

## Anyon Colliders

A time-dependent quantum Hall particle collider to reveal fractional statistics in the Laughlin sequence

Master's thesis in Erasmus Mundus Master in Nanoscience and Nanotechnology

SUSHANTH VARADA

DEPARTMENT OF MICROT TECHNOLOGY AND NANOSCIENCE - MC2

CHALMERS UNIVERSITY OF TECHNOLOGY

Gothenburg, Sweden 2023

[www.chalmers.se](http://www.chalmers.se)



MASTER'S THESIS 2023

# Anyon Colliders

A time-dependent quantum Hall particle collider to reveal  
fractional statistics in the Laughlin sequence

SUSHANTH VARADA



Department of Microtechnology and Nanoscience - MC2  
*Applied Quantum Physics Laboratory*  
Dynamics and Thermodynamics of Nanoscale devices group  
CHALMERS UNIVERSITY OF TECHNOLOGY  
Gothenburg, Sweden 2023

Anyon Colliders

A time-dependent quantum Hall particle collider to reveal  
fractional statistics in the Laughlin sequence

SUSHANTH VARADA

© SUSHANTH VARADA, 2023.

Supervisors: Dr. Christian Spånslätt<sup>1</sup>, Dr. Matteo Acciai<sup>1</sup>,

Examiner: Prof. Janine Splettstößer<sup>1</sup>

Co-Supervisor: Dr. George Simion<sup>3</sup>

Co-Promotor: Prof. Kristiaan De Greve<sup>2,3</sup>

<sup>1</sup>Applied Quantum Physics Laboratory, MC2, Chalmers University, Sweden

<sup>2</sup>Department of Electrical Engineering, KU Leuven, Belgium

<sup>3</sup>IMEC, Leuven, Belgium

Master's Thesis 2023

Department of Microtechnology and Nanoscience - MC2

Applied Quantum Physics Laboratory

Dynamics and Thermodynamics of Nanoscale devices group

Chalmers University of Technology

SE-412 96 Gothenburg

Telephone +46 31 772 1000

Cover: Schematic of a time-dependent anyon collider setup

Typeset in L<sup>A</sup>T<sub>E</sub>X

Printed by Chalmers Reproservice

Gothenburg, Sweden 2023

Anyon Colliders

A time-dependent quantum Hall particle collider to reveal fractional statistics in the Laughlin sequence

SUSHANTH VARADA

Department of Microtechnology and Nanoscience - MC2

Applied Quantum Physics Laboratory

Chalmers University of Technology

## Abstract

Elementary particles in nature (3+1 dimensions) are classified into bosons and fermions based on their exchange statistics. However, more general statistics, intermediate between fermionic and bosonic, are possible in 2+1 dimensions. Quasiparticles obeying this intermediary statistics are called anyons. A particularly relevant phase of matter hosting anyons is the fractional quantum Hall effect, where anyonic statistics has recently been demonstrated. Generally, exchange statistics is expected to be accessible in interference experiments, such as in the Hong-Ou-Mandel effect. In this setup, fermions show vanishing current correlations due to anti-bunching caused by the Pauli exclusion principle. Bosons, instead, bunch together due to Bose-Einstein statistics causing a surge in the current correlations. Can Hong-Ou-Mandel interferometry be extended to probe the fractional statistics of anyons?

In this thesis, we investigate this question in a fractional quantum Hall setup in the Laughlin sequence (filling factor  $\nu = 1/(2n + 1)$ ,  $n \in \mathbb{Z}^+$ ), where two anyons collide at a quantum point contact with a tunable time delay. Previous studies investigating similar systems relate current correlations of quasiparticle collisions with braiding between injected anyons and quasi-particle-hole excitations at the tunneling quantum point contact, which emerge due to thermal or quantum fluctuations. However, it remains unclear whether the presently studied Hong-Ou-Mandel effect probes the universal exchange phase ( $\vartheta$ ) picked up by the quasiparticles or other parameters, such as the non-universal scaling dimension ( $\delta$ ). We show that  $\vartheta$  accumulated by the incoming anyons due to interaction with quasi-particle-hole pairs at the quantum point contact cancel out in time-sensitive two-particle interferometry. Instead, the key quantity measured through current correlations is the non-universal  $\delta$  of the quasi-particle-hole excitations.

Keywords: Anyons, Edge states, Fractional quantum Hall effect, Topological quantum matter, Quantum interference effects.



## Acknowledgements

I am grateful to my supervisors, Christian Spånslätt, Matteo Acciai, and Janine Splettstößer, for their unwavering support and guidance throughout my master's thesis project. Their expertise, encouragement, and valuable insights have shaped my academic career. I express my sincere gratitude for their mentorship during my PhD applications and for being the *Giants* who helped me see further in my research journey. Furthermore, I thank my co-promoters, Kristiaan De Greve and George Simion, for their constructive feedback on my thesis. Finally, I extend my heartfelt appreciation to the Applied Quantum Physics (*AQP*) and Quantum Device Physics (*QDP*) lab members for productive discussions and the opportunity to learn about their research.

Sushanth Varada, Gothenburg, August 2023



# List of Acronyms

Below is the list of acronyms that have been used throughout this thesis listed in alphabetical order:

2DEG	Two-Dimensional Electron Gas
AC	Alternating Current
DC	Direct Current
DOS	Density of States
FQH	Fractional Quantum Hall
HBT	Hanbury Brown-Twiss
HOM	Hong-Ou-Mandel
IQH	Integer Quantum Hall
LL	Landau Levels
QPC	Quantum Point Contact



# Nomenclature

Below is the nomenclature of parameters and variables that have been used throughout this thesis.

## Parameters

$h$	Planck's constant
$k_B$	Boltzmann constant
$q$	Charge of particle
$\nu$	Filling factor
$v$	Velocity of the edge mode
$\vartheta$	Statistical exchange phase (or) Braiding angle
$\delta$	Scaling dimension of tunneling quasiparticles excited at the QPC
$\theta$	Temperature
$\Lambda$	Tunneling amplitude
$\alpha$	UV or short distance cut-off
$\omega_c$	Energy cut-off
$\Omega$	Frequency of applied voltage pulse
$T$	Time period of applied voltage pulse
$\tau_d$	Delay between injection/arrival of two input signals or particles

## Variables

$\mathcal{G}_{R,L}$	Equilibrium bosonic Green's function
$G_{+,-}$	Green's function
$p_{l,m}$	Photoassisted coefficient



# Contents

<b>List of Acronyms</b>	<b>ix</b>
<b>Nomenclature</b>	<b>xi</b>
<b>List of Figures</b>	<b>xv</b>
<b>1 Introduction</b>	<b>1</b>
1.1 Partition Noise and Two-particle Interferometry . . . . .	2
1.2 Integer Quantum Hall Effect . . . . .	4
1.3 Fractional Quantum Hall Effect . . . . .	6
1.4 Experimental Realization of Anyon Colliders . . . . .	8
1.5 Goal of the thesis . . . . .	9
<b>2 Theory</b>	<b>11</b>
2.1 Time Evolution Pictures in Quantum Mechanics . . . . .	11
2.2 Landau Levels and Linear Dispersion Model . . . . .	13
2.3 1D Chiral Fermions and Bosonization . . . . .	14
2.4 Bosonic Hamiltonian and Quasiparticle Operator . . . . .	17
2.5 Temporal Voltage Drive . . . . .	19
<b>3 Particle collider in the FQH regime</b>	<b>21</b>
3.1 Tunneling current in a weak backscattering QPC . . . . .	21
3.2 Zero-frequency backscattered noise . . . . .	26
3.3 Two input sources and photoassisted coefficients . . . . .	27
3.4 Analysis in the DC regime . . . . .	29
3.5 AC Analysis: Hong-Ou-Mandel Effect . . . . .	30
<b>4 Exchange phase erasure in anyon time domain interferometry</b>	<b>33</b>
4.1 Auxiliary state and Tunneling operator . . . . .	33
4.2 Tunneling current in HOM configuration . . . . .	35
4.3 Exchange phase erasure in HOM noise ratio . . . . .	38
4.4 Interpreting the braiding phase erasure . . . . .	42
<b>5 Conclusion</b>	<b>47</b>
<b>6 Outlook</b>	<b>49</b>
<b>Bibliography</b>	<b>51</b>

<b>A Bosonic Green's Function</b>	<b>I</b>
<b>B Fourier Transform of the Green's Function</b>	<b>IV</b>
B.1 Finite temperature Green's function . . . . .	IV
B.2 Temperature independent Green's function . . . . .	VI
<b>C Photoassisted Coefficients</b>	<b>VII</b>
<b>D Integral of the Equilibrium Green's Function</b>	<b>IX</b>

# List of Figures

1.1	Pictorial representation of particle exchange statistics in (3+1)D and (2+1)D	1
1.2	A particle scattered by a potential barrier . . . . .	2
1.3	The <i>fermionic anti-bunching</i> and <i>bosonic bunching</i> in the Hong-Ou-Mandel interference of indistinguishable particles . . . . .	3
1.4	Illustrations detailing the integer quantum Hall effect . . . . .	5
1.5	Pictorial examples showcasing the formation of chiral edge modes in the integer quantum Hall effect . . . . .	6
1.6	Diagrams elucidating the occupation of the density of states in the integer and fractional quantum Hall effect and a plot of Hall resistance . . . . .	7
1.7	Schematic of the three-QPC mesoscopic anyon collider setup with the measurement circuitry . . . . .	9
1.8	A naive expectation of the Hong-Ou-Mandel noise ratio for anyons at $\nu = 1/3$	10
2.1	Linearizing the Landau levels near the Fermi points to obtain a linear dispersion model . . . . .	14
3.1	A four terminal Laughlin fractional quantum Hall setup operating in the Hanbury Brown-Twiss configuration . . . . .	22
3.2	Plots of backscattered current and zero-frequency noise for a DC bias as a function of $q\nu V_{DC}\omega_c^{-1}$ for zero and finite temperature cases . . . . .	30
3.3	A four terminal Laughlin fractional quantum Hall setup operating in the Hong-Ou-Mandel configuration . . . . .	31
3.4	A plot of the standard Hong-Ou-Mandel noise ratio $\mathcal{R}$ as a function of the time delay $\tau_d/T$ between the input signals . . . . .	32
4.1	The four terminal Laughlin FQH setup operating in the HOM configuration with ideal time-resolved anyon sources. . . . .	34
4.2	Pictorial representation of different cases arising in the calculation of the tunneling current . . . . .	37
4.3	A plot of the anyonic HOM noise ratio $\mathcal{R}$ as a function of delay $\tau_d/T$ between the arrival times of two injected anyons at the collider QPC . . . . .	41
4.4	Diagrams representing different subprocesses occurring between the injected anyons and the quasi-particle-hole pairs excited at the QPC . . . . .	43
4.5	Time domain braiding between the injected anyons and QPC quasi-particle-hole excitations caused due to thermal or quantum fluctuations. . . . .	44



# 1

## Introduction

Quantum Mechanics is a very successful theoretical framework, tested by numerous experiments, that describes the fundamental constituents of matter and their interactions. Its conceptions were formulated by Schrödinger, Heisenberg, and Born in 1926-1927 [1] and further developed as elaborated in Ref. [2]. Quantum mechanics classifies indistinguishable particles in 3+1 dimensional (D) nature (3 spatial + 1 time dimension) into bosons and fermions. This limitation to only two possible types of particles in (3+1)D can be understood by examining their exchange statistics. Imagine interchanging two identical particles twice. This scenario is equivalent to encircling one particle around the other by forming a loop that changes the wavefunction by an arbitrary phase<sup>1</sup> [ $\Psi(x_1, x_2) \rightarrow e^{i\Phi}\Psi(x_2, x_1) \rightarrow e^{2i\Phi}\Psi(x_1, x_2)$ ]. Permitting only local deformations<sup>2</sup>, this loop can be shrunk to a point in three space dimensions, as illustrated in Fig. 1.1a.

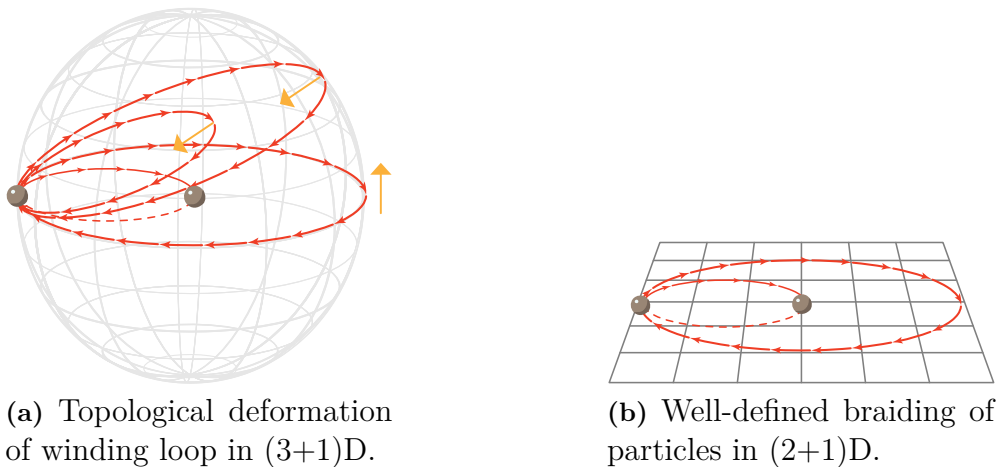


**Figure 1.1:** Pictorial representation of particle exchange statistics in three and two dimensions. (a) The winding loop (red trajectory) formed by moving one particle around the other is shrunk to a point through continuous deformations in the third dimension, as depicted by the orange arrows. (b) In two dimensions, the winding loop cannot be topologically deformed to a point because one particle intersects the path of the other particle. This constraint, exclusive to (2+1)D, leads to fractional exchange statistics.

<sup>1</sup>This representation is Abelian, meaning that the wavefunction is a scalar quantity that only acquires a phase after a braiding operation (exchange of two particles). There are more complicated types of anyons, where a non-abelian representation applies: in that case, the wavefunction is a multi-component object that transforms according to a unitary matrix [3–5]. In this case, the order in which consecutive braiding operations are performed is important [6].

<sup>2</sup>Continuous deformations of a geometry or structure that only include stretching, bending, and shrinking. These transformations do not involve operations like tearing and cutting.

Therefore, winding one particle around the other in (3+1)D is topologically equivalent to not moving the particles. Thus, the wavefunction of the particles remains unaltered under two such exchanges. Consequently, the particle wavefunction can only change by a phase factor  $e^{i\Phi}$  of either  $+1$  or  $-1$  under a single exchange [ $\Psi(x_1, x_2) \rightarrow e^{i\Phi}\Psi(x_2, x_1)$ ]. Bosons, defined by a many-body wavefunction that is symmetric when exchanging two particles, can be described by an accumulated exchange phase of  $\Phi = 0$ . In contrast, fermions with an anti-symmetric wave function pick up an exchange phase of  $\Phi = \pi$ , such that  $e^{i\pi} = -1$  and  $e^{2i\pi} = 1$ . Two-dimensional systems lack the extra dimension to topologically deform this winding loop to a point, as depicted in Fig. 1.1b. Therefore, encircling one particle around the other is non-trivial in (2+1)D systems and the wavefunction can acquire *any* phase  $\Phi = \vartheta$ . Particles described by these wavefunctions are termed *anyons* and were predicted in the late 1970s [7–9]. Anyons are neither bosons nor fermions and are governed by fractional exchange statistics that is possible for point particles only in 2 spatial + 1 time dimensions [10, 11]. The renewed interest in exploring the properties of anyons stems from the experimental observation of their fractional statistics with potential applications in topological quantum computing [6, 12]. Generally, the exchange statistics of indistinguishable particles is expected to be accessible through interference experiments. The fractional statistics of Abelian anyons were detected in two seminal experiments [13, 14], each utilizing a different type of interferometer. These experiments attracted much attention and instigated several theoretical studies. Moreover, the anyon collider (anyon interferometry) experiment was reproduced independently by three different experimental groups [15–17]. In this chapter, we begin by describing two-particle interferometry for particles in (3+1)D and discuss the prospects of extending the idea to anyons in (2+1)D. The remainder of the chapter introduces key concepts required throughout the thesis.

## 1.1 Partition Noise and Two-particle Interferometry

Consider a source emitting a stream of  $N$  particles impinging onto a potential barrier. The particles are either transmitted or reflected independently, with a probability of  $\mathcal{T}$  and  $1 - \mathcal{T}$ , respectively, as depicted in Fig. 1.2. The detector on the right-hand side clicks only when a particle successfully tunnels through the barrier. The average number of particles the detector measures is then represented by  $\langle N_1 \rangle = N\mathcal{T}$ . The deviations from this average manifest as fluctuations, described by  $\Delta N_1 = N_1 - \langle N_1 \rangle$ . The variance is obtained by auto-correlating  $\Delta N_1$  as

$$\langle \Delta N_1 \Delta N_1 \rangle = \langle \Delta N_1^2 \rangle = \langle (N_1 - \langle N_1 \rangle)^2 \rangle = \langle N_1 \rangle (1 - \mathcal{T}). \quad (1.1)$$

Equation (1.1) represents the *partition noise* that occurs due to the random partitioning

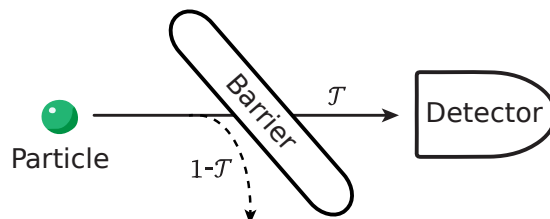


**Figure 1.2:** Particle scattered by a potential barrier into a transmitted or reflected signal with probabilities  $\mathcal{T}$  and  $1 - \mathcal{T}$ , respectively.

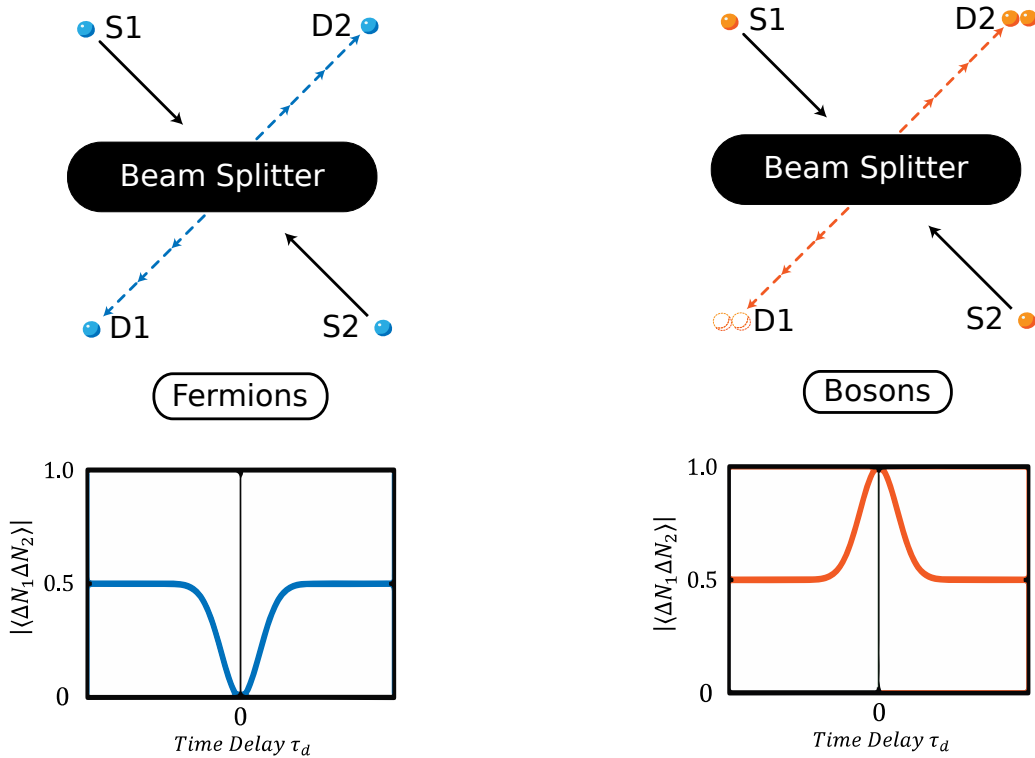


**Figure 1.3:** Illustration of the *fermionic anti-bunching* and *bosonic bunching* in the Hong-Ou-Mandel interference. The beam splitter is symmetric with a transmission (and reflection) probability of  $1/2$ . A different behavior in fluctuations emerges when two bosons or fermions arrive simultaneously ( $\tau_d = 0$ ) at the beam splitter. Fluctuations are suppressed for fermions because they avoid each other due to the Pauli exclusion principle. Conversely, fluctuations surge for bosons as they tend to occupy the same state because of their underlying Bose-Einstein statistics.

of the stream of particles into transmitted and reflected signals. Likewise, the fluctuations in the occupation number of the reflected beam are given by  $\Delta N_2 = N_2 - \langle N_2 \rangle$ . The cross-correlation  $\langle N_1 N_2 \rangle$  between the number of particles tunneling through the barrier ( $\mathcal{T}$ ) and those being deflected ( $1 - \mathcal{T}$ ) is always zero because each particle can be either transmitted ( $N_1 = 1, N_2 = 0$ ) or reflected ( $N_1 = 0, N_2 = 1$ ). Using this, we can extrapolate the following relation:

$$\langle \Delta N_1 \Delta N_2 \rangle = -\langle \Delta N_1^2 \rangle = -\langle \Delta N_2^2 \rangle. \quad (1.2)$$

Thus, both auto- and cross-correlations contain identical information about the partition noise that describes the statistical fluctuations in the detected number of particles. This relation remains valid regardless of whether the particle (as shown in Fig. 1.2) is a fermion or boson. However, to reveal the quantum statistics of indistinguishable particles, we need to consider two-particle interferometry [18, 19].

Figure 1.3 represents a Hong-Ou-Mandel (HOM) interferometer [20] with two sources and detectors separated by a beam splitter. A non-zero time delay ( $\tau_d \neq 0$ ) between particles arriving at the beam splitter from *Source 1* (S1) and *Source 2* (S2) results in a 50% cross-correlation of fluctuations at the two detectors (averaged over a long time).  $\langle \Delta N_1 \Delta N_2 \rangle = 0.5$ , holds true if the transmission of the beam splitter is  $1/2$ , irrespec-

tive of the particles being either fermions or bosons. However, a very different behavior arises for a vanishing time delay  $\tau_d = 0$ . If two identical fermions arrive at the beam splitter simultaneously, they will avoid each other because they cannot occupy the same quantum state due to the Pauli exclusion principle [21–24]. Therefore, each detector will always measure a particle definitively without fluctuations:  $\Delta N_1 = \Delta N_2 = 0$ . The cross-correlation  $\langle \Delta N_1 \Delta N_2 \rangle = 0$  indicates uncorrelated fluctuations that do not vary in time. This phenomenon observed in HOM interferometry is called *fermion antibunching*. It is characterized by the Pauli dip, which is the suppression of partition noise<sup>3</sup> as a function of  $\tau_d$ , shown in Fig. 1.3. Bose-Einstein statistics show that multiple bosons can occupy the same quantum state. Consequently, two indistinguishable bosons at  $\tau_d = 0$  always leave the beam splitter together towards either of the detectors. Hence, the probability of finding two bosons at *Detector 1* (D1) and zero bosons at *Detector 2* (D2) or vice versa is equal. This phenomenon of *boson bunching* surges the fluctuations in one detector  $\Delta N_{1/2} = 1 - 0 = 1$ , while concurrently reducing the fluctuations in the other  $\Delta N_{2/1} = 1 - 2 = -1$ . Therefore, the fluctuations at the two detectors are perfectly anti-correlated with  $\langle \Delta N_1 \Delta N_2 \rangle = -1$ . As illustrated in Fig. 1.3, this correlation  $|\langle \Delta N_1 \Delta N_2 \rangle|$  is characterized by a peak in the partition noise as a function of  $\tau_d$ . Hence, the underlying exchange statistics of particles is made manifest in noise measurements. Can this concept be extended to probe the fractional statistics of anyons?

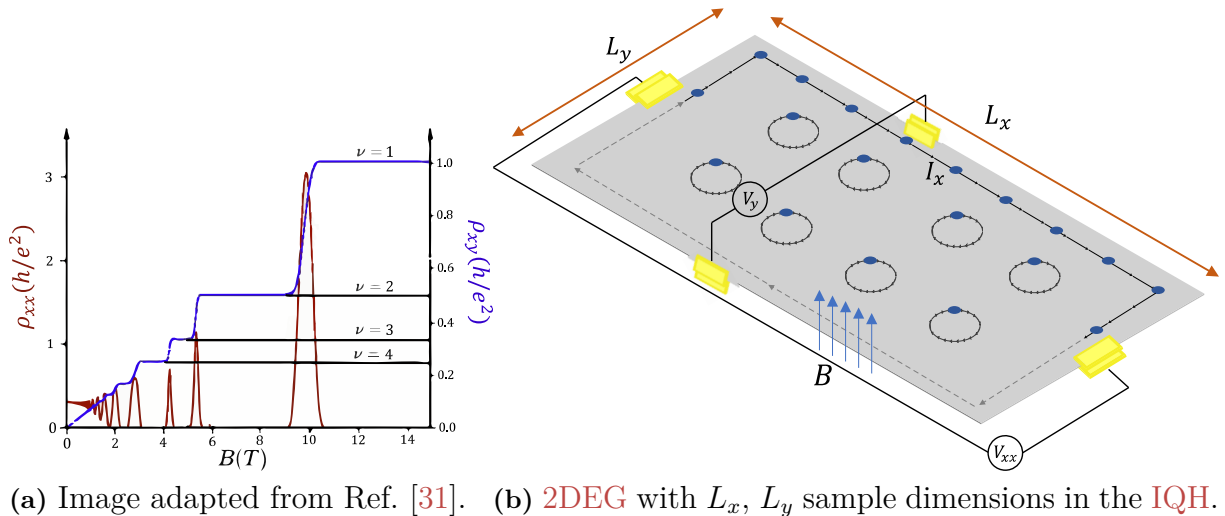
To answer this, we require (i) sources that emit anyons, (ii) channels to guide them towards a (iii) beam splitter for quasiparticles. Fractional Quantum Hall systems are a promising testbed that hosts anyons [25]. Furthermore, the components required to assemble a HOM setup can be implemented in (2+1)D quantum Hall systems [23, 24, 26–28]. Hence, in the following sections, we briefly introduce the integer quantum Hall effect and extend the concept to the fractional Hall regime before discussing anyon interferometry.

## 1.2 Integer Quantum Hall Effect

When a current-carrying conductor is placed in a perpendicular magnetic field ( $B_\perp$ ), the electrons deflect from their trajectory due to the Lorentz force. This mechanism gives rise to the classical Hall effect in which the transverse resistivity  $\rho_{xy}$  is directly proportional to the strength of the applied magnetic field  $\vec{B}$ . In contrast, the longitudinal resistivity  $\rho_{xx}$  is independent of the  $\vec{B}$ -field and assumes a constant value depending on the scattering time  $\tau$  (as  $\tau \rightarrow \infty$   $\rho_{xx} \rightarrow 0$ ) [29]. Increasing the strength of the  $\vec{B}$ -field at low temperature causes a phase transition in the 2D classical Hall system. It results in the quantization of the relationship between the magnetic field ( $\vec{B}$ ) and the Hall resistivity  $\rho_{xy}$  as plotted in Fig. 1.4a. It is the integer quantum Hall (IQH) effect discovered by von Klitzing in 1980, using samples prepared by Dorda and Pepper [30] for which he was awarded the 1985 Nobel Prize. The experimental data shows that the longitudinal resistivity  $\rho_{xx} = 0$ , as long as  $\rho_{xy}$  lies on a plateau with the value

$$\rho_{xy} = \frac{h}{e^2} \frac{1}{\nu}, \nu \in \mathbb{Z}^+, \quad (1.3)$$

<sup>3</sup>For electrons,  $\langle N_1 \rangle$  is given by  $\langle I_1 \rangle (t/e)$  where  $\langle I_1 \rangle$  is the average current measured over the time interval  $t$ , and so  $\langle \Delta N_1 \Delta N_1 \rangle$  is related to the current fluctuations, or shot noise  $\langle S_{11} \rangle$ .



(a) Image adapted from Ref. [31]. (b) 2DEG with  $L_x$ ,  $L_y$  sample dimensions in the IQH.

**Figure 1.4:** (a) A plot of the longitudinal resistivity  $\rho_{xx}$  and transverse resistivity  $\rho_{xy}$  as a function of the magnetic field ( $\vec{B}$ ) in the IQH effect.  $\rho_{xx}$  is independent of the  $\vec{B}$ -field and spikes to a finite value only when  $\rho_{xy}$  transits onto the next plateau as a function of the  $\vec{B}$ -field. (b)  $V_{xx}$  and  $V_y$  are the measured voltages in the longitudinal and transverse directions of the sample in the IQH regime. The sample's bulk exhibits insulating behavior because the electrons are trapped in closed circular orbits. Concurrently, electricity is conducted at the edges without any dissipation due to the formation of skipping orbits.

where  $h$  is Planck's constant and  $e$  is the charge of an electron,  $\nu$  is measured to be an integer with remarkable accuracy. Moreover,  $\rho_{xx}$  spikes to a finite value only during the transition of  $\rho_{xy}$  to the next plateau as a function of the  $\vec{B}$ -field. The vanishing  $\rho_{xx}$  for  $\rho_{xy} \neq 0$  indicates the presence of a perfect dissipationless conductor that does not oppose the flow of electrons. However, examining the conductivity tensor  $\sigma$  reveals the existence of an insulator with a vanishing longitudinal conductivity

$$\sigma_{xx} = \frac{\rho_{xx}}{\rho_{xx}^2 + \rho_{xy}^2} = 0, \text{ for } \rho_{xx} = 0, \rho_{xy} \neq 0. \quad (1.4)$$

Therefore, in the IQH regime, the system is an insulator and conductor concurrently. Classically, the strong perpendicular magnetic field causes the electrons in the sample bulk to move in circular orbits with an angular frequency  $\omega_B$  (cyclotron frequency<sup>4</sup>), as depicted in Fig. 1.4b. As the electrons are trapped in these closed orbits, they do not conduct electricity transforming the bulk into an insulator. However, at the edge of the sample, the closed orbits form connected skipping orbitals that facilitate electron transport in only one direction. Therefore, the 1D boundary of the sample acts as a *chiral* conductor. Quantum mechanics shows that the strong magnetic field discretizes the energy spectrum into energy levels equally spaced by the cyclotron energy<sup>5</sup>  $\hbar\omega_B$ . These levels that encompass a macroscopic number of degenerate energy states are called Landau levels (LL). A confining potential  $\mathcal{V}_{confine}(y)$  arises due to the finite boundary of the sample. This potential is zero within the bulk and increases towards the edge of

<sup>4</sup>The cyclotron frequency is given by  $\omega_B = eB/m$ , where  $m$  is the mass of an electron.

<sup>5</sup>Energy associated with the cyclotron motion of charged particles in a magnetic field.

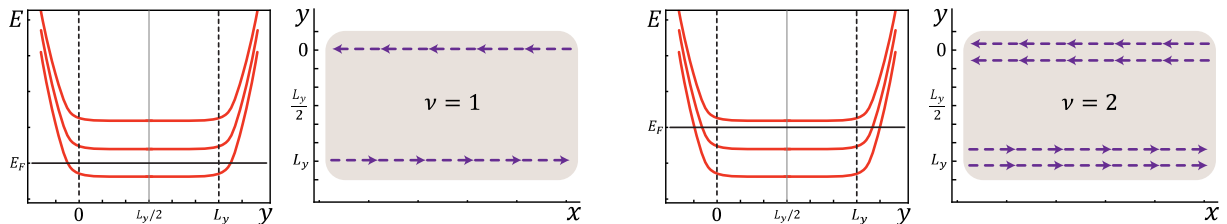
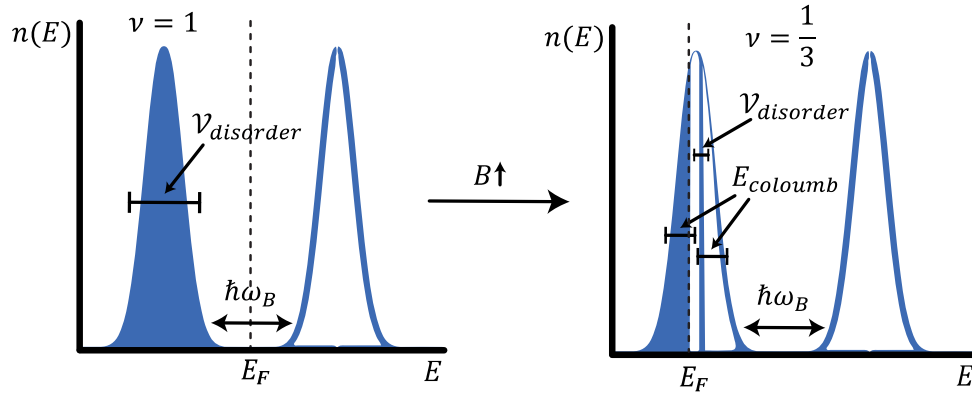


**Figure 1.5:** Bending of LLs at the edges  $(0, L_y)$  of the 2DEG sample due to the confining potential  $\mathcal{V}_{confiner}(y)$ .  $n$  edge modes emerge when the Fermi level  $E_F$  intersects the LLs at  $2n$  points that result in  $n$  filled LLs corresponding to the filling factor  $\nu = n$  in the IQH regime. The cases for  $\nu = 1, 2$  are depicted to the left and right, respectively.

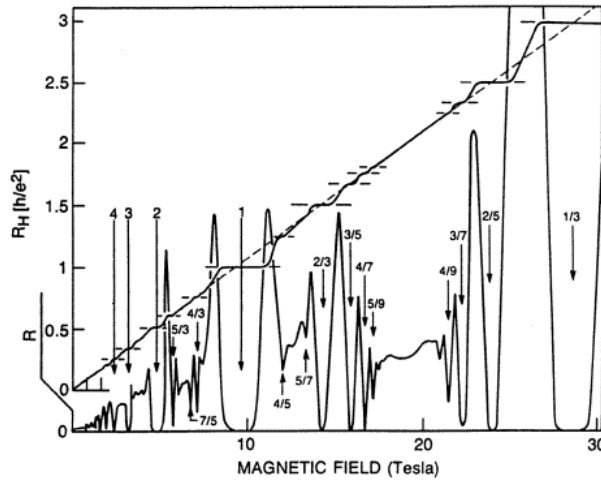
the sample to restrict the electrons. Consequently, the energy states close to the edge are raised by  $\mathcal{V}_{confiner}(y)$  that bend the associated LL at the sample boundary. The band situated in the bulk of the sample has filled states, making it an insulator. Whereas the bent LL having empty states available above the Fermi energy give rise to 1D conductors at the edge of the sample. The two Fermi points (intersection of  $E_F$  with the bent energy spectrum) shown in Fig. 1.5 lead to two chiral edge states with opposite group velocities ( $v$ ): right moving state at  $y = L_y$ , with positive  $v$ , and left moving state at  $y = 0$  with negative  $v$ . The spatial separation of the chiral modes suppresses the backscattering of electrons from right-moving to left-moving or vice versa, forming perfect chiral conductors. Therefore, the edge states are immune to scattering caused by impurities that “smoothly deform” LL [31]. Furthermore,  $E_F$  lying between the gap of  $n^{th}$  and  $n + 1^{th}$  LL intersects them at  $2n$  points, spawning  $\nu = n$  [where  $n \in \mathbb{Z}^+$ ] chiral modes at each edge. Notably, the filling factor  $\nu$  corresponds to the number of filled LL and IQH effect manifests at integer-number values of  $\nu$ . Hence, the chiral edge modes in the quantum Hall systems facilitate robust one-way channels to guide particles for interferometry experiments.

### 1.3 Fractional Quantum Hall Effect

In a realistic sample with disorder due to underlying lattice impurities, the density of states (DOS)  $n(E)$  and the corresponding LL do not assume a perfect train of Dirac  $\delta$  functions. They instead have a Gaussian or Lorentzian profile, as illustrated in Fig. 1.6a. If the strength of the random potential introduced by the disorder is smaller than the splitting of LL:  $\hbar\omega_B > \mathcal{V}_{disorder}$ , it helps stabilize the edge modes and makes the plateaus better discernable in the IQH effect [31]. If the  $\vec{B}$ -field is further increased ( $\hbar\omega_B$  increases) in very pristine samples, other plateaus emerge at fractional values  $\nu \in \mathbb{Q}$ , as plotted in Fig. 1.6b. The most prominent and simple states lie on plateaus with odd denominators  $\nu = 1/(2n+1)$ ,  $n \in \mathbb{Z}^+$ . These states are explained by the emergence of a single-edge mode and are termed the Laughlin sequence [32]. The edge states for other filling factors are more complicated [33, 34] and fall outside the scope of this study. The fractional quantum Hall effect [35] can be understood by considering the Coulomb interaction between electrons. These interactions lift the degeneracy of the macroscopic states embedded in a LL, leading to a spectrum of states of width proportional to  $E_{coulomb}$ . The DOS corresponding to different energy scales do not overlap as long as  $\hbar\omega_B > E_{coulomb} > \mathcal{V}_{disorder}$ . This spectrum consists of partially filled LL that exhibit small excitation gaps at fractional filling factors



(a) DOS and occupation of LL in a  $\vec{B}$ -field ignoring the particle spin.



(b) Image taken from Ref. [36].

**Figure 1.6:** (a) Transition of DOS from IQH to FQH regime.  $\hbar\omega_B$  is the cyclotron energy, and  $\mathcal{V}_{disorder}$  represents the strength of the random potential introduced by the disorder. The width of the integer filled LLs ( $\nu = n$ , where  $n \in \mathbb{Z}^+$ ) are proportional to  $\mathcal{V}_{disorder}$ . These levels spread out as the magnetic field increases, making the plateaus more discernable in the limit  $\hbar\omega_B > \mathcal{V}_{disorder}$  in the IQH regime. The Coulomb interaction  $E_{coulomb}$  between the electrons becomes prominent as we transition to the FQH regime. These interactions lift the degeneracy of the macroscopic states resulting in a spectrum of states whose width is proportional to  $E_{coulomb}$ . This spectrum has gaps at fractional values, and the filled states are discernable when  $\hbar\omega_B > E_{coulomb} > \mathcal{V}_{disorder}$ . The case for  $\nu = 1/3$  is shown here. (b) A plot depicting the Hall resistance  $R_H$  as a function of the magnetic field  $\vec{B}$  in the context of the FQH effect.

where the Hall states are observed. Figure 1.6a depicts a Laughlin state with a single gap at  $\nu = \frac{1}{3}$ . Fractionally charged quasiparticle excitations with  $q^* = q\nu$  above such collective ground state of correlated electrons have been predicted [25, 32, 37] and recently confirmed [13, 14] to be emergent Abelian anyons. These fractional charges can be detected by implementing a Quantum Point Contact (QPC) [38, 39] in the FQH system, as initially suggested by Kane and Fisher in Ref. [40]. The QPC is a narrow constriction that partially distorts the trajectory of chiral edge modes by imposing a negative voltage

polarization that depletes the underlying **2DEG**. Tuning the voltage polarization varies the transmission of the **QPC** by closing or opening the edge modes. Therefore, a **QPC** is analogous to a beam splitter that transmits or reflects impinging particles with specific probabilities. Tunneling of quasiparticles through the quantum Hall liquid between the edge modes corresponds to a backscattering event. The transmission probability through the **QPC** in the weak-backscattering limit is  $\mathcal{T} \approx 1$ . Therefore, the tunneling events corresponding to the reflection probability  $1 - \mathcal{T} \ll 1$  are so rare that the quasiparticles backscatter without any correlation between them. This stochastic tunneling generates zero-temperature shot noise

$$S = 2q^* \langle I_T \rangle, \text{ in the limit } eV \gg k_B \theta, \quad (1.5)$$

where  $I_T$  is the tunneling current through the **QPC**,  $q^*$  is the effective charge,  $k_B$  is the Boltzmann constant, and  $\theta$  is the temperature. The shot noise measurements proved the existence of fractionally charged quasiparticles in **FQH** systems at filling factors  $\nu = 1/3$  and  $\nu = 2/3$  [41, 42]. The **FQH** system with a **QPC** in the weak backscattering limit can generate a dilute beam of quasiparticles. Therefore, it acts as a stochastic anyon source [40] to implement the **HOM** interferometer to collide anyons.

## 1.4 Experimental Realization of Anyon Colliders

The direct observation of fractional statistics is much more subtle than detecting the fractional charge of anyons. Combining the elements discussed in Sections 1.2 and 1.3, a two-particle anyon collider at filling factor  $\nu = 1/3$  was proposed in Ref. [43] and realized in Ref. [14]. **QPC1** and **QPC2** of the setup shown in Fig. 1.7 are **DC** biased into a weak backscattering regime with transmission probabilities  $\mathcal{T}_s = \mathcal{T}_1 = \mathcal{T}_2$  by  $V_{DC1}$  and  $V_{DC2}$ , respectively. Due to the tunneling of  $q^* = q/3$  quasiparticles at random, these **QPCs** serve as sources that emit anyons following a Poisson distribution. This random emission implies that the *source* **QPCs** are not time-resolved and do not permit control over the emission times of the quasiparticles. The tunneling currents  $I_1$  and  $I_2$  carrying the quasiparticles interfere at the collider **cQPC** with a transmission probability  $\mathcal{T}$ . The shot noise accompanied by  $I_3$  and  $I_4$  embeds the information about the exchange statistics of anyons. The cross-correlation between the output currents describes the shot noise as

$$S_{I_3 I_4}(\text{classical}) = -2q\nu(1-p)\mathcal{T}_s\mathcal{T}(1-\mathcal{T})(I_1 + I_2), \quad (1.6)$$

where  $p$  is the exclusion (quasi)probability. Equation 1.6 originates from an intuitive classical model, which suggests an interpretation of the exchange statistics in terms of the exclusion probability. A fermionic behavior with  $p = 1$  results in vanishing shot noise, as discussed in Sec. 1.1. At  $\nu = 1/3$ , the fractional exchange phase  $\Phi = \pi/3$  is closer to bosons ( $\Phi = 0$ ) than fermions ( $\Phi = \pi$ ). Therefore,  $p$  is predicted to be negative ( $p < 0$ ), ensuing a negative cross-correlation  $S_{I_3 I_4} < 0$ . Thus, the classical model generalizes the Pauli dip and associates the negative value of the exclusion probability  $p$  with the fractional statistics of anyons in a non-rigorous manner. A quantum mechanical treatment of the current cross-correlations for abelian anyons with an exchange phase  $\Phi = \pi/m$  (for  $m \geq 3$ ) leads to the following result for the shot noise:

$$S_{I_3 I_4}(\text{quantum}) = 2q\nu \frac{-2}{m-2} \mathcal{T}(I_1 + I_2) \implies P = \frac{S_{I_3 I_4}}{2q\nu \mathcal{T}(I_1 + I_2)} = \frac{-2}{m-2}. \quad (1.7)$$

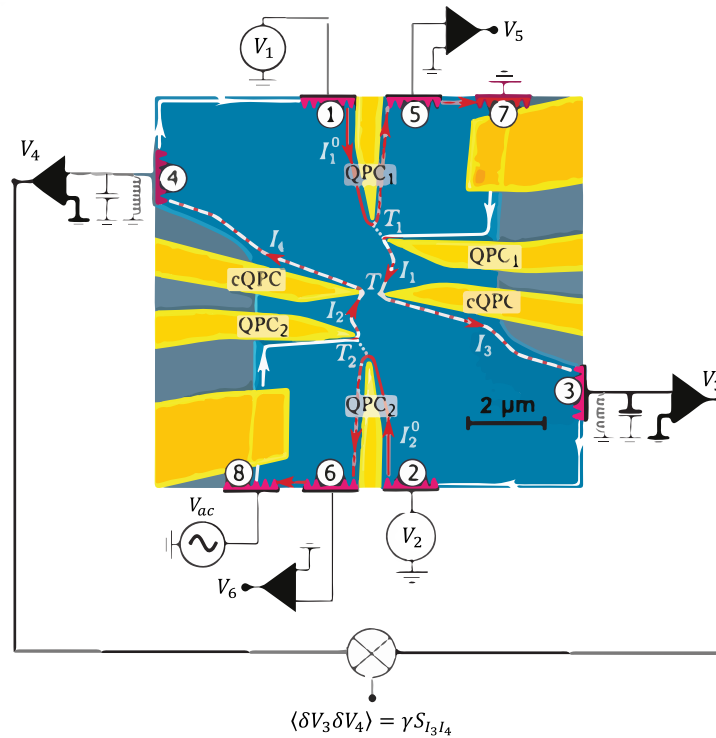


**Figure 1.7:** False color scanning micrograph of the mesoscopic anyon collider setup with the measurement circuitry (image taken from Ref. [14]). The quasiparticle tunneling currents  $I_1$  and  $I_2$  originating from the DC biased QPC 1 and 2 interfere at the collider cQPC with a transmission probability  $\mathcal{T}$ . Contacts 3 and 4 collect the output signals  $I_3$  and  $I_4$  to compute the current cross-correlations.

Equation (1.7) describes a generalized Fano factor  $P$  that is only dependent on the exchange phase of anyons. The experimental demonstration measured  $P = -2 \pm 0.1$ , which agrees with the prediction of the theoretical model that  $P = -2$  at  $\nu = 1/m = 1/3$  [43]. Later theoretical investigations [44, 45] have re-interpreted the Fano factor  $P$  to be directly associated with braiding between anyons interfering at the cQPC of the setup depicted in Fig. 1.7. This implies that the experiment in Ref. [14] is the first evidence of Abelian anyon fractional statistics through shot noise measurements at  $\nu = 1/3$ .

## 1.5 Goal of the thesis

Probing the fractional statistics of anyons through Hong-Ou-Mandel interferometry is the primary focus of this thesis. We expect that the HOM interference will reveal the underlying quantum statistics of anyons through current correlations that depend on the tunable time delay ( $\tau_d$ ) between particles arriving at the beam splitter. This expectation aligns with the HOM effect obtained for fermions and bosons, as explained in Sec. 1.1.

Earlier descriptions of anyon colliders [43] employed DC biased Poissonian sources of anyons that generate a random stream of quasiparticles without any control over their emission times. However, we require a time-resolved emission of anyons that enables us to modulate the time delay ( $\tau_d$ ) between the arrival of quasiparticles at the collider

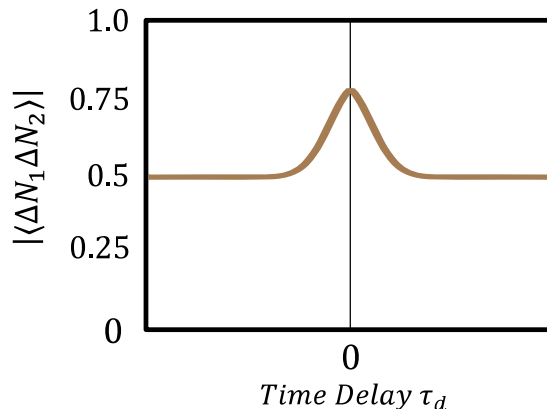


**Figure 1.8:** Visual representation of a naive expectation regarding the fluctuations in **HOM** interferometry of anyons in the Laughlin sequence at  $\nu = 1/3$ . This depiction showcases an accumulated exchange phase of  $\vartheta = \pi/3$  as described by Eq. (1.8).

**QPC** to perform the **HOM** interferometry. The correlations describing the **HOM** curves of fermions and bosons represented in Fig. 1.3 are defined by [18]

$$|\langle \Delta N_1 \Delta N_2 \rangle| = \frac{1}{2} [1 + |J|^2 \cos(\vartheta)], \quad (1.8)$$

where  $|J|$  represents the spatial overlap between two incident wavefunctions at the beam splitter, and  $\vartheta$  denotes the acquired exchange phase. Taking  $|J| = 1$  at null delay  $\tau_d = 0$ , the fluctuations described in Eq. (1.8) entirely depend on the accumulated statistical exchange phase  $\vartheta$ . Building upon the success of the **HOM** interference in uncovering the exchange statistics of fermions and bosons, we investigate:

- How would the fluctuations in the **HOM** interferometry manifest due to the fractional statistics of anyons?
- How would the **HOM** noise curves presented in Fig. 1.3 be influenced by the acquired exchange phase of the colliding anyons?
- Would anyons generate intermediate noise fluctuations, corresponding to  $\vartheta = \pi/(2n+1)$ , where  $n \in \mathbb{Z}^+$  in the Laughlin sequence? (as portrayed in Fig. 1.8 for  $n = 1$ ).
- What distinguishes the interference between colliding anyons in the **HOM** interferometry from those in fermions and bosons?

Providing insights into these questions is the main motivation for this work.

# 2

## Theory

This chapter briefly overviews the theoretical tools necessary to describe edge transport of anyons in the Laughlin fractional quantum Hall states. Initially, we digress to discuss the concept of quantum time evolution pictures, which is a foundational framework utilized throughout this thesis. We then discuss the formulation of Landau levels and chiral edge modes in the IQH regime before generalizing it to Laughlin FQH edges. Subsequently, we describe the technique of bosonization of 1D systems and demonstrate the utility of the introduced theory toolbox in describing an out-of-equilibrium Laughlin FQH edges.

### 2.1 Time Evolution Pictures in Quantum Mechanics

There are three different equivalent approaches to treating time dependence in quantum mechanics [46, 47], and they find utility in distinct contexts. It is also possible to transform between these time evolution pictures.

**Schrödinger picture:** The quantum states  $|\varphi(t)\rangle_S$  evolve with time, while the operators are fixed at an initial time  $t_0$ ,  $O_S(t) = O(t_0)$ . One can introduce a time evolution operator acting on the quantum states  $|\varphi(t)\rangle_S = U(t, t_0) |\varphi(t_0)\rangle$  and evolve them according to the Schrödinger equation,  $i\hbar\partial_t |\varphi(t)\rangle_S = H |\varphi(t)\rangle_S$ , from which we obtain

$$i\hbar\partial_t U(t, t_0) |\varphi(t_0)\rangle = HU(t, t_0) |\varphi(t_0)\rangle. \quad (2.1)$$

For a time-dependent Hamiltonian  $H$ , Eq. (2.1) gives us  $U(t, t_0) = \mathcal{T} \left[ e^{-\frac{i}{\hbar} \int_{t_0}^t dt' H(t')} \right]$ , where  $\mathcal{T}$  is the time ordering operator that orders a product of time-dependent operators in descending sequence of time. When the Hamiltonian is independent of time, Eq. (2.1) simplifies to  $U(t, t_0) = e^{-\frac{i}{\hbar}(t-t_0)\mathcal{H}}$ .

**Heisenberg picture:** The quantum states are stationary in time  $|\varphi(t)\rangle_H = |\varphi(t_0)\rangle$ , while the operators procure a time dependence through the time evolution operator  $O_H(t) = U^\dagger(t, t_0)O(t_0)U(t, t_0)$ . The equation of motion for an observable in the Heisenberg picture is given by

$$i\hbar\partial_t O(t) = [O(t), H(t)] + (\partial_t O)(t). \quad (2.2)$$

Suppose the operator does not explicitly depend on time; its time evolution boils down to  $i\hbar\partial_t O(t) = [O(t), H(t)]$ , where the expression  $[O(t), H(t)]$  represents the commutator between the operators  $O(t)$  and  $H(t)$  defined as  $[O(t), H(t)] = O(t)H(t) - H(t)O(t)$ .

**Interaction picture:** It is also termed<sup>1</sup> the *mixed picture* because both the quantum states and operators carry part of the time dependence. This picture is beneficial for constructing perturbative expansions and dealing with the time evolution of observables caused by interactions. Consider the Hamiltonian of the form  $H = \mathcal{H} + \mathcal{V}(t)$ , where  $\mathcal{H}$  is a known time-independent operator and  $\mathcal{V}(t)$  is a non-diagonalizable complex operator carrying the time dependence. In the interaction picture, the operator  $O(t_0)$  evolves with the trivial  $\mathcal{H}$  like in the Heisenberg picture:  $O_I(t) = e^{\frac{i}{\hbar}(t-t_0)\mathcal{H}}O(t_0)e^{-\frac{i}{\hbar}(t-t_0)\mathcal{H}} = O_H^{(0)}(t)$ <sup>2</sup>. Whereas  $U_I(t, t_0) = e^{\frac{i}{\hbar}(t-t_0)\mathcal{H}}U(t, t_0)$ , acting on the quantum states evolve according to the Schrodinger equation only with respect to the non-trivial interaction term  $\mathcal{V}_I(t) = e^{\frac{i}{\hbar}(t-t_0)\mathcal{H}}\mathcal{V}(t)e^{-\frac{i}{\hbar}(t-t_0)\mathcal{H}}$  as follows:

$$\partial_t |\varphi(t)\rangle_I = \partial_t U_I(t, t_0) |\varphi(t_0)\rangle = -\frac{i}{\hbar} \mathcal{V}_I(t) U_I(t, t_0) |\varphi(t_0)\rangle. \quad (2.3)$$

Equation (2.3) is analogous to Eq. (2.1) with which we can express  $U_I(t, t_0)$  as a function of the interaction part  $\mathcal{V}_I(t)$  as:  $U_I(t, t_0) = \mathcal{T} \left[ e^{-\frac{i}{\hbar} \int_{t_0}^t dt' \mathcal{V}_I(t')} \right]$ . This expression is useful to establish a bridge between operators in the Heisenberg and interaction pictures to construct perturbative expansions

$$O_I(t) = e^{\frac{i}{\hbar}(t-t_0)\mathcal{H}}O(t_0)e^{-\frac{i}{\hbar}(t-t_0)\mathcal{H}} = U_I(t, t_0)O_H(t)U_I^\dagger(t, t_0). \quad (2.4)$$

Equation (2.4) spawns a perturbative expansion for  $O_H(t)$ :

$$\begin{aligned} O_H(t) &= \tilde{\mathcal{T}} \left[ e^{\frac{i}{\hbar} \int_{t_0}^t dt' \mathcal{V}_I(t')} \right] O_I(t) \mathcal{T} \left[ e^{-\frac{i}{\hbar} \int_{t_0}^t dt' \mathcal{V}_I(t')} \right], \\ O_H(t) &= \tilde{\mathcal{T}} \left[ 1 + \frac{i}{\hbar} \int_{t_0}^t dt' \mathcal{V}_I(t') + \frac{1}{2} \left( \frac{i}{\hbar} \right)^2 \int_{t_0}^t dt' \mathcal{V}_I(t') \int_{t_0}^t dt'' \mathcal{V}_I(t'') + \dots \right] \times O_H^{(0)}(t), \\ &\quad \times \mathcal{T} \left[ 1 - \frac{i}{\hbar} \int_{t_0}^t dt' \mathcal{V}_I(t') + \frac{1}{2} \left( -\frac{i}{\hbar} \right)^2 \int_{t_0}^t dt' \mathcal{V}_I(t') \int_{t_0}^t dt'' \mathcal{V}_I(t'') + \dots \right], \\ O_H(t) &= O_H^{(0)}(t) - \frac{i}{\hbar} \int_{t_0}^t dt' [O_H^{(0)}(t), \mathcal{V}_I(t')] \\ &\quad + \left( -\frac{i}{\hbar} \right)^2 \int_{t_0}^t dt' \int_{t_0}^t dt'' [[O_H^{(0)}(t), \mathcal{V}_I(t')], \mathcal{V}_I(t'')] + \dots \end{aligned} \quad (2.5)$$

Taking the expectation value of Eq. (2.5) over an equilibrium state characterized by the equilibrium density matrix  $\rho_0(t)$  retrieves the Kubo formula as the first-order perturbation term in the following series [48].

$$\begin{aligned} \langle O_H(t) \rangle_0 &= \langle O_H^{(0)}(t) \rangle_0 - \frac{i}{\hbar} \int_{t_0}^t dt' \langle [O_H^{(0)}(t), \mathcal{V}_I(t')] \rangle_0 \\ &\quad - \frac{1}{\hbar^2} \int_{t_0}^t dt' \int_{t_0}^t dt'' \langle [[O_H^{(0)}(t), \mathcal{V}_I(t')], \mathcal{V}_I(t'')] \rangle_0 + \dots \end{aligned} \quad (2.6)$$

<sup>1</sup>The *interaction picture* is alternatively referred to as the *Dirac picture*.

<sup>2</sup> $O_H^{(0)}(t)$  is the time evolution of  $O(t_0)$  with a time-independent Hamiltonian in the Heisenberg picture.

## 2.2 Landau Levels and Linear Dispersion Model

We mathematically model the **LL** restricted by a confining potential  $\mathcal{V}_{confiner}(y)$  [31, 49], as discussed in Sec. 1.2. We fix a Landau gauge with vector potential  $\mathbf{A} = yB\vec{x}$ , such that  $\nabla \times \mathbf{A} = -B\vec{z}$ , describes a magnetic field acting perpendicular to the x-y plane. With momentum  $p_\mu = -i\hbar\partial_\mu$ , the Hamiltonian is given by

$$H = \frac{1}{2m} \left( p_x + \frac{e}{c}By \right)^2 + \frac{1}{2m}p_y^2 + \mathcal{V}_{confiner}(y). \quad (2.7)$$

Because the system exhibits translational invariance in the  $y$ -direction, the energy eigenstates of  $p_y$  can be expressed as plane waves, and the composite eigenstate of the system can be written using separation of variables as  $\varphi(x, y) = e^{ikx}\Phi(y)$ . Considering the slow spatial variation of the confining potential  $\partial_y\mathcal{V}_{confiner}(y) \ll \hbar\omega_c/l_B$ , where  $l_B$  is the magnetic length<sup>3</sup> defined as  $\sqrt{\hbar/eB}$ , we can approximate  $\mathcal{V}_{confiner}(y)$  by a constant potential. It transforms the Hamiltonian into

$$-\frac{\hbar^2}{2m}\partial_y^2 + \frac{1}{2}m\omega_c^2(y - kl_B^2)^2 + \mathcal{V}_{confiner}(y_0). \quad (2.8)$$

Equation (2.8) resembles the Hamiltonian for a harmonic oscillator in the  $y$ -direction with a center displaced from the origin by  $y_0$ . The wavefunctions satisfying the time-dependent Schrödinger equation are given by

$$\varphi(x, y) = e^{ikx - \omega_k t} \Phi(y - kl_B^2), \quad (2.9)$$

with corresponding eigenenergies

$$\hbar\omega_k = \left( n + \frac{1}{2} \right) \hbar\omega_c + \mathcal{V}_{confiner}(kl_B^2). \quad (2.10)$$

The above equations imply that the wavefunctions are localized at  $y_0 = kl_B^2$ , and the spatial localization of **LLs** depend on  $k$  ( $y \propto k$ ). As described in Sec. 1.2, the low energy excitations of the **LL** lie on the chiral edges with  $\hbar\omega_k \approx E_F$ . We only consider these low energy excitations close to the two Fermi points at  $k = \pm k_F$ , where  $E_F$  intersects the **LLs**, and ignore the rest of the energy spectrum to model the chiral edge states. Hence, it is acceptable to linearize the spectrum around the Fermi points, as shown in Fig. 2.1. This process is analogous to the standard linearization procedure of non-interacting 1D electron systems with two Fermi points, as detailed in Ref. [50]. We then establish the linear dispersion relations with the right/left moving branches as  $\epsilon_{R/L}(k) = \pm\hbar v(k \mp k_F)$ , with  $v = \partial\omega_k/\partial k|_{k=k_F}$ . To formulate the Hamiltonian in the framework of second quantization, consider a right-moving chiral edge mode corresponding to a **LL** with zero momentum at the Fermi point  $k_F = 0$ . By setting  $\hbar = 1$ , we obtain  $\epsilon_R(k) = vk$ , such that

$$\mathcal{H}_{edge,R} = v \sum_k k c_{k,R}^\dagger c_{k,R}, \quad (2.11)$$

where  $c_{k,R}$  annihilates an electron with momentum  $k$  on the right-moving edge mode. However, an infinite number of fermions in the *Dirac sea* occupy the states  $k \in (-\infty, 0]$ ,

<sup>3</sup> $l_B$  the is characteristic length scale that determines the spatial extent of the Landau levels in  $B_\perp$

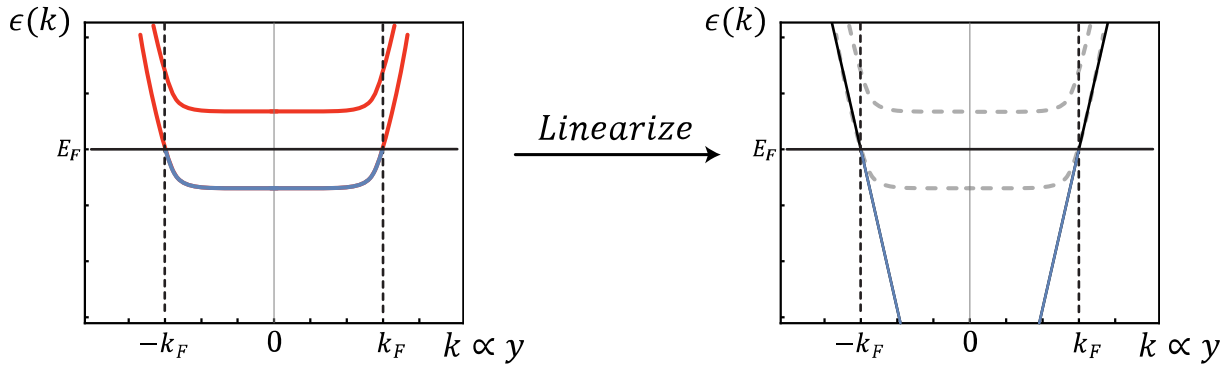


**Figure 2.1:** The Hamiltonian in Eq. (2.8) implies that the spatial localization of the LLs depend on  $k$ , as  $y \propto k$ . To model the physics of the edge modes, we only consider the low energy states close to the Fermi points where the Fermi level  $E_F$  intersects the LLs. Following the standard linearization procedure of a non-interacting 1D electron gas model [50], we linearize the low energy spectrum of the LLs into the linear dispersion model near the Fermi points at  $k = \pm k_F$ .

making the expectation value of the number operator  $\sum_k c_{k,R}^\dagger c_{k,R}$  divergent. Since this is an artifact of the linearization procedure, the physically relevant quantity is the excess number operator with respect to the ground state  $|0\rangle_0$ . It is obtained by introducing the normal ordering as  $:c_{k,R}^\dagger c_{k,R}:\equiv c_{k,R}^\dagger c_{k,R} - \langle c_{k,R}^\dagger c_{k,R} \rangle_0$ . Therefore, we only examine the finite excess number of fermions with respect to the ground state  $|0\rangle_0$ . Now, we introduce the fermionic field operators in real space that satisfy the usual anti-commutation relation:  $\{\psi_R(x), \psi_R^\dagger(y)\} = \delta(x - y)$ , and are defined as

$$\psi_R(x) = \frac{1}{\sqrt{L}} \sum_{k=-\infty}^{+\infty} e^{ikx} c_{k,R} \quad \psi_R^\dagger(x) = \frac{1}{\sqrt{L}} \sum_{k=-\infty}^{+\infty} e^{-ikx} c_{k,R}^\dagger, \quad (2.12)$$

where  $L$  is the size of the 1D system. Applying the above identities in Eq. (2.11) leads to the following Hamiltonian in the thermodynamic limit of  $L \rightarrow \infty$ :

$$\mathcal{H}_{edge,R} = \int_{-\infty}^{\infty} dx : \psi_R^\dagger(x) (-iv\partial_x) \psi_R(x) :. \quad (2.13)$$

Repeating the same construction for the left-moving edge, one obtains

$$\mathcal{H}_{edge,L} = \int_{-\infty}^{\infty} dx : \psi_L^\dagger(x) (iv\partial_x) \psi_L(x) : \quad (2.14)$$

and the total edge hamiltonian is therefore  $\mathcal{H}_{edge} = \mathcal{H}_{edge,R} + \mathcal{H}_{edge,L}$

## 2.3 1D Chiral Fermions and Bosonization

The *chirality* of the 1D edge modes can be demonstrated by evolving the fermionic field operators in time with  $\mathcal{H}_{edge,R}$  in the Heisenberg picture to obtain their equation of motion. Considering the fermionic creation operator  $\psi_R^\dagger$  on the right-moving edge in equilibrium

$$\partial_t \psi_R^\dagger(x, t) = i [\mathcal{H}_{edge,R}(y), \psi_R^\dagger(x, t)] = v \int_{-\infty}^{\infty} dy [\psi_R^\dagger(y) \partial_y \psi_R(y), \psi_R^\dagger(x, t)]. \quad (2.15)$$

Using the identity  $[A, BC] = \{A, B\}C - B\{A, C\}$  [51], with  $A = \psi_R^\dagger(x, t)$ ,  $B = \psi_R^\dagger(y)$ ,  $C = \partial_y \psi_R(y)$ , and applying the anti-commutation relation  $\{\psi_R^\dagger(x), \psi_R^\dagger(y)\} = 0$ , we obtain

$$\partial_t \psi_R^\dagger(x, t) = v \int_{-\infty}^{\infty} dy \psi_R^\dagger(y) \left\{ \psi_R^\dagger(x, t), \partial_y \psi_R(y) \right\}. \quad (2.16)$$

Changing the order of operations  $\left\{ \psi^\dagger(x, t), \partial_y \psi(y) \right\} = \partial_y \left\{ \psi^\dagger(x, t), \psi(y) \right\}$ , and using the commutation relation  $\left\{ \psi^\dagger(x), \psi(y) \right\} = \delta(x - y)$

$$\partial_t \psi_R^\dagger(x, t) = v \int_{-\infty}^{\infty} dy \psi_R^\dagger(y) \partial_y \delta(x - y) = -v \partial_x \psi_R^\dagger(x). \quad (2.17)$$

To obtain the above expression we used the identity:  $\int dz f(z) \partial_z \delta(z) = -\partial_z f(z) \Big|_{z=0}$ . Performing similar calculations for  $\psi_R$ , the equation of motions are:

$$\partial_t \psi_R^\dagger(x, t) + v \partial_x \psi_R^\dagger(x) = 0 \quad \partial_t \psi_R(x, t) + v \partial_x \psi_R(x) = 0. \quad (2.18)$$

The above expressions represent right-moving chiral waves propagating at speed  $v$ . In the absence of boundary conditions, their solutions take the form  $\psi^\dagger(x - vt)$  and  $\psi(x - vt)$ , respectively. Performing the above calculations for the left-moving edge will produce the following equations of motion:

$$\partial_t \psi_L^\dagger(x, t) - v \partial_x \psi_L^\dagger(x) = 0 \quad \partial_t \psi_L(x, t) - v \partial_x \psi_L(x) = 0, \quad (2.19)$$

with solutions of the form  $\psi_L^\dagger(x + vt)$  and  $\psi_L(x + vt)$ , propagating in the opposite direction. The linear 1D fermionic system allows an exact description in terms of bosonic density fluctuations that are unique to the one-dimensional setting. To develop this description, we introduce the density fluctuation operator [50] that creates particle-hole excitations in the infinite Dirac sea. We concentrate on the right-moving particles and drop the subscript  $R$  in the subsequent calculations for brevity. A similar approach can be followed to develop an equivalent description for left-movers.

$$\rho^{(p)}(l) = \sum_k : c_{k+l}^\dagger c_k : \quad (\text{for } l \neq 0 \text{ only}). \quad (2.20)$$

Note that  $\rho^{(p)}$  does not alter the particle count of the system (i.e.,  $|N\rangle_0$  to  $|N + n\rangle_0$ , where  $n \in \mathbb{Z}$ )<sup>4</sup> and  $\partial_t \rho_{R/L}$  have corresponding right and left chiral evolutions in time. Using the identities in Eq. (2.12),  $\rho^{(p)}(x) = : \psi^\dagger(x) \psi(x) :$  can be re-written as

$$\begin{aligned} \rho^{(p)}(x) &= \frac{1}{L} \sum_k : c_k^\dagger c_k : + \frac{1}{L} \sum_{l \neq 0} e^{-ilx} \sum_k : c_{k+l}^\dagger c_k :, \\ &= \frac{N}{L} + \frac{1}{L} \sum_{l > 0} \left( e^{-ilx} \rho^{(p)}(l) + e^{ilx} \rho^{(p)}(-l) \right), \end{aligned} \quad (2.21)$$

where  $N$  is the number operator defined as  $N = \sum_k : c_k^\dagger c_k : = \sum_k \left( c_k^\dagger c_k - \langle c_k^\dagger c_k \rangle_0 \right)$ . Using the identities from the derivation of Eq. (2.16) and by omitting the superscript  $(p)$  for brevity, the commutation relations of the particle density operators are expressed as

$$[\rho(m), \rho(l)] = \sum_{kk'} \left[ c_{k+m}^\dagger c_k, c_{k'+l}^\dagger c_{k'} \right] = \sum_k \left( c_{k+m+l}^\dagger c_k - c_{k+l}^\dagger c_{k-m} \right). \quad (2.22)$$

<sup>4</sup>Connecting Hilbert spaces with different particle numbers is taken care by the Klein factors that alter  $|N\rangle_0$  by one as  $F^\dagger |N\rangle_0 = |N + 1\rangle_0$  and  $F |N\rangle_0 = |N - 1\rangle_0$ .

It generates the following two cases:

$$\begin{aligned} [\rho(m), \rho(l)] &= 0 && \text{for } m \neq -l, \\ &= \sum_k \left( \langle c_k^\dagger c_k \rangle_0 - \langle c_{k-m}^\dagger c_{k-m} \rangle_0 \right) = -\frac{Lm}{2\pi} && \text{for } m = -l, \end{aligned}$$

that can be formulated in a compact way as

$$[\rho(m), \rho(l)] = -\frac{Lm}{2\pi} \delta(m+l). \quad (2.23)$$

Equation (2.23) is analogous to a bosonic commutation relation that allows us to define bona fide bosonic creation and annihilation operators for  $l > 0$

$$b_l = \sqrt{\frac{2\pi}{Ll}} \rho(-l) = \sqrt{\frac{2\pi}{Ll}} \sum_k : c_{k-l}^\dagger c_k : \quad b_l^\dagger = \sqrt{\frac{2\pi}{Ll}} \rho(l) = \sqrt{\frac{2\pi}{Ll}} \sum_k : c_{k+l}^\dagger c_k : \quad (2.24)$$

Akin to fermions, we define bosonic field operators in real space

$$\varphi(x) = \frac{i}{\sqrt{L}} \sum_{l>0} \frac{e^{ilx}}{\sqrt{l}} b_l e^{-\alpha l/2} \quad \varphi^\dagger(x) = -\frac{i}{\sqrt{L}} \sum_{l>0} \frac{e^{-ilx}}{\sqrt{l}} b_l^\dagger e^{-\alpha l/2}, \quad (2.25)$$

where the factor  $e^{-\alpha l/2}$ , in which  $\alpha$  is a UV or short distance cut-off, is introduced by hand to regulate divergences. It is convenient to define a new field  $\phi$ , also called a *compact* boson. This bosonic field is constrained within a spatial dimension, with its values wrapping around periodically as they traverse through this dimension

$$\phi(x) = \varphi(x) + \varphi^\dagger(x) = \frac{i}{\sqrt{L}} \sum_{l>0} \frac{1}{\sqrt{l}} e^{-\alpha l/2} (b_l e^{ilx} - b_l^\dagger e^{-ilx}). \quad (2.26)$$

Combining the results from Eqs. (2.21), (2.24), and (2.26), we can express the density fluctuation operator (particle density) as

$$\rho^{(p)}(x) =: \psi^\dagger(x) \psi(x) := \frac{N}{L} - \frac{1}{\sqrt{2\pi}} \partial_x \phi(x). \quad (2.27)$$

In the thermodynamic limit  $L \rightarrow \infty$ , we omit the first term in the above equation. We can further define the total charge density by introducing the charge  $q$  in Eq. (2.27) as

$$\rho(x) = -q \frac{1}{\sqrt{2\pi}} \partial_x \phi(x). \quad (2.28)$$

From the commutation of  $\psi(x)$  with  $b_l$ , it can be shown that  $\psi(x) |N\rangle_0$  is an eigenstate of the bona fide bosonic annihilation operator with an eigenvalue  $\alpha_l(x)$ ,  $l > 0$ . We can describe  $\psi(x) \propto e^{\sum_{l>0} \alpha_l(x) b_l^\dagger} |N-1\rangle_0$ , because coherent states are known to be the eigenstates of the bosonic annihilation operator [52]. Generalizing it to any state  $|N\rangle$ , we obtain the Mattis-Mandelstam formula [53, 54]

$$\psi(x) |N\rangle = \frac{F}{\sqrt{L}} e^{i \frac{2\pi N x}{L}} e^{\sum_{l>0} \alpha_l(x) b_l^\dagger} e^{-\sum_{l>0} \alpha_{*l}(x) b_l} |N\rangle. \quad (2.29)$$

Finally, using the identity  $e^A e^B = e^{A+B} e^{C/2}$ , if  $C = [A, B]$  and  $[A, C] = [B, C] = 0$  [51], and Eqs. (2.26), (2.29) we can write

$$\psi(x) = \frac{F}{\sqrt{L}} e^{i\frac{2\pi Nx}{L}} e^{-i\sqrt{2\pi}\varphi^\dagger(x)} e^{-i\sqrt{2\pi}\varphi(x)}, \quad \psi^\dagger(x) = \frac{F^\dagger}{\sqrt{L}} e^{-i\frac{2\pi Nx}{L}} e^{i\sqrt{2\pi}\varphi^\dagger(x)} e^{i\sqrt{2\pi}\varphi(x)}, \quad (2.30)$$

$$\psi(x) = \frac{F}{\sqrt{2\pi\alpha}} e^{i\frac{2\pi Nx}{L}} e^{-i\sqrt{2\pi}\phi(x)}, \quad \psi^\dagger(x) = \frac{F^\dagger}{\sqrt{2\pi\alpha}} e^{-i\frac{2\pi Nx}{L}} e^{i\sqrt{2\pi}\phi(x)}, \quad (2.31)$$

where the operators in Eq. (2.30) are normal ordered (cf. Sec. 2.2), while the operators in Eq. (2.31) are not.

## 2.4 Bosonic Hamiltonian and Quasiparticle Operator

The operators presented in Eq. (2.31), which are exponentiated bosons, are known as *vertex operators* [55]. They describe electrons propagating in a chiral edge mode and are instrumental in rewriting the Hamiltonian defined in Eq. (2.13) in terms of bosonic fields.

$$\mathcal{H}_{edge,R} = \frac{v\pi}{L} N_R(N_R + 1) + \frac{v}{2} \int_{-\frac{L}{2}}^{\frac{L}{2}} dx : [\partial_x \phi_R(x)]^2 : . \quad (2.32)$$

The zero-mode contribution (first term in the above Hamiltonian) will be dropped in the thermodynamic limit of  $L \rightarrow \infty$ . This bosonic Hamiltonian is complemented by the Kac-Moody commutation relation [50] that governs the bosonic fields as

$$[\phi_R(x, t), \phi_R(y, t)] = \frac{i}{2} \text{sgn}(x - y), \quad (2.33)$$

where  $\text{sgn}(x - y)$  is the signum function. Equations (2.31), (2.32), and (2.33) are useful to develop a description for a wide range of interacting 1D systems, including the FQH edge modes [56]. The pre-factor operators (Klein factors and exponentiated number operators) in Eq. (2.31) can be ignored because they are not important for the calculations in this thesis. To determine the charge associated with the fermionic operators, we compute its commutation with  $\rho(x)$  using the identity  $[e^A, B] = [A, B]e^A$  and Eq. (2.33) [57, 58].

$$\begin{aligned} [\rho_R(x), \psi_R^\dagger(y)] &= \frac{q}{2\pi\sqrt{\alpha}} \partial_x [e^{i\sqrt{2\pi}\phi_R(y)}, \phi_R(x)] = iq \partial_x [\phi_R(y), \phi_R(x)] \psi_R^\dagger(y), \\ &= \frac{q}{2} \partial_x \text{sgn}(x - y) \psi_R^\dagger(y) = q \delta(x - y) \psi_R^\dagger(y). \end{aligned} \quad (2.34)$$

Equation (2.34) implies that  $\psi_R^\dagger(x)$  and  $\psi_R(x)$  describe the creation and annihilation of fermions with a charge  $q$ . The statistical exchange phase accumulated by these fermionic excitations is determined by exchanging the vertex operators defined in Eq. (2.31) at different spatial coordinates  $x, y$ . To proceed, we use the Baker-Campbell-Hausdorff identity  $e^A e^B = e^B e^A e^{[A, B]}$  and Eq. (2.33).

$$\psi_R(x) \psi_R(y) = \psi_R(y) \psi_R(x) e^{-2\pi[\phi_R(x), \phi_R(y)]} \implies \psi_R(x) \psi_R(y) = \psi_R(y) \psi_R(x) e^{-i\pi \text{sgn}(x-y)}. \quad (2.35)$$

Here, the acquired phase is given by  $\Phi = -\pi$  for  $x > y$  and  $\Phi = \pi$  for  $x < y$ . Hence, the fermionic excitations described by the vertex operators accumulate a statistical exchange phase of  $|\Phi| = \pi$ , effectively retrieving the fermionic anticommutation relation. We now introduce the filling factor  $\nu$  into the charge density operator defined in Eq. (2.28) and the vertex operators from Eq. (2.31), in the following manner

$$\rho_R(x) = -q \frac{1}{\sqrt{2\pi}} \sqrt{\nu} \partial_x \phi_R(x), \quad (2.36)$$

$$\psi_{qp(R)}(x) = \frac{1}{\sqrt{2\pi\alpha}} e^{-i\sqrt{2\pi}\sqrt{\nu}\phi_R(x)} \quad \psi_{qp(R)}^\dagger(x) = \frac{1}{\sqrt{2\pi\alpha}} e^{i\sqrt{2\pi}\sqrt{\nu}\phi_R(x)}. \quad (2.37)$$

By following a similar approach as we used to examine the charge and statistical phase associated with fermionic vertex operators, we deduce

$$[\rho_R(x), \psi_{qp(R)}^\dagger(y)] = \frac{q\sqrt{\nu}}{2\pi\sqrt{\alpha}} \partial_x [e^{i\sqrt{2\pi}\sqrt{\nu}\phi_R(y)}, \phi_R(x)] = q\nu\delta(x-y)\psi_{qp(R)}^\dagger(y), \quad (2.38)$$

$$\psi_{qp(R)}(x)\psi_{qp(R)}(y) = \psi_{qp(R)}(y)\psi_{qp(R)}(x)e^{-2\pi[\phi_R(x), \phi_R(y)]} = \psi_{qp(R)}(y)\psi_{qp(R)}(x)e^{-i\pi\nu\text{sgn}(x-y)}. \quad (2.39)$$

Hence, the operators presented in Eq. (2.37) create and annihilate a fractional charge of  $q\nu$  and acquire a statistical exchange phase of  $|\Phi| = \pi\nu$ . Therefore, these quasiparticle creation and annihilation operators describe the anyonic excitations in the **FQH** edge modes. To simplify the derived results, we rescale the bosonic field  $\sqrt{2\pi\nu}\phi_R(x) \rightarrow \phi_R(x)$  to obtain (presented equations are extended to encompass both left and right edges)

$$\mathcal{H}_{edge(L/R)} = \frac{v}{4\pi\nu} \int_{-\infty}^{\infty} dx [(\partial_x \phi_{L/R})^2], \quad (2.40)$$

$$\psi_{qp(L/R)}(x) = \frac{1}{\sqrt{2\pi\alpha}} e^{-i\phi_{L/R}(x)}, \quad (2.41)$$

$$[\phi_{L/R}(x, t), \phi_{L/R}(y, t)] = \mp i\pi\nu\text{sgn}(x-y), \quad (2.42)$$

$$\rho_{L/R}(x) = \pm q \frac{\partial_x \phi_{L/R}(x)}{2\pi}. \quad (2.43)$$

Until now, we utilized a single boson field description of an **FQH** edge state hosting one kind of quasiparticle. However, a broader description of the edge states exists, employing multiple boson fields and offering a precise definition of the statistical exchange phase or braiding angle  $\vartheta$ . Following the Haldane-Halperin hierarchal description of quantum Hall states [34], Wen derived an effective theory for generic Abelian **FQH** edge modes hosting distinct kinds of quasiparticles [59]. The theory describes the edge states with  $n$ -boson fields  $\phi(x, t) = (\phi_1, \phi_2, \dots, \phi_n)^T$  and a charge vector  $\mathbf{q} = (q_1, q_2, \dots, q_n)^T$  that determines the units of charge carried by quasiparticles of each kind  $\mathbf{l} = (l_1, l_2, \dots, l_n)^T$ . The  $K$ -matrix consisting of integer elements is given by

$$K = \begin{pmatrix} p_1 & 0 & 0 & \dots \\ 0 & p_2 & 0 & \dots \\ 0 & 0 & \ddots & \dots \\ \vdots & \vdots & \vdots & p_n \end{pmatrix}, \quad (2.44)$$

where  $p_j, j = 1, \dots, n$  are odd integers. It defines each edge mode's filling factor  $\nu_j = 1/p_j$  and governs the commutation relation between the bosonic fields.

$$\boldsymbol{\nu} = \mathbf{q}^T K^{-1} \mathbf{q}, \quad (2.45)$$

$$\mathbf{e}_1^* = \mathbf{q}^T K^{-1} \mathbf{1}, \quad (2.46)$$

$$\left[ \phi_{i(L/R)}(x, t), \partial_y \phi_{j(L/R)}(y, t) \right] = \mp 2i\pi (K^{-1})_{ij} \delta(x - y). \quad (2.47)$$

This is the so-called symmetric basis in which all charge vector elements  $q_j = 1$ . The commutation relation in Eq. (2.47) together with the Hamiltonian

$$\mathcal{H}_{edge(L/R)} = \frac{1}{4\pi} \sum_{i,j=1}^n \int_{-\infty}^{\infty} dx \partial_x \phi_{i(L/R)} v_{ij} \partial_x \phi_{j(L/R)}, \quad (2.48)$$

where  $v_{ij}$  are elements of a positive definite matrix  $V$ , generalizes the single bosonic edge mode Hamiltonian in Eq. (2.40) to multiple edge modes. The diagonal elements  $v_{ij}|_{i=j}$  of the matrix  $V$  assign a velocity to each edge mode, whereas the off-diagonal elements  $v_{ij}|_{i \neq j}$  describe the short-range interactions between these edge modes. The statistical exchange phase accumulated by the interaction of such quasiparticles is given by

$$\vartheta = \pi \mathbf{1}^T K^{-1} \mathbf{1}. \quad (2.49)$$

We adopt the above conventions for all the subsequent calculations in the thesis.

## 2.5 Temporal Voltage Drive

We now analyze the influence of a generic time-dependent voltage pulse  $V(t)$  on the time evolution of the edge modes. Our methodology closely follows the approach presented in Ref. [60]. Here, we consider that a voltage pulse is applied to the right-moving chiral edge mode at  $x = x_R$ . The voltage source is described by the function  $U_R(x, t) = \Theta(-x + x_R)V(t)$ . The Heaviside function ensures that the voltage source is only defined within the contact, i.e., the region  $x \in (-\infty, x_R)$ . The voltage pulse couples to the edge mode via the Hamiltonian

$$\mathcal{H}_g = \int dx U_R(x, t) \rho_R(x). \quad (2.50)$$

At  $t = -\infty$ , the system is in equilibrium, and the edge modes' time evolution is only attributed to the Hamiltonian  $\mathcal{H}_{edge,R}$ . When the applied voltage drive couples to the system at  $t = -\infty + \epsilon$ , the system is driven out of equilibrium, and the time evolution is also carried by  $\mathcal{H}_g$ . We use the Heisenberg picture introduced in Sec. 2.1 to derive the equation of motion of the bosonic field operator with respect to the non-equilibrium Hamiltonian  $H = \mathcal{H}_{edge,R} + \mathcal{H}_g$ .

$$\begin{aligned} \partial_t \phi_R(x, t) &= i [\mathcal{H}_{edge,R}(y), \phi_R(x, t)] + i [\mathcal{H}_g(y), \phi_R(x, t)], \\ &= i \frac{v}{4\pi\nu} \int_{-\infty}^{\infty} dy \left[ (\partial_y \phi_R(y))^2, \phi_R(x, t) \right] - i \frac{q}{2\pi} \int_{-\infty}^{\infty} dy U_R(y, t) [\partial_y \phi_R(y), \phi_R(x, t)]. \end{aligned} \quad (2.51)$$

By using the identity  $[AB, C] = A[B, C] + [A, C]B$  [51], Kac Moody commutation relations, and following a similar procedure as outlined in Sec. 2.3, we simplify the integrals in Eq. (2.51) to obtain

$$\begin{aligned}\partial_t \phi_R(x, t) &= -v \int_{-\infty}^{\infty} dy \partial_y \phi_R(y) \delta(x - y) + q\nu \int_{-\infty}^{\infty} dy U_R(y, t) \delta(x - y), \\ \partial_t \phi_R(x, t) &= -v \partial_x \phi_R(x) + q\nu U_R(x, t).\end{aligned}\tag{2.52}$$

The above equation can be solved with Green's function approach. To this end, we define a differential operator  $\mathcal{L} = (\partial_t + v\partial_x)$ , and define a general solution of the form  $\phi(x, t) = \phi_0(x - vt, 0) + A(x, t)$ , where  $\phi_0(x - vt, 0)$  is the solution of Eq. (2.52) when  $U_R(x, t) = 0$ . This substitution gives us an equation relating the ansatz function  $A(x, t)$  with the voltage drive as

$$(\partial_t + v\partial_x) A(x, t) = q\nu U_R(x, t) \implies \mathcal{L}A(x, t) = q\nu U_R(x, t).\tag{2.53}$$

We now introduce Green's function, which is the impulse response of the differential operator  $\mathcal{L}$

$$\mathcal{L}G(x, x'; t, t') = \delta(x - x')\delta(t - t').\tag{2.54}$$

By its definition [61],  $G(x, x'; t, t')$  encodes all the output responses of a linear time-invariant system for all input frequencies. Therefore, convoluting our generic input  $U_R(x, t)$  with  $G(x, x'; t, t')$  will fetch us the output response  $A(x, t)$

$$A(x, t) = q\nu \int \int dx' dt' G(x, x'; t, t') U_R(x', t').\tag{2.55}$$

Equation (2.53) can be recovered by applying the differential operator  $\mathcal{L}$  on Eq. (2.55), and using the property (2.54). We now substitute the Green's function of the operator  $\mathcal{L}$  in Eq. (2.55) to obtain

$$G(x, x'; t, t') = \Theta(t - t') \delta(v(t - t') - (x - x')), \tag{2.56}$$

$$A(x, t) = q\nu \int_{-\infty}^t dt' U_R(x - v(t - t'), t'), \tag{2.57}$$

$$\phi_R(x, t) = \phi_{R0}(x - vt, 0) + q\nu \int_{-\infty}^t dt' U_R(x - v(t - t'), t'). \tag{2.58}$$

Using the bosonization identity from Eq. (2.41), the time evolution of the quasiparticle field operator can be derived by a simple substitution

$$\psi_{qp(R)}(x) = \frac{1}{\sqrt{2\pi\alpha}} e^{-i\phi_{R0}(x-vt,0)} e^{-iq\nu \int_{-\infty}^t dt' U_R(x-v(t-t'),t')}. \tag{2.59}$$

Notably, the field operators evolve chirally despite an arbitrary voltage pulse driving the system out of equilibrium. The chiral evolution of the applied time-dependent voltage drive is a direct consequence of the chirality of the edge modes. It is an intrinsic property of quantum Hall edge states and can be validated in both the fermionic and bosonic descriptions.

# 3

## Particle collider in the FQH regime

In the previous chapters, we introduced the essential ingredients required to describe time-resolved two-particle interferometry for anyons. To reiterate, the Hamiltonian  $\mathcal{H}_{edge(L/R)}$  described in Eq. (2.40) models the quantum Hall edge modes that act as transmission lines for the left or right-moving quasiparticles. Equation (2.50) describes the Hamiltonian that couples time-dependent input voltage sources to these edge modes propagating in either direction. In this chapter, we model the effects of a QPC (taking the role of a beam splitter) introduced in an FQH setup in the Laughlin sequence, i.e., states with filling factors  $\nu = 1/(2n + 1)$ , where  $n \in \mathbb{Z}^+$ . In the weak backscattering regime<sup>1</sup>, the QPC topologically deforms the edge modes without entirely depleting the quantum Hall fluid and forms a narrow constriction, as shown in Fig. 3.1. The QPC allows tunneling between the counter-propagating edge modes at the position  $x = x_{QPC}$ . Here, the quasiparticles stochastically tunnel between the opposite edge modes with a small, and for simplicity assumed energy independent, amplitude  $|\Lambda| \ll 1$ . A tunneling Hamiltonian that effectively describes the most relevant tunneling process in this configuration reads

$$H_\Lambda = \Lambda \psi_{qp(L)}^\dagger(x_{QPC}, t) \psi_{qp(R)}(x_{QPC}, t) + h.c., \quad (3.1)$$

where  $h.c.$  is the hermitian conjugate  $[\Lambda^* \psi_{qp(R)}^\dagger(x_{QPC}) \psi_{qp(L)}(x_{QPC})]$  and  $\psi_{qp}(x, t)$ ,  $\psi_{qp}^\dagger(x, t)$  are the quasiparticle creation and annihilation operators introduced in Sec. 2.4. As follows, we will drop the subscript notation of  $qp$  from the operators for all the subsequent calculations for brevity. The space-time coordinate  $(x, t)$  denotes arbitrary points in the setup at the space coordinate  $x$  and time coordinate  $t$ . Note that the chiral evolution of the edge modes induces the following relation between these coordinates:

$$\psi_R(x, t) \rightarrow \psi_R(x - vt, 0) \quad \psi_L(x, t) \rightarrow \psi_L(x + vt, 0). \quad (3.2)$$

We now analyze the collider setup in the FQH regime operated in different configurations by computing the tunneling current and backscattered noise. A similar analysis was performed in the Refs. [62, 63] applying Schwinger-Keldysh contour formalism.

### 3.1 Tunneling current in a weak backscattering QPC

A time-dependent voltage source  $V_R(t)$  is coupled to the right-moving edge mode via *Source 2* terminal at the spatial coordinate  $x = x_R$ , in the setup shown in Fig. 3.1. The voltage source  $V_L(t)$  connected to the left-moving edge mode at  $x = x_L$  is switched off, and its terminal *Source 1* is grounded. The considered setup is geometrically symmetric

---

<sup>1</sup>In the strong backscattering regime, the QPC fully depletes the underlying quantum Hall fluid, permitting only stochastic electron tunneling through the depleted region.

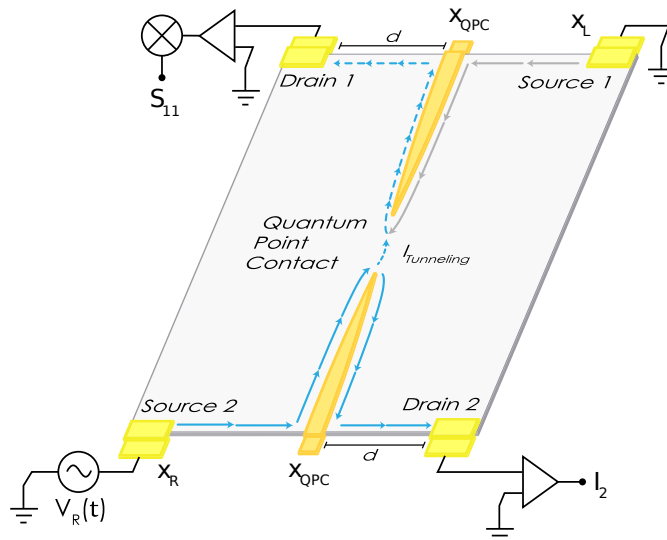


**Figure 3.1:** The four terminal setup driven by a single input source is dubbed to be operating in the Hanbury Brown-Twiss (HBT) configuration [64, 65]. The voltage source  $V_R(t)$  is defined in the region  $x < x_R$ , coupled to the right-moving edge via the Source 2 terminal. The QPC is at the position  $x_{QPC}$ , and the Source 1 terminal at  $x_L$  is grounded. The Drain 2 terminal collects the unperturbed current  $I_R$  (depicted by  $I_2$  in the schematic), and the Drain 1 terminal collects the tunneling current. All the terminals are equidistant from the QPC by a distance  $d$ .

such that the Source and Drain terminals are equidistant from the position of QPC. We assign the parameter  $d$  to measure the distance between the components of the setup as follows:  $x_L - x_R = 2d$ ;  $x_L - x_{QPC} = d$ ;  $x_{QPC} - x_R = d$ . The terminal *Drain 2* is used to collect the transmitted (or unperturbed) current  $I^{(0)}$  driven by  $V_R(t)$  in the right-moving lower edge mode of the setup. The tunneling current at the QPC, which is also utilized to compute the backscattered noise (refer to Sec. 3.2 for more details), is measured by the *Drain 1* terminal coupled to the left-moving upper edge mode. As our first step, we compute the current operator  $I$  from the continuity equation relating the charge density  $\rho$  to the current density  $J$ . Due to the inherent one-dimensionality of the current carrying edge modes, we have

$$\partial_x J(x, t) + \partial_t \rho(x, t) = 0, \text{ and } I(x, t) = J(x, t). \quad (3.3)$$

For a right-moving chiral edge mode  $\partial_t \rho_R(x, t) = -v \partial_x \rho_R(x, t)$ , cf. Sec. 2.3. Therefore,

$$\partial_x I_R(x, t) = v \partial_x \rho_R(x, t) \rightarrow I_R(x, t) = v \rho_R(x, t) = -qv \frac{\partial_x \phi_R(x, t)}{2\pi}. \quad (3.4)$$

The QPC is tuned to operate in the weak backscattering regime with a weak tunneling amplitude ( $|\Lambda| \ll 1$ ). This diminutive amplitude allows us to treat the tunneling at  $x = x_{QPC}$  as a perturbation to the system being driven out of equilibrium by  $V_R(t)$ . Therefore, we can utilize the perturbative expansion introduced in Sec. 2.1 [cf. Eq. (2.5)] to compute the tunneling current  $I_T(t)$ . While the time-dependent current operator is constructed as a power series in perturbation theory [48], components of the expansion consisting of powers of  $\Lambda$  greater than three can be neglected because of the small tunneling

amplitude  $|\Lambda| \ll 1$ . As mentioned earlier, the Hamiltonian  $\mathcal{H}_{edge(L/R)}$  defined in Eq. (2.40) (cf. Sec. 2.5) models the FQH edge modes propagating in either direction. Therefore, we use two copies of Eq. (2.40) defined in both the left-moving ( $L$ ) and right-moving ( $R$ ) subspaces (cf. Sec. 2.2) to model the transport phenomenon in the Laughlin FQH setup depicted in Fig. 3.1. We now consider the Hamiltonian of the form  $H = \mathcal{H} + \mathcal{V}(t)$ , where  $\mathcal{H}$  is the initial unperturbed non-equilibrium Hamiltonian described as

$$\mathcal{H} = \mathcal{H}_{edge} + \mathcal{H}_g = \frac{v}{4\pi\nu} \int_{-\infty}^{\infty} dx \left[ (\partial_x \phi_L)^2 + (\partial_x \phi_R)^2 \right] + \int_{-\infty}^{\infty} dx U_R(x, t) \rho_R(x). \quad (3.5)$$

The time dependence is now carried by the tunneling Hamiltonian introduced in Eq. (3.1), which gives us  $\mathcal{V}(t) = H_\Lambda(t)$ . Using Eq. (2.5), the time evolution of the current operator in a single QPC setup for a second-order perturbation at the space-time coordinates  $(y, t)$ , given that  $y > x_{QPC}$  can be written as

$$\begin{aligned} I_R(y, t) &= I^{(0)}(y, t) + i \int_{-\infty}^t dt' \left[ H_\Lambda^{(0)}(x_{QPC}, t'), I_R^{(0)}(y, t) \right] \\ &\quad + i^2 \int_{-\infty}^t dt' \int_{-\infty}^{t'} dt'' \left[ H_\Lambda^{(0)}(x_{QPC}, t''), \left[ H_\Lambda^{(0)}(x_{QPC}, t'), I_R^{(0)}(y, t) \right] \right] + \mathcal{O}(\Lambda^3). \end{aligned} \quad (3.6)$$

We proceed with a piece-wise calculation of  $I_R(y, t) = I^{(0)}(y, t) + I^{(1)}(y, t) + I^{(2)}(y, t)$ .

**Zeroth order:** It is the time evolution of the right-moving current operator  $I_R(y, t)$  with the initial unperturbed non-equilibrium Hamiltonian ( $\mathcal{H}$ ) which is already given by Eq. (3.4). We use the general formula of the right-moving chiral boson from Eq. (2.58)

$$\phi_R(y, t) = \phi_{R0}(y - vt, 0) + q\nu \int_{-\infty}^t dt' U_R(y - v(t - t'), t').$$

The voltage source is coupled to the system at  $x_R$ , such that  $U_R(y, t) = \Theta(-y + x_R) V_R(t)$ .

$$\begin{aligned} I^{(0)}(y, t) &= -qv \frac{\partial_y \phi_{R0}(y, t)}{2\pi} - q^2 \nu \int_{-\infty}^t dt' \partial_y \Theta(-y + x_R + (t - t')v) V_R(t'), \\ &= -qv \frac{\partial_y \phi_{R0}(y, t)}{2\pi} + q^2 \nu \int_{-\infty}^t dt' \delta\left(t - t' + \frac{-y + x_R}{v}\right) V_R(t'), \\ &= -qv \frac{\partial_y \phi_{R0}(y, t)}{2\pi} + q^2 \nu V_R\left(t + \frac{-y + x_R}{v}\right). \end{aligned} \quad (3.7)$$

**First order:** As  $H_\Lambda(x_{QPC}, t') = H_\Lambda^\dagger(x_{QPC}, t')$ , we apply the identity  $[A + A^\dagger, B] = [A, B] - ([A, B])^\dagger$ , if  $B = B^\dagger$  [51] and bosonize the tunneling Hamiltonian using the identities in Eq. (2.41) to simplify the calculations. We then have

$$\begin{aligned} I^{(1)}(y, t) &= i \int_{-\infty}^t dt' \left[ \Lambda \psi_L^\dagger(x_{QPC}, t') \psi_R(x_{QPC}, t') + h.c., \right. \\ &\quad \left. - qv \frac{\partial_y \phi_{R0}(y, t)}{2\pi} + q^2 \nu V_R\left(t + \frac{-y + x_R}{v}\right) \right] \\ &= i \int_{-\infty}^t dt' \left[ \Lambda \psi_L^\dagger(x_{QPC}, t') \psi_R(x_{QPC}, t'), -qv \frac{\partial_y \phi_{R0}(y, t)}{2\pi} \right] - h.c., \\ &= -\frac{iqv\Lambda}{(2\pi)^2 \alpha} \int_{-\infty}^t dt' e^{-iqv \int_{-\infty}^{t'+(x_R-x_{QPC})/v} d\tau} V_R(\tau) \left[ e^{i\phi_{L0}(x_{QPC}, t')} e^{-i\phi_{R0}(x_{QPC}, t')}, \partial_y \phi_{R0}(y, t) \right] - h.c.. \end{aligned}$$

Taking into account that the operators in the left-moving and right-moving edge modes commute, we apply the identities  $[e^A, B] = [A, B]e^A$  and  $[AB, C] = A[B, C] + [A, C]B$  and the Kac-Moody commutation relation [cf. Eq. (2.50)] to obtain

$$\begin{aligned}
 &\implies \left[ e^{i\phi_{L0}(x_{QPC}, t')} e^{-i\phi_{R0}(x_{QPC}, t')}, \partial_y \phi_{R0}(y, t) \right] = e^{i\phi_{L0}(x_{QPC}, t')} \left[ e^{-i\phi_{R0}(x_{QPC}, t')}, \partial_y \phi_{R0}(y, t) \right], \\
 &= e^{i\phi_{L0}(x_{QPC}, t')} \left[ -i\phi_{R0}(x_{QPC}, t'), \partial_y \phi_{R0}(y, t) \right] e^{-i\phi_{R0}(x_{QPC}, t')}, \\
 &= -ie^{i\phi_{L0}(x_{QPC}, t')} \left[ -2i\pi\nu\delta(x_{QPC} - y + v(t - t')) \right] e^{-i\phi_{R0}(x_{QPC}, t')}, \\
 &= -2\pi\nu\delta(x_{QPC} - y + v(t - t')) e^{i\phi_{L0}(x_{QPC}, t')} e^{-i\phi_{R0}(x_{QPC}, t')}.
 \end{aligned}$$

Using the above result and by reabsorbing the pre-factors,  $I^{(1)}(y, t)$  can be rewritten in terms of quasiparticle annihilation and creation operators as

$$I^{(1)}(y, t) = iq\nu \int_{-\infty}^t dt' \delta\left(t - t' + \frac{x_{QPC} - y}{v}\right) \left( \Lambda\psi_L^\dagger(x_{QPC}, t')\psi_R(x_{QPC}, t') - h.c. \right). \quad (3.8)$$

The region of interest is after the pulse injection point, i.e., at  $y > x_{QPC} > x_R$ . It implies  $x_{QPC} - y < 0$ , ensuring  $t' = t + (x_{QPC} - y)/v$  falls within the time interval  $(-\infty, t)$ . We enforce this condition using a Heaviside function and apply the identity  $\int dt f(t)\delta(t - t_0) = f(t_0)$  to obtain

$$I^{(1)}(y, t) = iq\nu\Theta(y - x_{QPC}) \left( \Lambda\psi_L^\dagger(2x_{QPC} - y + vt, 0)\psi_R(y - vt, 0) - h.c. \right). \quad (3.9)$$

**Second order:** To compute the contribution of the second-order perturbation term, we utilize the previously derived expression of the commutator  $\left[ H_\Lambda^{(0)}(x_{QPC}, t'), I_R^{(0)}(y, t) \right]$  in the calculation of  $I^{(1)}(y, t)$  as follows

$$\begin{aligned}
 I^{(2)}(y, t) &= i^2 \int_{-\infty}^t dt' \int_{-\infty}^{t'} dt'' \left[ H_\Lambda^{(0)}(x_{QPC}, t''), \right. \\
 &\quad \left. q\nu\delta\left(t - t' + \frac{x_{QPC} - y}{v}\right) \left( \Lambda\psi_L^\dagger(x_{QPC}, t')\psi_R(x_{QPC}, t') - h.c. \right) \right]. \quad (3.10)
 \end{aligned}$$

To reduce the number of operators appearing during the expansion of Eq. (3.10), we neglect the terms that zero out when we evaluate the expectation value of  $I^{(2)}(y, t)$ . Upon careful analysis, it is clear that components containing an equal number of quasiparticle creation and annihilation operators in the left-moving and right-moving subspaces will contribute to  $\langle I^{(2)}(y, t) \rangle$ . We only retain non-vanishing contributions and drop the notation of denoting  $x_{QPC}$  from the space-time coordinate  $(x_{QPC}, t)$  in subsequent calculations.

$$\begin{aligned}
 I^{(2)}(y, t) &= i^2 q\nu \int_{-\infty}^t dt' \int_{-\infty}^{t'} dt'' \delta\left(t - t' + \frac{x_{QPC} - y}{v}\right) \left[ H_\Lambda^{(0)}(t''), \Lambda\psi_L^\dagger(t')\psi_R(t') - h.c. \right], \\
 &= q\nu|\Lambda|^2\Theta(y - x_{QPC}) \int_{-\infty}^{\tilde{t}} dt'' \left[ \psi_L^\dagger(t'')\psi_R(t''), \psi_R^\dagger(\tilde{t})\psi_L(\tilde{t}) \right] - h.c., \quad (3.11)
 \end{aligned}$$

where  $\tilde{t} = t + (x_{QPC} - y)/v$  and  $\psi_{L/R}(t'') = \psi_{L/R}(x_{QPC} \pm vt'', 0)$ . We next compute the expectation value of the time-evolved current operator with respect to the density matrix  $\rho_0(t_0)$  over the ground state of the system (by omitting the subscript notation  $\langle \cdot \rangle_0$ )

for brevity). Consider the ground state in equilibrium at  $t_0 = -\infty$ , and that the input voltage source, tunneling at the QPC (treated as perturbation), transpired at later times.

$$\langle I_R(y, t) \rangle = \langle I^{(0)}(y, t) \rangle + \langle I^{(1)}(y, t) \rangle + \langle I^{(2)}(y, t) \rangle \text{ [cf. Eq. (2.6)],} \quad (3.12)$$

$$\langle I^{(0)}(y, t) \rangle = -qv \left\langle \frac{\partial_y \phi_{R0}(y, t)}{2\pi} \right\rangle + q^2 \nu \left\langle V_R \left( t + \frac{-y + x_R}{v} \right) \right\rangle,$$

$$\langle I^{(1)}(y, t) \rangle = q^2 \nu V_R \left( t + \frac{x_R - y}{v} \right). \quad (3.13)$$

By definition, the compact boson field  $\phi \propto b_q - b_q^\dagger$  [cf. Eq. (2.26)] creates and destroys particle-hole pairs. Therefore, the expectation value of the first term in the above equation reduces to zero without any counter-balancing operators acting on the equilibrium state. Furthermore, the vanishing expectation value of the quasiparticle creation and annihilation operators  $\langle \psi_{qp} \rangle = 0$ , result in a zero contribution from  $I^{(1)}(y, t)$

$$\langle I^{(1)}(y, t) \rangle = iq\nu\Lambda \left\langle \psi_L^\dagger(2x_{QPC} - y + vt, 0) \psi_R(y - vt, 0) - h.c. \right\rangle = 0. \quad (3.14)$$

To calculate the expectation value of the second order contribution, we expand the commutator in Eq. (3.11) and split the current as  $I^{(2)}(y, t) = \int dt'' (a - b) - h.c.$ , where  $a = \psi_L^\dagger(t'') \psi_R(t'') \psi_R^\dagger(\tilde{t}) \psi_L(\tilde{t})$  and  $b = \psi_R^\dagger(\tilde{t}) \psi_L(\tilde{t}) \psi_L^\dagger(t'') \psi_R(t'')$ . We compute each term separately by bosonizing the quasiparticle operators. The evaluation of  $\langle a \rangle$  is detailed in the subsequent calculations

$$\langle I^{(2)}(y, t) \rangle = q\nu |\Lambda|^2 \Theta(y - x) \int_{-\infty}^{\tilde{t}} dt'' \left\langle \psi_L^\dagger(t'') \psi_R(t'') \psi_R^\dagger(\tilde{t}) \psi_L(\tilde{t}) \right\rangle - \langle b \rangle - h.c.,$$

$$\langle a \rangle = \left\langle e^{i\phi_{L0}(t'')} e^{-i\phi_{L0}(\tilde{t})} \right\rangle \left\langle e^{-i\phi_{R0}(t'')} e^{i\phi_{R0}(\tilde{t})} \right\rangle e^{iq\nu \int_{-\infty}^{\tilde{t}} d\tau V_R(\tau) - iq\nu \int_{-\infty}^{\tilde{t}} d\tau V_R(\tau)},$$

where  $\tilde{t} = t + (x_R - y)/v$  and  $\bar{t} = t'' + (x_R - x_{QPC})/v$ . Applying the property of time translational invariance and the exponentiated bosonic correlation formula [55]

$$\left\langle \prod_{k=1}^n e^{O_k} \right\rangle = e^{\sum_{j < k} \langle O_j O_k \rangle} e^{\frac{1}{2} \sum_{k=1}^n \langle O_k^2 \rangle}, \quad (3.15)$$

$$\langle a \rangle = e^{\langle \phi_{L0}(t'' - \tilde{t}) \phi_{L0}(0) \rangle - \langle \phi_{L0}^2(0) \rangle} e^{\langle \phi_{R0}(t'' - \tilde{t}) \phi_{R0}(0) \rangle - \langle \phi_{R0}^2(0) \rangle} e^{iq\nu \int_{\tilde{t}}^{\tilde{t}} d\tau V_R(\tau)}.$$

Proceeding further, we utilize the expression of the equilibrium bosonic Green's function [31, 66, 67] evaluated in Appendix A. It is a mathematical construct used to describe the correlation between bosonic excitations at different space-time points in a quantum system at thermal equilibrium. We now rewrite the expectation value  $\langle a \rangle$  as

$$\langle a \rangle = e^{\mathcal{G}_L(t'' - \tilde{t})} e^{\mathcal{G}_R(t'' - \tilde{t})} e^{iq\nu \int_{\tilde{t}}^{\tilde{t}} d\tau V_R(\tau)} = G_-^2(x_{QPC}, y, t, t'') \left( e^{iq\nu \int_{\tilde{t}}^{\tilde{t}} d\tau V_R(\tau)} \right), \quad (3.16)$$

$$G_-^2(x_{QPC}, y, t, t'') = \left( \frac{\alpha}{\alpha - i(x_{QPC} - y + v(t - t''))} \frac{\pi k_B \theta \left( \frac{x_{QPC} - y}{v} + t - t'' \right)}{\sinh \left( \pi k_B \theta \left( \frac{x_{QPC} - y}{v} + t - t'' \right) \right)} \right)^{2\nu},$$

where  $k_B$  is the Boltzmann constant and  $\theta$  is the temperature. We drop the arguments of Green's function in the subsequent calculations for brevity. Following a similar procedure

to compute  $\langle b \rangle$  and *h.c.*, we write down the final expression of  $\langle I^{(2)}(y, t) \rangle$ , neglecting the intermediate calculation steps:

$$\begin{aligned} \langle I^{(2)}(y, t) \rangle &= q\nu|\Lambda|^2\Theta(y-x) \int_{-\infty}^{\tilde{t}} dt'' \left( G_-^2 - G_+^2 \right) \left[ e^{iq\nu \int_{\tilde{t}}^t d\tau V_R(\tau)} - e^{-iq\nu \int_{\tilde{t}}^t d\tau V_R(\tau)} \right], \\ &= 2iq\nu|\Lambda|^2\Theta(y-x) \int_{-\infty}^{\tilde{t}} dt'' \left( G_-^2 - G_+^2 \right) \sin \left( q\nu \int_{\tilde{t}}^t d\tau V_R(\tau) \right); G_+^2 = (G_-^2)^\dagger. \end{aligned} \quad (3.17)$$

Combining the results, the final time evolved current after turning on the perturbation is

$$\begin{aligned} \langle I_R(y, t) \rangle &= q^2\nu V_R \left( t + \frac{x_R - y}{v} \right) + \\ &2iq\nu|\Lambda|^2\Theta(y-x) \int_{-\infty}^{\tilde{t}} dt'' \left( G_-^2 - G_+^2 \right) \sin \left( q\nu \int_{\tilde{t}}^t d\tau V_R(\tau) \right). \end{aligned} \quad (3.18)$$

The first term ( $\langle I^{(0)}(y, t) \rangle$ ) in Eq. (3.18) is a direct portrayal of Ohm's law ( $V \propto I$ ) obeyed by the edge mode in the absence of any perturbation. The second-order average term ( $\langle I^{(2)}(y, t) \rangle$ ) depicts the expectation value of the tunneling current ( $\langle I_T(t) \rangle$ ) expanded to the leading order in  $\Lambda$ . Whereas  $I^{(1)}(y, t)$  is the tunneling current operator  $I_T(t)$ , denoting the backscattered current from the lower edge to the upper edge measured in *Drain 1*. By proper choice of spatial coordinates, we generalize the computed results as

$$I_T(t) = iq\nu \left( \Lambda \psi_L^\dagger(t) \psi_R(t) - \Lambda^\dagger \psi_R^\dagger(t) \psi_L(t) \right), \quad (3.19)$$

$$\langle I_T(t) \rangle = q\nu|\Lambda|^2 \int_{-\infty}^t dt' \left\langle \left[ \psi_L^\dagger(t) \psi_R(t), \psi_R^\dagger(t') \psi_L(t') \right] + \left[ \psi_L^\dagger(t') \psi_R(t'), \psi_R^\dagger(t) \psi_L(t) \right] \right\rangle. \quad (3.20)$$

## 3.2 Zero-frequency backscattered noise

The zero-frequency shot noise [19] can be computed by cross-correlating the time-evolved current fluctuations  $\Delta I(t)$  measured in the *Drain* terminals (cf. Sec. 1.1). The unsymmetrical form of the noise is defined as

$$S^{(ij)}(\omega = 0) = \lim_{T \rightarrow \infty} \frac{2}{T} \int_{-T/2}^{T/2} dt \int_{-\infty}^{\infty} ds \left\langle \Delta I^{(i)}(t+s) \Delta I^{(j)}(t) \right\rangle, \quad (3.21)$$

where  $s$  is a time variable denoting the delay between the fluctuations. The fluctuation in the time evolution of the generic current operator is given by  $\Delta I(t) = I(t) - \langle I(t) \rangle$ . Similar to the formulation of the tunneling current operator (cf. Sec. 3.1), we expand Eq. (3.21) to the leading order in the tunneling amplitude. In other words, we restrict the perturbative expansion of the time-dependent current operator to include terms with pre-factors  $\Lambda^n$  for  $n < 2$  due to the diminutive tunneling amplitude  $|\Lambda| \ll 1$  in the weak backscattering regime.

$$\left\langle \Delta I_R^{(i)}(t+s) \Delta I_R^{(j)}(t) \right\rangle = \langle (I_R(t+s) - \langle I_R(t+s) \rangle) (I_R(t) - \langle I_R(t) \rangle) \rangle. \quad (3.22)$$

Discarding the vanishing components and retaining only non-zero contributions, we obtain

$$\begin{aligned} \left\langle \Delta I_R^{(i)}(t+s) \Delta I_R^{(j)}(t) \right\rangle &= \left\langle I^{(0)}(t+s) I^{(0)}(t) \right\rangle + \left\langle I^{(1)}(t+s) I^{(1)}(t) \right\rangle \\ &+ \left\langle I^{(0)}(t+s) I^{(2)}(t) \right\rangle + \left\langle I^{(2)}(t+s) I^{(0)}(t) \right\rangle = S^{(00)} + S^{(11)} + S^{(02)} + S^{(20)}. \end{aligned} \quad (3.23)$$

We only focus on the backscattered noise  $S^{(11)}$  that arises due to the quasiparticle tunneling at the **QPC**. The residual noise components scale proportionally with temperature ( $\theta$ ) and become insignificant at very low temperatures. Our calculations are constricted to low temperatures with an upper bound  $V_{R/L} > k_B\theta$ .

$$S^{(11)} = (q\nu\Theta(y-x)|\Lambda|)^2 \lim_{T \rightarrow \infty} \frac{2}{T} \int_{-T/2}^{T/2} dt \int_{-\infty}^{\infty} ds \left\langle \psi_L^\dagger(t+s)\psi_R(t)\psi_R^\dagger(t+s)\psi_L(t) \right\rangle + h.c..$$

The backscattered noise has a similar mathematical form as that of  $\langle I^{(2)}(y,t) \rangle$ , entailing a similar calculation method (cf. Sec. 3.1). Therefore, we state the final generalized noise expressions ignoring the intermediate computation steps:

$$S^{(11)} = (q\nu|\Lambda|)^2 \lim_{T \rightarrow \infty} \frac{2}{T} \int_{-T/2}^{T/2} dt \int_{-\infty}^{\infty} ds \langle I_T(t+s)I_T(t) \rangle, \quad (3.24)$$

$$S^{(11)} = (q\nu|\Lambda|)^2 \lim_{T \rightarrow \infty} \frac{4}{T} \int_{-T/2}^{T/2} dt \int_{-\infty}^{\infty} ds G_+^2(0,0,s,0) \cos\left(q\nu \int_t^{t+s} d\tau V_R(\tau)\right). \quad (3.25)$$

### 3.3 Two input sources and photoassisted coefficients

So far, we have derived results for a single source setup. However, we must now extend our analysis to a two-source case because we aim to model the **HOM** interferometry. In addition to the previously defined input source  $U_R(y,t)$  in the region  $x < x_R$ , we introduce another voltage source  $U_L(y,t) = \Theta(y-x_L)V_L(t)$  in the region  $x > x_L$  that couples to the left-moving chiral edge mode modifying the quasiparticle and bosonic field operators as

$$\phi_L(y,t) = \phi_{L0}(y+vt,0) + q\nu \int_{-\infty}^t dt' U_L(y+v(t-t'),t'), \quad (3.26)$$

$$\psi_L(t) = \frac{1}{\sqrt{2\pi\alpha}} e^{-i\phi_{L0}(y+vt,0)} e^{-iq\nu \int_{-\infty}^{t+y/v-x_L/v} dt' V_L(t')}. \quad (3.27)$$

It is apparent that the additional source term augments a phase factor corresponding to the applied voltage  $V_L(t)$  altering the previously computed observables as (results stated after enforcing the symmetric conditions of the setup in Fig. 3.1 and by writing  $G_\pm(x_{QPC}, y, t, t'')$  as  $G_\pm$  and  $G_+(0,0,s,0)$  as  $G_+(0,s)$  for brevity):

$$\langle I_T(t) \rangle = 2iq\nu|\Lambda|^2 \int_{-\infty}^t dt'' (G_-^2 - G_+^2) \sin\left(q\nu \int_{t''}^{t-d/v} d\tau [V_R(\tau) - V_L(\tau)]\right), \quad (3.28)$$

$$S^{(11)} = (q\nu|\Lambda|)^2 \lim_{T \rightarrow \infty} \frac{4}{T} \int_{-T/2}^{T/2} dt \int_{-\infty}^{\infty} ds G_+^2(0,s) \cos\left(q\nu \int_t^{t+s} d\tau [V_R(\tau) - V_L(\tau)]\right) \quad (3.29)$$

By coupling two voltage sources to both the chiral edge modes, we can now operate the Laughlin **FQH** setup in both the **HOM** (collider regime) [20] and **HBT** configurations (by setting either of the inputs to 0) [64, 65]. To extend our examination with relevance to experiments, we assume that the voltage source drives the system periodically with a time-period  $T$  (angular frequency  $\Omega$ ). This approach stems from the practical challenges associated with achieving single-pulse detection, leading to the frequent use of periodic sources in experimental setups. Consequently, the tunneling current satisfies:  $\langle I_T(t) \rangle = \langle I_T(t+T) \rangle$ , because the sinusoidal function in Eq. (3.28) is periodic in time. Therefore,

averaging the tunneling current over one cycle of  $T$  would suffice to further our analysis. We split the applied effective voltage bias into **AC** [ $V_{AC}(\tau) = V_R^{AC}(\tau) - V_L^{AC}(\tau)$ ] and **DC** [ $V_{DC}(\tau) = V_R^{DC}(\tau) - V_L^{DC}(\tau)$ ] components [68] to rearrange the sine term as follows:

$$\begin{aligned} \langle \overline{I_T(t)} \rangle &= 2iq\nu|\Lambda|^2 \frac{1}{T} \int_0^T dt \int_{-\infty}^t dt'' (G_-^2 - G_+^2) \sin \left( q\nu \int_{t''}^{t-d/v} d\tau [V_{AC}(\tau) + V_{DC}] \right), \\ &= q\nu|\Lambda|^2 \frac{1}{T} \int_0^T dt \int_{-\infty}^t dt'' (G_-^2 - G_+^2) e^{iq\nu \int_{t''}^{t-d/v} d\tau V_{AC}(\tau)} e^{iq\nu V_{DC}(t-t''-d/v)} - h.c.. \end{aligned}$$

Due to the periodicity of  $V_{AC}(\tau)$ , the exponential can be expressed as a Fourier series by introducing the photoassisted coefficients [69, 70] elaborated in Appendix C.

$$\langle \overline{I_T(t)} \rangle = \frac{q\nu|\Lambda|^2}{T} \int_0^T dt \int_{-\infty}^t dt'' (G_-^2 - G_+^2) \sum_{l=-\infty}^{\infty} \sum_{m=-\infty}^{\infty} p_l^* p_m e^{il\Omega t} e^{-im\Omega t''} e^{iQ\Omega(t-t'')} - h.c.,$$

where  $Q\Omega = q\nu V_{DC}$ ,  $G_{\pm}^2 = G_{\pm}^2(x_{QPC}, y, t, t'')$ , and  $p_{l/m}$  is the photoassisted coefficient. Performing a change of variables  $t - t'' = -t'$  by subtracting  $t''$  from the time arguments transforms the observable into<sup>2</sup>

$$\langle \overline{I_T(t)} \rangle = \frac{q\nu|\Lambda|^2}{T} \int_0^T dt \int_{-\infty}^0 dt' (G_-^2 - G_+^2) \sum_{l=-\infty}^{\infty} \sum_{m=-\infty}^{\infty} p_l^* p_m e^{i\Omega t(l-m)} e^{-i\Omega t'(l+Q)} - h.c.,$$

where  $G_{\pm}^2 = G_{\pm}^2(x_{QPC}, y, -t', 0)$ . We drop the space coordinates from Green's function and change the order of operations to obtain  $(1/T) \int_0^T dt e^{-i\Omega t(l-m)} = 1$ , which yields  $l = m$  within a single period  $T$  of the applied periodic voltage pulses.

$$\begin{aligned} \langle \overline{I_T(t)} \rangle &= q\nu|\Lambda|^2 \int_{-\infty}^0 dt' (G_+^2(-t', 0) - G_-^2(-t', 0)) \sum_{l=-\infty}^{\infty} |p_l|^2 [e^{i\Omega t'(l+Q)} - e^{-i\Omega t'(l+Q)}], \\ \langle \overline{I_T(t)} \rangle &= 2iq\nu|\Lambda|^2 \sum_{l=-\infty}^{\infty} |p_l|^2 \int_{-\infty}^0 dt' (G_+^2(-t', 0) - G_-^2(-t', 0)) \sin(\Omega t'(l+Q)). \end{aligned} \quad (3.30)$$

As  $G_-^2(-t', 0) = G_+^2(t', 0)$ , we can simplify Eq. (3.30) by treating the integral as follows:

$$\begin{aligned} \langle \overline{I_T(t)} \rangle &= 2iq\nu|\Lambda|^2 \sum_{l=-\infty}^{\infty} |p_l|^2 \left[ \int_{-\infty}^0 dt' G_+^2(-t', 0) \sin(\Omega t'(l+Q)) \right. \\ &\quad \left. - \int_{-\infty}^0 dt' G_+^2(t', 0) \sin(\Omega t'(l+Q)) \right]. \end{aligned}$$

Applying the substitution  $t' = -t'$ , to the first integral in the above equation, we obtain

$$\langle \overline{I_T(t)} \rangle = -2iq\nu|\Lambda|^2 \sum_{l=-\infty}^{\infty} |p_l|^2 \int_{-\infty}^{\infty} dt' G_+^2(t', 0) \sin(\Omega t'(l+Q)). \quad (3.31)$$

Expressing the sinusoidal in exponents leads to the Fourier transform of Green's function calculated in Appendix B. It reformulates  $\langle \overline{I_T(t)} \rangle$  into summation of  $p_l$

$$\begin{aligned} \langle \overline{I_T(t)} \rangle &= q\nu|\Lambda|^2 \sum_{l=-\infty}^{\infty} |p_l|^2 \left[ \int_{-\infty}^0 dt' G_+^2(t') e^{-i\Omega t'(l+Q)} - \int_{\infty}^0 dt' G_+^2(t') e^{-i\Omega t'(l+Q)} \right], \\ &= q\nu|\Lambda|^2 \sum_{l=-\infty}^{\infty} |p_l|^2 [P_{2\nu}(\Omega(l+Q)) - P_{2\nu}(-\Omega(l+Q))]. \end{aligned} \quad (3.32)$$

<sup>2</sup>The constant global phase factor  $e^{-i\Omega(l+Q)d/v}$  appearing in  $\langle \overline{I_T(t)} \rangle$  can be ignored in our calculation.

Following a similar procedure, we connect with the photoassisted coefficients to compute the photoassisted shot noise [71, 72]. We expand the cosine term in Eq. (3.29) to obtain

$$S^{(11)} = \lim_{T \rightarrow \infty} \frac{2(q\nu|\Lambda|)^2}{T} \int_{-T/2}^{T/2} dt \int_{-\infty}^{\infty} ds G_+^2(s) e^{-iQ\Omega s} \sum_{l=-\infty}^{\infty} \sum_{m=-\infty}^{\infty} p_l^* p_m e^{i\Omega t(l-m)} e^{-i(l+m)\Omega s/2} + h.c..$$

Considering the periodic nature of the voltage pulses, the above equation boils down to the Fourier transform of  $G_+^2(s)$  (cf. Appendix B).

$$\begin{aligned} S^{(11)} &= 2(q\nu|\Lambda|)^2 \sum_{l=-\infty}^{\infty} |p_l|^2 \int_{-\infty}^{\infty} ds G_+^2(s) [e^{-i(l+Q)\Omega s} + e^{i(l+Q)\Omega s}], \\ &= 2(q\nu|\Lambda|)^2 \sum_{l=-\infty}^{\infty} |p_l|^2 [P_{2\nu}(\Omega(l+Q)) + P_{2\nu}(-\Omega(l+Q))]. \end{aligned} \quad (3.33)$$

### 3.4 Analysis in the DC regime

Driving the Laughlin FQH setup with a pure DC bias  $Q \neq 0$ , where  $Q = q\nu V_{DC}/\Omega$  by zeroing out the AC component  $W = 0$ , where  $W = q\nu V_{AC}/\Omega$ , transforms the photoassisted coefficient to  $p_l(W = 0) = -J_l(0) = \delta_{l,0} = \delta(l)$  (cf. Appendix C). The noise and current expressions in the DC regime read as

$$\begin{aligned} \overline{\langle I_T(t) \rangle} &= \langle I_T(t) \rangle = q\nu|\Lambda|^2 \sum_{l=-\infty}^{\infty} |\delta(l)|^2 [P_{2\nu}(\Omega(l+Q)) - P_{2\nu}(-\Omega(l+Q))], \\ &= \frac{2q\nu|\Lambda|^2}{\Gamma(2\nu)\omega_c} \left( \frac{2\pi k_B\theta}{\omega_c} \right)^{2\nu-1} \left| \Gamma\left(\nu + \frac{iq\nu V_{DC}}{2\pi k_B\theta}\right) \right|^2 \sinh\left(\frac{q\nu V_{DC}}{2k_B\theta}\right). \end{aligned} \quad (3.34)$$

$$\begin{aligned} S^{(11)} &= 2(q\nu|\Lambda|)^2 \sum_{l=-\infty}^{\infty} |\delta(l)|^2 [P_{2\nu}(\Omega(l+Q)) + P_{2\nu}(-\Omega(l+Q))], \\ &= \frac{(2q\nu|\Lambda|)^2}{\Gamma(2\nu)\omega_c} \left( \frac{2\pi k_B\theta}{\omega_c} \right)^{2\nu-1} \left| \Gamma\left(\nu + \frac{iq\nu V_{DC}}{2\pi k_B\theta}\right) \right|^2 \cosh\left(\frac{q\nu V_{DC}}{2k_B\theta}\right). \end{aligned} \quad (3.35)$$

The temperature-dependent behavior of the system at  $\nu = 1/3$  for a sweep of the dimensionless DC parameter ( $q\nu V_{DC}\omega_c^{-1}$ , where  $\omega_c$  is the energy cut-off, cf. Appendix A) from -0.5 to 0.5 are plotted in Fig. 3.2. As discussed in Sec. 3.2, our computations pertain to low temperatures bounded by the limit  $V_{applied} > k_B\theta$ . The perfectly overlapping curves Fig. 3.2 indicate the negligible impact of finite temperature effects within this regime. However, this limit is no longer valid for a diminishing applied voltage  $V_{DC} \rightarrow 0$  where the relatively significant temperature diverges the current and noise responses of the system. Notably, this divergent behavior is persistent in a multiple QPC setup as both  $V_{applied}$  and  $\theta$  tend towards zero [73]. The DC analysis reveals another aspect of the nature of the tunneling particles at the QPC. In the temperature independent regime (cf. Appendix B.2), we can derive  $\langle I_T(t) \rangle \propto V_{applied}^{2\nu-1}$  from Eq. (B.16) which suggests the power law governing the relation between tunneling current and the applied input voltage.  $\nu = 1$  refers to the tunneling current caused by electrons that dwindle to zero as  $V_{applied} \rightarrow 0$ . In contrast, the Laughlin sequence with  $\nu = 1/(2n+1)$ , where  $n \in \mathbb{Z}^+$ , exhibits an asymptotic current due to the tunneling of quasiparticles at the QPC. It illustrates the dominance of

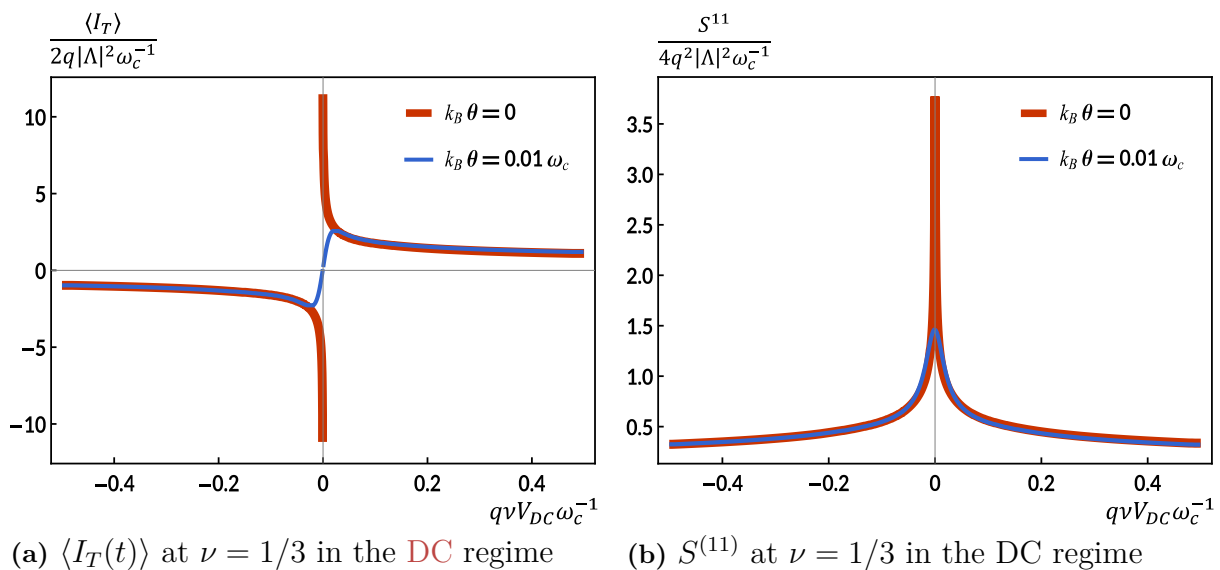


**Figure 3.2:** Plots of backscattered current and zero-frequency noise as a function of the dimensionless parameter  $q\nu V_{DC}\omega_c^{-1}$  at zero ( $k_B\theta = 0$ , in red) and finite temperature ( $k_B\theta = 0.01\omega_c$ , in blue). The curves overlap perfectly within the limit  $V_{DC} > k_B\theta$ . This limit is no longer valid in the region where the temperature-independent curves diverge.

quasiparticle tunneling over electron tunneling as a low-energy perturbation to the FQH system [74]. Furthermore, we can establish a relationship between the photoassisted shot noise and tunneling current as the following:

$$S^{(11)} = 2q\nu \langle I_T(t) \rangle \coth\left(\frac{q\nu V_{DC}}{2k_B\theta}\right). \quad (3.36)$$

Sending  $\theta$  to the infinitesimal limit ( $\theta \rightarrow 0$ ) at  $V_{DC} > 0$  retrieves  $S = 2q\nu \langle I_T(t) \rangle$ . As discussed in Sec. 1.3, this theoretical argument was instrumental in discovering fractional charges through current-noise measurements.

### 3.5 AC Analysis: Hong-Ou-Mandel Effect

We aim to realize the HOM effect by colliding two identical excitations at the QPC in the Laughlin FQH setup. The *Source 1* and *Source 2* terminals in Fig. 3.3 are driven by two periodic voltage pulses identical in amplitude but separated in time by a tunable delay  $\tau_d$ . When we drive the system with two voltage pulses of equal amplitudes, it zeroes out the contribution from the DC components due to the effective voltage seen by the system  $\Delta V = V_R(t) - V_L(t + \tau_d) = V_{AC}(t) + \cancel{V_{DC}} - V_{AC}(t + \tau_d) - \cancel{V_{DC}}$ , leading to  $Q = q\nu V_{DC}/\Omega = 0$ . Furthermore, the tunable time delay alters the general form of the photoassisted coefficient presented in Eq. (C.4) in Appendix C as follows:

$$p_{I(HOM)} = \int_{-T/2}^{T/2} dt \frac{1}{T} e^{i\Omega t} e^{-iq\nu \int_0^t d\tau V_{AC}(\tau)} e^{iq\nu \int_0^t d\tau V_{AC}(\tau + \tau_d)}. \quad (3.37)$$

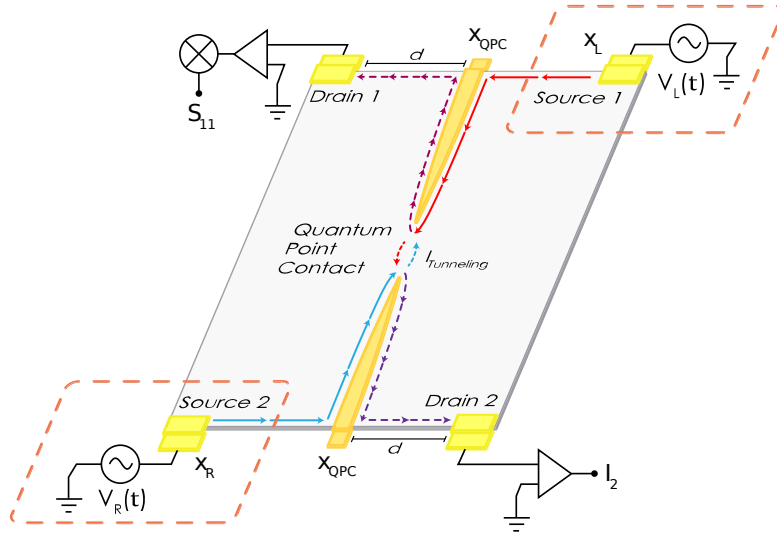


**Figure 3.3:** The four terminal Laughlin FQH setup in the HOM configuration. The voltage sources  $V_R(t)$  and  $V_L(t)$  are defined in the regions  $x < x_R$  and  $x > x_L$  at the Source terminals 2 and 1, respectively. Identical periodic voltage pulses are applied at these Source terminals in the HOM configuration that drive the FQH setup out-of-equilibrium. The Drain terminals measure the backscattered current and zero-frequency noise.

By changing the order of operations and considering the periodic nature of input voltage,

$$\begin{aligned}
 p_{l(HOM)} &= e^{-iq\nu \int_0^{t_d} d\tau V_{AC}(\tau)} \int_{-T/2}^{T/2} dt \frac{1}{T} e^{i\Omega t} \sum_{m=-\infty}^{\infty} \sum_{n=-\infty}^{\infty} p_m e^{-im\Omega t} p_n^* e^{in\Omega(t+\tau_d)}, \\
 &= e^{-iq\nu \int_0^{t_d} d\tau V_{AC}(\tau)} \sum_{n=-\infty}^{\infty} p_{n+l} p_n^* e^{in\Omega\tau_d} = \sum_{n=-\infty}^{\infty} p_{n+l} p_n^* e^{in\Omega\tau_d}.
 \end{aligned} \tag{3.38}$$

Hence, the photoassisted coefficient for HOM  $p_{l(HOM)}$ <sup>3</sup> is a function of the generic photoassisted coefficient  $p_n$  and time delay  $\tau_d$ . Although a broader class of HOM collisions exist that involve input voltages with distinct amplitudes and temporal shapes [62, 66], we only consider sinusoidal input for our analysis. Detailed calculations of  $p_n$  for a sinusoidal input are presented in Appendix C. A substantial time delay between the input signals in the HOM experiment is equivalent to driving the system independently through Sources 1 and 2 in the HBT configuration. Therefore, it is a standard practice to normalize the HOM noise with the HBT noise by defining a ratio  $\mathcal{R}$  that is only a function of the time delay  $\tau_d$ . Typically, the noise caused by particles tunneling at the QPC is overshadowed by the equilibrium fluctuation  $S^{(0)}$  that is independent of  $V_{applied}$ . For this reason, we focus on the excess noise  $\Delta S = S^{(11)} - S^{(0)}$  by subtracting the background fluctuations to define the standard HOM noise ratio as

$$\mathcal{R}(\tau_d) = \frac{S_{HOM}^{(11)} - S^{(0)}}{S_{HBT/R}^{(11)} + S_{HBT/L}^{(11)} - 2S^{(0)}}. \tag{3.39}$$

<sup>3</sup>As Eqs. (3.31) and (3.33) involve the square modulus of  $p_n$ , we can safely ignore the constant global phase factor  $e^{-iq\nu \int_0^{t_d} d\tau V_{AC}(\tau)}$  appearing in  $p_{l(HOM)}$

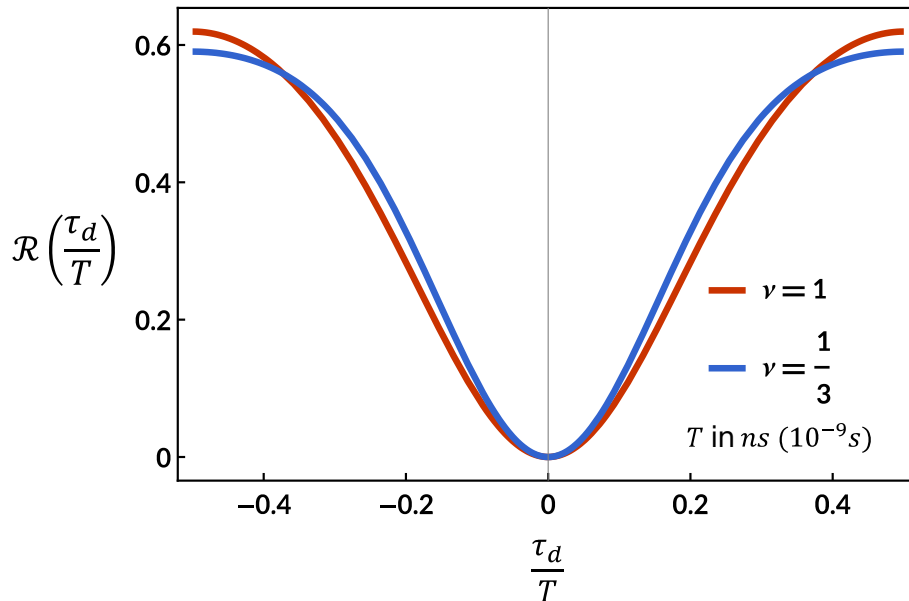


**Figure 3.4:** A plot of the standard **HOM** noise ratio  $\mathcal{R}$  as a function of the dimensionless delay parameter  $\tau_d/T$ . Identical sinusoidal input pulses with frequency  $\Omega$  (in GHz range) are considered at temperature  $k_B\theta = 0.01\Omega$  for filling factors  $\nu = 1$  and  $\nu = 1/3$ .

Note that we observe a vanishing **HOM** noise ratio even at a fractional filling factor of  $\nu = 1/3$  in Fig. 3.4. This behavior can be justified by examining the nature of excitations induced by the voltage sources in the **FQH** regime. As discussed in Sec. 1.1, a controllable source of quasiparticles is a primary ingredient required to perform anyonic **HOM**. However, the conventional voltage sources (marked by orange boxes in Fig. 3.3) cannot excite a single fractionally charged quasiparticle using any of the Lorentzian, sinusoidal, or square voltage drives [66]. Moreover, even the minimal excitation<sup>4</sup> in the **FQH** regime corresponds to an integer number of electrons instead of a fractional charge [62]. Thus, the **HOM** dip observed at fractional filling factors in Fig. 3.4 should not be interpreted as stemming from the fractional statistics of quasiparticle excitations. Therefore, the feasibility of employing controllable sources emitting single quasiparticles restricts the possibility of performing **HOM** for anyons to probe their fractional statistics. In the next Chapter, we explore this possibility by formally considering a prepared auxiliary state describing the time-controlled injection of a single quasiparticle excitation.

<sup>4</sup>Minimal excitations in a non-interacting system are typically characterized by a single particle excitation above the Fermi level, free from any additional particle-hole pair excitations that generate noise [75]. This notion can be extended to the context of strongly correlated **FQH** states by imposing that these minimal excitations do not generate any excess noise apart from thermal noise. Interestingly, the required voltage drive remains a Lorentzian pulse carrying an integer charge [62].

# 4

## Exchange phase erasure in anyon time domain interferometry

As outlined in previous chapters, we require time-resolved sources capable of injecting fractional excitations into the Laughlin FQH setup to explore anyon correlations in HOM interferometry. In the following, we theoretically model such ideal quasiparticle sources to describe the interference between anyon collisions at the QPC to probe their fractional statistics. Our theoretical description relies on an auxiliary state, as detailed in Sec. 4.1. Despite the experimental impracticability of such ideal quasiparticle sources, a mapping has been derived in Ref. [63], showing that an infinitely narrow,  $\delta$ -like voltage pulse  $V(t) = 2\pi\delta(t)/e$  (where  $e$  is the charge of an electron) is formally equivalent to the description of an ideal quasiparticle source, as described in Sec. 4.1. As a result, from an experimental point of view, the features we describe in this chapter can be approximately mimicked by driving the FQH collider with extremely narrow voltage pulses carrying an average fractional charge.

### 4.1 Auxiliary state and Tunneling operator

In the absence of excitations, we denote the ground state of the Laughlin FQH system in Fig. 4.1 with  $|0\rangle$ . To model an ideal time-resolved generic source of anyons capable of exciting any kind  $\mathbf{l} = (l_1, l_2, \dots, l_n)^T$  of quasiparticle, we adopt the  $K$ -matrix formalism introduced in Sec. 2.4. A single quasiparticle injection is then denoted by an auxiliary state  $|\varphi\rangle$ , which is just the system's ground state dressed by a single quasiparticle excitation [43, 76]. It is defined as  $|\varphi\rangle = \psi_{\mathbf{l}_1}^\dagger(x, t)|0\rangle$ , where  $\psi_{\mathbf{l}_1}^\dagger$  is the quasiparticle creation operator (cf. Sec. 2.4) that adds a single quasiparticle of kind  $\mathbf{l}_1$ <sup>1</sup> to the system at position  $x$  and time  $t$ . As our system hosts a single type of quasiparticles, we omit the subscript  $\mathbf{l}_1$  from the operators and switch to the following edge modes description:

left-moving edge ( $L$ )  $\rightarrow$  upper edge ( $u$ )      right-moving edge ( $R$ )  $\rightarrow$  lower edge ( $d$ ).

This notation facilitates a succinct description of various subprocesses arising at the QPC, which will be elucidated later in the chapter. We next introduce an operator  $A(t)$  describing tunneling quasiparticles at the QPC to distinguish various quantities in the theory clearly. Considering the weak tunneling amplitude to be real, i.e.,  $\Lambda \in \mathbb{R}$ , we compactly express the tunneling Hamiltonian as

$$H_\Lambda = \Lambda [A(t) + A^\dagger(t)], \quad (4.1)$$

---

<sup>1</sup>A non-interacting FQH system with a single edge mode hosts identical quasiparticles of a single kind.

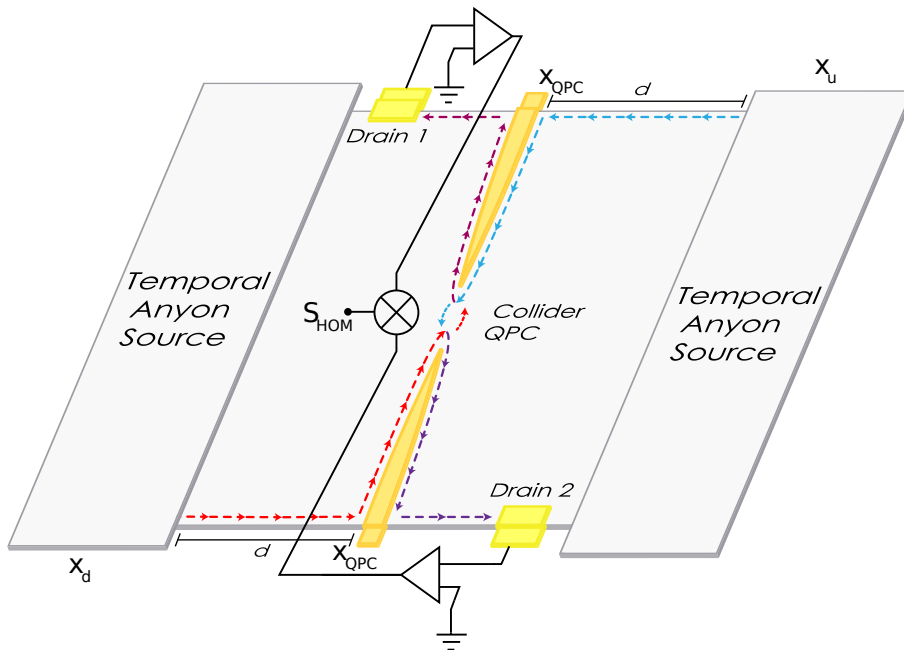


**Figure 4.1:** The four terminal Laughlin FQH setup in HOM configuration with ideal time-resolved anyon sources. *Temporal Anyon Source* is modeled by an auxiliary state  $|\varphi\rangle = \psi_u^\dagger(x_u, t_u)\psi_d^\dagger(x_d, t_d)|0\rangle$  that injects anyons in the upper ( $u$ ) and lower ( $d$ ) edges at positions  $x_u, x_d$  and times  $t_u, t_d$ , respectively. The resulting HOM noise due to anyon collisions at the QPC ( $x = x_{QPC}$ ) is measured by the *Drain* terminals.

where  $A(t) = \psi_u^\dagger(x_{QPC}, t)\psi_d(x_{QPC}, t)$ . From the bosonization formalism introduced in Sec. 2.3, it is apparent that the chiral edge modes host quasiparticles of the form  $\psi \propto e^{-i\phi}$ . The tunneling operator can thus be written as  $A(t) = e^{i\mathbf{1}_1\phi_u(x_{QPC}, t)}e^{-i\mathbf{1}_1\phi_d(x_{QPC}, t)}$ , which describes the creation of a quasi-particle-hole pair at the QPC. These tunneling quasi-particle-hole pairs can be attributed to either thermal excitations or quantum fluctuations occurring at different times, and their correlations are determined by the scaling dimension  $\delta$ . The scaling dimension appears as a power-law exponent that governs the decay of the equilibrium Green's function of the tunneling quasiparticles (quasiholes) taken as

$$\langle A(t)A^\dagger(t')\rangle_0 = \langle A^\dagger(t)A(t')\rangle_0 = \left[ \frac{\pi k_B \theta \alpha}{\sinh(\pi k_B \theta |t - t'|)} \right]^{4\delta} e^{-i2\pi\delta \text{sgn}(t-t')}. \quad (4.2)$$

Note that Eq. (4.2) is analogous to  $G_\pm^2$  quantity from Eq. (3.16) derived (cf. Appendix A) in Sec. 3.1. The term consisting of the UV cut-off parameter can be conformally mapped to the exponential with  $\text{sgn}$  function by selecting a suitable contour in the complex plane [77]. By comparing Eqs. (3.16) and Eq. (4.2) we arrive at the relation  $\nu = 2\delta$  which further implies that  $\vartheta = 2\pi\delta$  for the Laughlin edge states. Here,  $\vartheta$  is the braiding phase given by  $\pi\nu$ . This equivalence holds for non-interacting edges hosting Abelian anyons. However, in general, the scaling dimension  $\delta$  is a non-universal parameter affected by neutral modes or  $1/f$  noise [74, 78–82]. In contrast, the filling factor  $\nu$  and the statistical exchange phase  $\vartheta$  are universal parameters that are intrinsic characteristics of the FQH system insensitive to such external influences. Additionally, distinguishing between  $\vartheta$  from the non-universal effects of  $2\pi\delta$  is of high experimental relevance. If left unaccounted for, this coincidence

between  $\delta$  and  $\nu$ , dictated by the theory of non-interacting Abelian edges, could lead to misinterpretations about detecting fractional statistics through standard **HOM** noise ratio measurements. To compute observable quantities such as average backscattered current and noise, we replace the system's ground state  $|0\rangle$  with the prepared auxiliary state  $|\varphi\rangle$ . As shown in Fig. 4.1, the *Temporal Anyon Sources* operating in **HOM** configuration drive the Laughlin **FQH** setup out-of-equilibrium by injecting two time-resolved quasiparticles into the system. It is modeled by dressing the ground state of the system with a quasiparticle excitation on both the upper and lower edges as  $|\varphi\rangle = \psi_u^\dagger(x_u, t_u)\psi_d^\dagger(x_d, t_d)|0\rangle$ .

## 4.2 Tunneling current in HOM configuration

The tunneling current operator from Eq. (3.19) derived in Sec. 3.1 using Heisenberg's equation of motion can be written in the framework of tunneling operators as  $I_T(t) = iq\nu\Lambda [A(t) - A^\dagger(t)]$ . Using Eq. (3.20) expressed in terms of the tunneling operators, we calculate the expectation value of the tunneling current with respect to the auxiliary state  $\langle\varphi| \cdot |\varphi\rangle = \langle\cdot\rangle_{qp}$  as follows:

$$\begin{aligned} \langle I_T(t) \rangle &= q\nu\Lambda^2 \int_{-\infty}^t dt' \left\langle \left[ \psi_u^\dagger(t)\psi_d(t), \psi_d^\dagger(t')\psi_u(t') \right] + \left[ \psi_u^\dagger(t')\psi_d(t'), \psi_d^\dagger(t)\psi_u(t) \right] \right\rangle_{qp}, \\ &= q\nu\Lambda^2 \int_{-\infty}^t dt' \left[ \langle A(t)A^\dagger(t') \rangle_{qp} + \langle A(t')A^\dagger(t) \rangle_{qp} - \langle A^\dagger(t)A(t') \rangle_{qp} - \langle A^\dagger(t')A(t) \rangle_{qp} \right]. \end{aligned} \quad (4.3)$$

We are interested in injecting a quasiparticle into the upper and lower edges at the locations  $x_u > x_{QPC}$  and  $x_d < x_{QPC}$  at times  $t_u$  and  $t_d$  in the non-equilibrium driving of the Laughlin **FQH** setup in **HOM** configuration. The quasiparticle creation operator  $e^{i\mathbf{1}_1\phi_{u/d}(x_{u/d}, t_{u/d})}$  acting on the edges creates a stable localized disturbance (soliton) in each bosonic field. Consequently, the bosonic fields evolving chirally with a velocity  $v$  accumulate a phase due to the Kac Moody commutation relations (cf. Sec. 2.4)[83]

$$\phi_u(x, t_u) \rightarrow \phi_u(x, t_u) + 2\pi K^{-1}\mathbf{1}_1\Theta(-(x + v(t - t_u)) + x_u), \quad (4.4)$$

$$\phi_d(x, t_d) \rightarrow \phi_d(x, t_d) + 2\pi K^{-1}\mathbf{1}_1\Theta(x - v(t - t_d) - x_d). \quad (4.5)$$

The injected quasiparticles interfere at the position  $x = x_{QPC}$  when there is zero time delay  $\tau_d = 0$ . Enforcing the symmetric conditions of the setup in Fig. 4.1 generates constant offset components ( $d/v$ ) that correspond to the relative position of the **QPC** with respect to the anyon sources in the setup. By absorbing the offset terms into the injection times, the accumulated phase can be simplified to a function of time arguments. However,  $t_u$  and  $t_d$  will now represent the arrival times of the injected anyons at the **QPC** that is inherently controlled by the injection times  $(t_u, t_d)$ . Hence, we continue with the same notation without loss of generality

$$\phi_{u/d}(t_{u/d}) \rightarrow \phi_{u/d}(t_{u/d}) + 2\pi K^{-1}\mathbf{1}_1\Theta(t_{u/d} - t). \quad (4.6)$$

Therefore, from the bosonic description of the tunneling operator, it is clear that the exponentiated phase factors out of the non-equilibrium correlation function leading to the relation [holds for all combinations of observables appearing in Eq. (4.3)]

$$\langle A^\dagger(t)A(t') \rangle_{qp} = \langle A^\dagger(t)A(t') \rangle_0 e^{-i2\pi\mathbf{1}_1 K^{-1}\mathbf{1}_1[-\Theta(t_d - t) + \Theta(t_u - t) + \Theta(t_d - t') - \Theta(t_u - t')]}. \quad (4.7)$$

The obtained phase component  $\vartheta = \pi \mathbf{1}_1 K^{-1} \mathbf{1}_1$ , is the standard definition of the statistical braiding angle between two quasiparticles of the same kind introduced in Sec. 2.4. Equation (4.7) demonstrates that the injected quasiparticles acquire a non-trivial exchange phase by interacting (braiding) with the quasi-particle-hole pairs created at the QPC due to thermal or quantum fluctuation. In the HOM configuration, the product accumulates a braiding phase  $\vartheta$  only when both the arrival times of the quasiparticles  $t_d$  and  $t_u$  fall within the range of the QPC quasi-particle-hole pair creation times  $t$  and  $t'$ . Introducing  $\Phi = 2\vartheta [-\Theta(t_d - t) + \Theta(t_u - t) + \Theta(t_d - t') - \Theta(t_u - t')]$  for brevity.

$$\begin{aligned} \langle I_T(t) \rangle &= q\nu\Lambda^2 \int_{-\infty}^t dt' \left( \langle A(t)A^\dagger(t') \rangle_0 - \langle A^\dagger(t')A(t) \rangle_0 \right) e^{i\Phi} + \left( \langle A(t')A^\dagger(t) \rangle_0 - \langle A^\dagger(t)A(t') \rangle_0 \right) e^{-i\Phi}, \\ &= q\nu\Lambda^2 \int_{-\infty}^t dt' \left[ \frac{\pi k_B \theta \alpha}{\sinh(\pi k_B \theta |t - t'|)} \right]^{4\delta} \left( e^{-i2\pi\delta \text{sgn}(t-t')} - e^{-i2\pi\delta \text{sgn}(t'-t)} \right) \left( e^{i\Phi} - e^{-i\Phi} \right), \\ &= -4q\nu\Lambda^2 \int_{-\infty}^t dt' \left[ \frac{\pi k_B \theta \alpha}{\sinh(\pi k_B \theta |t - t'|)} \right]^{4\delta} \sin(\Phi) \sin(2\pi\delta) \text{sgn}(t - t'). \end{aligned} \quad (4.8)$$

The integral over  $dt'$  in Eq. (4.8) ranges from  $-\infty$  to  $t$ , implying that  $t'$  is limited to values less than  $t$  ( $t' < t$ ). This condition simplifies the integral to

$$\langle I_T(t) \rangle = -4q\nu\Lambda^2 \sin(2\pi\delta) \int_{-\infty}^t dt' \left[ \frac{\pi k_B \theta \alpha}{\sinh(\pi k_B \theta (t - t'))} \right]^{4\delta} \sin(\Phi). \quad (4.9)$$

We attempt to simplify the integral in Eq. (4.9), focusing on the sinusoidal function and by assuming  $t_d > t_u$ . However, we will accommodate the converse case in subsequent calculations. The controllable injection (arrival) times  $t_u$  and  $t_d$  impose different conditions on the temporal parameter  $t$ , modifying the integration bounds where the sinusoidal function is nonvanishing. We proceed with a piece-wise calculation of the conditions depicted pictorially in Fig. 4.2. and denote the equilibrium Green's function with  $\mathcal{J}(t - t')$ .

$t > t_d > t_u$ : By definition, the Heaviside functions  $\Theta(t_d - t)$  and  $\Theta(t_u - t)$  in  $\Phi$  vanish due to the imposed condition. The leftover terms generate a finite tunneling current only when the argument  $t'$  is between the arrival times such that  $t_d > t' > t_u$ .

$$\int_{-\infty}^t dt' \sin(2\vartheta [-\Theta(t_d - t) + \Theta(t_u - t) + \Theta(t_d - t') - \Theta(t_u - t')]) = \int_{t_u}^{t_d} dt' \sin(2\vartheta).$$

$t_d > t > t_u$ : The function  $\Theta(t_u - t)$  zeroes out while  $-\Theta(t_d - t) + \Theta(t_d - t')$  cancel out each other. The residual argument ensures a non-trivial tunneling current for  $t' < t_u$ .

$$\int_{-\infty}^t dt' \sin(2\vartheta [-\Theta(t_d - t) + \Theta(t_u - t) + \Theta(t_d - t') - \Theta(t_u - t')]) = - \int_{-\infty}^{t_u} dt' \sin(2\vartheta).$$

$t_d > t_u > t$ : It results in a null tunneling current because the quasiparticles never arrive at the QPC. All the Heaviside functions in  $\Phi$  cancel out each other, giving  $\langle I_T(t) \rangle = 0$ . Considering the three discussed scenarios, it is clear that the tunneling current is finite only when  $t > t_u$ . Modeling alternative cases based on conditions imposed by  $t_d$ .

$$\begin{aligned} \langle I_T(t) \rangle &= \sin(2\vartheta)\Theta(t - t_u) \left[ \Theta(t - t_d) \int_{t_u}^{t_d} dt' \mathcal{J}(t - t') - \Theta(t_d - t) \int_{-\infty}^{t_u} dt' \mathcal{J}(t - t') \right], \\ &= \sin(2\vartheta)\Theta(t - t_u) \left[ \Theta(t - t_d) \int_{-\infty}^{t_d} dt' \mathcal{J}(t - t') - \int_{-\infty}^{t_u} dt' \mathcal{J}(t - t') \right]. \end{aligned} \quad (4.10)$$

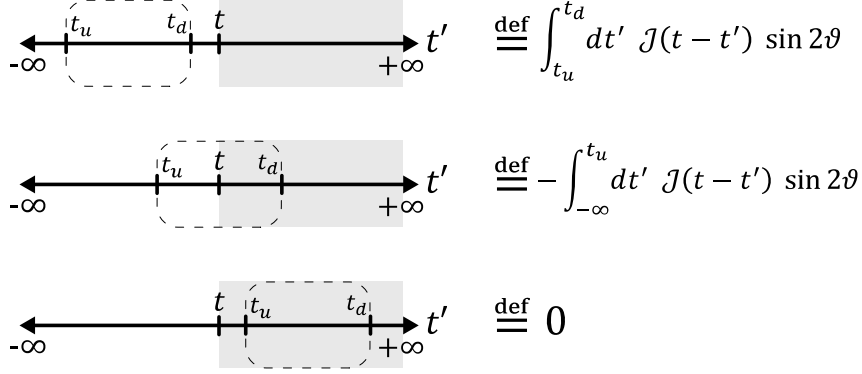


**Figure 4.2:** Pictorial representation of different cases arising in the calculation of  $\langle I_T(t) \rangle$ . The figure portrays a sliding window of controllable quasiparticle injection times that vary in the integration region over  $dt'$  ranging from  $-\infty$  to  $t$ . The shaded area represents the region outside the integration limits.

Entailing similar computations, the arrival times in Eq. (4.10) would swap for  $t_u > t_d$

$$\langle I_T(t) \rangle = \sin(2\vartheta)\Theta(t-t_d) \left[ \Theta(t-t_u) \int_{-\infty}^{t_u} dt' \mathcal{J}(t-t') - \int_{-\infty}^{t_d} dt' \mathcal{J}(t-t') \right]. \quad (4.11)$$

We introduce a tunable time delay  $\tau_d = t_d - t_u$  corresponding to the difference between injection (arrival) times of quasiparticles into the lower and upper edges. We focus on the integrals and perform a change of variables  $t \rightarrow t + t_u$ ,  $t' \rightarrow t' + t_u$  resulting in

$$\begin{aligned} \Theta(t) \left[ \Theta(t-\tau_d) \int_{-\infty}^{\tau_d} dt' \mathcal{J}(t-t') - \int_{-\infty}^0 dt' \mathcal{J}(t-t') \right] & \quad \text{for } t_d > t_u \implies \tau_d > 0, \\ \Theta(t) \left[ \Theta(t+\tau_d) \int_{-\infty}^{-\tau_d} dt' \mathcal{J}(t-t') - \int_{-\infty}^0 dt' \mathcal{J}(t-t') \right] & \quad \text{for } t_u > t_d \implies \tau_d < 0. \end{aligned} \quad (4.12)$$

Combining both cases, we obtain the following expression for tunneling current.

$$\langle I_T(t) \rangle = 4q\nu\Lambda^2 \sin(2\vartheta) \sin(2\pi\delta)\Theta(t) \left[ \int_{-\infty}^0 dt' \mathcal{J}(t-t') - \Theta(t-|\tau_d|) \int_{-\infty}^{|\tau_d|} dt' \mathcal{J}(t-t') \right].$$

The integral of the equilibrium Green's function in its general form has been evaluated in Appendix D. Building upon these results, we derive a closed-form expression for the tunneling current expressed in terms of the incomplete Beta function

$$\begin{aligned} \langle I_T(t) \rangle = 4q\nu\Lambda^2 (2\pi k_B \theta)^{4\delta-1} \alpha^{4\delta} \sin(2\vartheta) \sin(2\pi\delta)\Theta(t) & \left[ \mathcal{B} \left( e^{-2\pi k_B \theta t}; 2\delta, 1-4\delta \right) \right. \\ & \left. - \Theta(t-|\tau_d|) \mathcal{B} \left( e^{-2\pi k_B \theta (t-|\tau_d|)}; 2\delta, 1-4\delta \right) \right], \end{aligned} \quad (4.13)$$

where  $\mathcal{B}(x; a, b) = \int_0^x t^{a-1} (1-t)^{b-1}$ . It is apparent from the above equation that simultaneous injection of quasiparticles with zero delay  $\tau_d = 0$  results in a vanishing tunneling current. The HOM configuration in the null delay is equivalent to maintaining the system in equilibrium  $\langle A^\dagger(t)A(t') \rangle_{qp} = \langle A^\dagger(t)A(t') \rangle_0$ , that leads to  $\langle I_T(t) \rangle = 0$ . This outcome agrees with the results obtained in Sec. 3.3 [cf. Eq. (3.28)] where we drive the system

with identical voltage pulses that leads to a zero effective bias  $\Delta V = V_R(t) - V_L(t + \tau_d)$  at  $\tau_d = 0$ . The vanishing current, which also leads to a vanishing noise despite the ideal injection of time-resolved quasiparticles, can be attributed to the single-QPC geometry of the Laughlin FQH setup. The suppression of observables in the HOM configuration for quasiparticles does not render the conclusion that anyons obey Fermi-Dirac statistics. In contrast, it suggests a more intricate interaction of quasiparticles at the QPC than the straightforward interpretation of two injected anyons colliding/interfering with each other. By extending the present approach of auxiliary state, it is possible to explore such interplay between quasiparticles through further investigation of the HOM noise ratio, which will be the focus of subsequent sections.

### 4.3 Exchange phase erasure in HOM noise ratio

As our next step, we compute here the symmetrized noise power  $S^{(11)}(t, t') = \{I_T(t), I_T(t')\}$ , where  $\{\cdot\}$  is the anti-commutation of operators defined as  $I_T(t)I_T(t') + I_T(t')I_T(t)$ , measured in the *Drain* terminals of the Laughlin FQH setup depicted in Fig. 4.1. The zero-frequency noise in the HOM configuration is calculated by taking the expectation of  $S^{(11)}(t, t')$  with respect to the auxiliary state  $|\varphi\rangle$  defining two time-resolved quasiparticle excitations. Using the tunneling operator for backscattered current, we derive

$$\begin{aligned} S_{HOM}^{(11)} &= \int_{-\infty}^{\infty} \frac{dt}{T} \int_{-\infty}^{\infty} dt' \langle S^{(11)}(t, t') \rangle_{qp} = \int_{-\infty}^{\infty} \frac{dt}{T} \int_{-\infty}^{\infty} dt' \langle \{I_T(t), I_T(t')\} \rangle_{qp}, \\ &= (q\nu\Lambda)^2 \int_{-\infty}^{\infty} \frac{dt}{T} \int_{-\infty}^{\infty} dt' \left[ \langle A(t)A^\dagger(t') \rangle_{qp} + \langle A(t')A^\dagger(t) \rangle_{qp} + \langle A^\dagger(t)A(t') \rangle_{qp} + \langle A^\dagger(t')A(t) \rangle_{qp} \right]. \end{aligned} \quad (4.14)$$

Following a similar approach as in the calculation of the tunneling current, we use the identity in Eq. (4.7) and substitute  $\Phi = 2\vartheta [-\Theta(t_d - t) + \Theta(t_u - t) + \Theta(t_d - t') - \Theta(t_u - t')]$

$$\begin{aligned} S_{HOM}^{(11)} &= (q\nu\Lambda)^2 \int_{-\infty}^{\infty} \frac{dt}{T} \int_{-\infty}^{\infty} dt' \mathcal{J}(|t - t'|) \left( e^{-i2\pi\delta \text{sgn}(t-t')} + e^{-i2\pi\delta \text{sgn}(t'-t)} \right) \left( e^{i\Phi} + e^{-i\Phi} \right), \\ &= (2q\nu\Lambda)^2 \int_{-\infty}^{\infty} \frac{dt}{T} \int_{-\infty}^{\infty} dt' \left[ \frac{\pi k_B \theta \alpha}{\sinh(\pi k_B \theta |t - t'|)} \right]^{4\delta} \cos(\Phi) \cos(2\pi\delta). \end{aligned} \quad (4.15)$$

Our primary objective is to calculate *excess noise*, which is of experimental relevance as detailed in Sec. 3.5. Thus, we subtract the background fluctuations independent of quasiparticle injection from Eq. (4.15) to obtain excess HOM noise

$$\begin{aligned} \Delta S_{HOM}^{(11)} &= (2q\nu\Lambda)^2 \cos(2\pi\delta) \int_{-\infty}^{\infty} \frac{dt}{T} \int_{-\infty}^{\infty} dt' \left[ \frac{\pi k_B \theta \alpha}{\sinh(\pi k_B \theta |t - t'|)} \right]^{4\delta} (\cos(\Phi) - 1), \\ &= (2q\nu\Lambda)^2 \cos(2\pi\delta) \left[ \int_{-\infty}^{\infty} \frac{dt}{T} \int_t^{\infty} dt' \left[ \frac{\pi k_B \theta \alpha}{\sinh(\pi k_B \theta (t' - t))} \right]^{4\delta} (\cos(\Phi) - 1) \right. \\ &\quad \left. + \int_{-\infty}^{\infty} \frac{dt}{T} \int_{-\infty}^t dt' \left[ \frac{\pi k_B \theta \alpha}{\sinh(\pi k_B \theta (t - t'))} \right]^{4\delta} (\cos(\Phi) - 1) \right]. \end{aligned} \quad (4.16)$$

We simplify the integrals in Eq. (4.16) into regions generating non-trivial finite HOM noise by concentrating on  $(\cos(\Phi) - 1)$  term, assuming initially that  $t_d > t_u$ . We now

calculate the contribution of  $\mathcal{J}(t' - t)$  with the integral over  $dt'$  ranging from  $t$  to  $\infty$ .

$t > t_d > t_u$ : The Heaviside functions in  $\Phi$  cancel because the arrival times of the injected anyons at the QPC are out of the integral bounds. It generates a vanishing  $\Phi$  leading to a trivial noise contribution

$$\int_t^\infty dt' \mathcal{J}(t' - t)(\cos(0) - 1) = 0.$$

$t_d > t > t_u$ : The functions with the time argument  $t_u$  nullify as  $t' > t > t_u$ . If we have  $-\Theta(t_d - t) = -1$  combined with  $\Theta(t_d - t')$ , it would result in a phase of zero when  $t' < t$ . Hence, we only have a finite noise contribution when  $t' > t_d$ .

$$\int_t^\infty dt' \mathcal{J}(t' - t)(\cos(2\vartheta[-1 + \Theta(t_d - t')]) - 1) = \int_{t_d}^\infty dt' \mathcal{J}(t' - t)(\cos(2\vartheta) - 1).$$

$t_d > t_u > t$ : The Heaviside functions dependent on  $t$  cancel out each other. The leftover functions contribute to the noise only when  $t_d > t' > t_u$ .

$$\int_t^\infty dt' \mathcal{J}(t' - t)(\cos(2\vartheta[\Theta(t_d - t') - \Theta(t_u - t')]) - 1) = \int_{t_u}^{t_d} dt' \mathcal{J}(t' - t)(\cos(2\vartheta) - 1).$$

Combining all the cases, we obtain the final contribution

$$\begin{aligned} \int_t^\infty dt' &\implies \Theta(t_d - t) \left[ \Theta(t - t_u) \int_{t_d}^\infty dt' \mathcal{J}(t' - t) + \Theta(t_u - t) \int_{t_u}^{t_d} dt' \mathcal{J}(t' - t) \right], \\ \int_{-\infty}^\infty \frac{dt}{T} \int_t^\infty dt' &\implies \int_{t_u}^{t_d} \frac{dt}{T} \int_{t_d}^\infty dt' \mathcal{J}(t' - t) + \int_{-\infty}^{t_u} \frac{dt}{T} \int_{t_u}^{t_d} dt' \mathcal{J}(t' - t). \end{aligned} \quad (4.17)$$

Likewise, the contribution from the second term  $\mathcal{J}(t - t')$  in Eq. (4.16) with the integral over  $dt'$  ranging from  $-\infty$  to  $t$  is calculated to be

$$\int_{-\infty}^\infty \frac{dt}{T} \int_{-\infty}^t dt' \implies \int_{t_d}^\infty \frac{dt}{T} \int_{t_u}^{t_d} dt' \mathcal{J}(t - t') + \int_{t_u}^{t_d} \frac{dt}{T} \int_{-\infty}^{t_u} dt' \mathcal{J}(t - t'). \quad (4.18)$$

Taking both Eqs. (4.17) and (4.18) into account, we find excess HOM noise for  $t_d > t_u$

$$\Delta S_{HOM}^{(11)} = 2(2q\nu\Lambda)^2 \cos(2\pi\delta)(\cos(2\vartheta) - 1) \int_{t_u}^{t_d} \frac{dt}{T} \left[ \int_{t_d}^\infty dt' \mathcal{J}(t' - t) + \int_{-\infty}^{t_u} dt' \mathcal{J}(t - t') \right].$$

Considering the case when  $t_u > t_d$  will switch the arrival times in the above equation. Analogous to the tunneling current computations, introducing the tunable delay  $\tau_d = t_d - t_u$  and accounting for both cases gives the final HOM noise

$$\Delta S_{HOM}^{(11)} = 2(2q\nu\Lambda)^2 \cos(2\pi\delta)(\cos(2\vartheta) - 1) \int_0^{|\tau_d|} \frac{dt}{T} \left[ \int_{|\tau_d|}^\infty dt' \mathcal{J}(t' - t) + \int_{-\infty}^0 dt' \mathcal{J}(t - t') \right]. \quad (4.19)$$

As explained in Sec. 3.5, the HOM noise ratio  $\mathcal{R}(\tau_d)$  is calculated by normalizing the excess HOM noise with twice the value of excess noise in the HBT configuration. The auxiliary state defined by  $|\varphi\rangle = \psi_{u/d}^\dagger(x_{u/d}, t_{u/d}) |0\rangle$  corresponds to a single quasiparticle injection in

either of the upper or lower edges. Starting from Eq. (4.14), repeating the previous calculations using the **HBT** auxiliary state generates a phase  $\Phi_{\text{HBT}} = 2\vartheta [\Theta(t_u - t) - \Theta(t_u - t')]$  within the cosine function, leading to the following **HBT** noise:

$$\begin{aligned} \Delta S_{\text{HBT}}^{(11)} &= (2q\nu\Lambda)^2 \cos(2\pi\delta)(\cos(2\vartheta) - 1) \left[ \int_{-\infty}^{t_u} \frac{dt}{T} \int_{t_u}^{\infty} dt' \mathcal{J}(t' - t) + \int_{t_u}^{\infty} \frac{dt}{T} \int_{-\infty}^{t_u} dt' \mathcal{J}(t - t') \right], \\ &= 2(2q\nu\Lambda)^2 \cos(2\pi\delta)(\cos(2\vartheta) - 1) \left[ \int_{-\infty}^0 \frac{dt}{T} \int_0^{\infty} dt' \mathcal{J}(t' - t) \right]. \end{aligned} \quad (4.20)$$

Dividing Eq. (4.19) with Eq. (4.20) yields the standard **HOM** noise ratio as

$$\mathcal{R}(\tau_d) = \frac{\Delta S_{\text{HOM}}^{(11)}}{2\Delta S_{\text{HBT}}^{(11)}} = \frac{1 \cancel{(\cos(2\vartheta) - 1)} \int_0^{|\tau_d|} dt \left[ \int_{|\tau_d|}^{\infty} dt' \mathcal{J}(t' - t) + \int_{-\infty}^0 dt' \mathcal{J}(t - t') \right]}{2 \cancel{(\cos(2\vartheta) - 1)} \int_{-\infty}^0 dt \int_0^{\infty} dt' \mathcal{J}(t' - t)}. \quad (4.21)$$

It is clear from Eq. (4.21) that the information about the braiding phase is erased from the standard **HOM** noise ratio. This observation is a key result in this thesis. Using the relations derived in Appendix D, we can express  $\mathcal{R}(\tau_d)$  in terms of the incomplete Beta functions and rewrite the noise ratio as

$$\begin{aligned} \mathcal{R}(\tau_d) &= \frac{1 \int_0^{|\tau_d|} dt \left[ \mathcal{B}\left(e^{-2\pi k_B \theta t}; 2\delta, 1 - 4\delta\right) + \mathcal{B}\left(e^{2\pi k_B \theta(t - |\tau_d|)}; 2\delta, 1 - 4\delta\right) \right]}{2 \int_0^{\infty} dt \mathcal{B}\left(e^{-2\pi k_B \theta t}; 2\delta, 1 - 4\delta\right)}, \\ &= \frac{1}{2} \left[ 1 + \frac{\int_0^{|\tau_d|} dt \mathcal{B}\left(e^{2\pi k_B \theta(t - |\tau_d|)}; 2\delta, 1 - 4\delta\right) - \int_{-\infty}^0 dt \mathcal{B}\left(e^{2\pi k_B \theta(t - |\tau_d|)}; 2\delta, 1 - 4\delta\right)}{\int_{-\infty}^0 dt \mathcal{B}\left(e^{2\pi k_B \theta t}; 2\delta, 1 - 4\delta\right)} \right], \\ &= \frac{1}{2} [1 + \mathcal{F}(\tau_d, \delta, \theta)], \end{aligned} \quad (4.22)$$

where

$$\mathcal{F}(\tau_d, \delta, \theta) \equiv \frac{\int_0^{|\tau_d|} dt \mathcal{B}\left(e^{2\pi k_B \theta(t - |\tau_d|)}; 2\delta, 1 - 4\delta\right) - \int_{-\infty}^0 dt \mathcal{B}\left(e^{2\pi k_B \theta(t - |\tau_d|)}; 2\delta, 1 - 4\delta\right)}{\int_{-\infty}^0 dt \mathcal{B}\left(e^{2\pi k_B \theta t}; 2\delta, 1 - 4\delta\right)}. \quad (4.23)$$

The **HOM** noise ratio is thus solely dependent on the tunable delay ( $\tau_d$ ), scaling dimension of the tunneling **QPC** quasi-particle-hole pairs ( $\delta$ ), and temperature ( $\theta$ ). The presence of the exchange phase  $\vartheta$  in the excess noise expressions validate braiding between the quasi-particle-hole pairs excitations and the incoming injected anyons at the **QPC**. However, its erasure from  $\mathcal{R}(\tau_d)$  illustrates the cancellation of the acquired universal braiding phase through subprocesses (previously unaccounted for) occurring at the collider **QPC**. The relegation of the acquired  $\vartheta$  to a trivial phase is responsible for the **HOM** noise dip at zero time delay  $\tau_d = 0$  in a fractional filling factor  $\nu = 1/3$ , as depicted in Fig. 4.3. Interestingly, the width of the anyonic **HOM** dip is governed by the temperature  $\theta$ . The noise dip width demonstrates a progressive growth with decreasing temperatures, exhibiting an inverse relationship. It starkly contrasts the temperature-independent noise suppression observed in the **HOM** for electrons. Instead, the width of the Pauli dip for electrons is directly

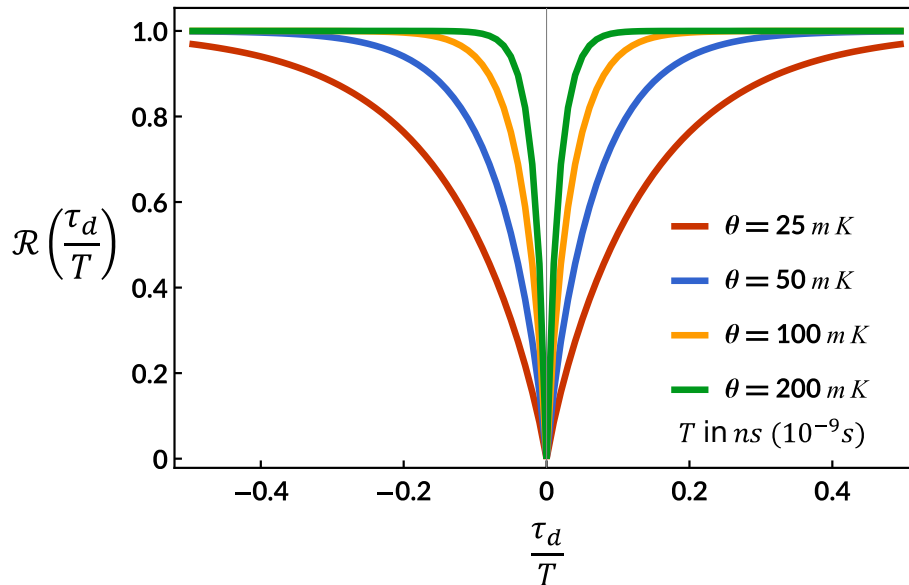


**Figure 4.3:** A plot of the **HOM** noise ratio  $\mathcal{R}$  as a function of the dimensionless delay parameter  $\tau_d/T$  at  $\nu = 1/3$  for varying temperatures  $\theta$  ranging from  $25 \text{ mK}$  –  $200 \text{ mK}$ . The parameter  $k_B$  is set to 1. Ideal time-resolved anyon injections at  $t_u$  and  $t_d$  into the upper and lower edges were modeled by the auxiliary state  $|\varphi\rangle = \psi_u^\dagger(x_u, t_u)\psi_d^\dagger(x_d, t_d)|0\rangle$ .

proportional to the temporal extension of the incoming electronic excitations that interfere at the **QPC** [23, 66, 84]. Equation (4.22) represents the time-sensitive interference between injected point-like anyons and the **QPC** quasi-particle-hole excitations as a function of temperature, scaling dimension, and delay. The temperature-dependent variation of the anyonic **HOM** noise ratio thus characterizes the modulation of the non-universal scaling dimension delta of the tunneling quasi-particle-hole pairs created at timescales  $t$  and  $t'$ . Despite the unique characteristics of the **HOM** ratio for anyons, it fails to capture information about the universal braiding phase  $\vartheta$  to probe fractional statistics. The erasure of the exchange phase from  $\mathcal{R}(\tau_d)$  might appear as a consequence of the standard normalization of **HOM** noise with the noise from the **HBT** configuration. Selecting a different normalization (of experimental relevance) for the **HOM** noise retains the braiding phase in  $\mathcal{R}^{(0)}(\tau_d)$  as illustrated in Eq. (4.24). However, in this case, the braiding phase cannot be disentangled from the other factors containing the scaling dimension  $\delta$ .

$$\mathcal{R}^{(0)}(\tau_d) = \frac{\Delta S_{HOM}^{(11)}}{S^{(0)}} = (\cos(2\vartheta) - 1) \frac{\int_0^{|\tau_d|} dt \left[ \int_{|\tau_d|}^{\infty} dt' \mathcal{J}(t' - t) + \int_{-\infty}^0 dt' \mathcal{J}(t - t') \right]}{\int_{-\infty}^{\infty} dt \int_{-\infty}^{\infty} dt' \mathcal{J}(|t' - t|)}. \quad (4.24)$$

Hence, we conclude that, contrary to fermions and bosons, the standard **HOM** ratio in a two-particle **FQH** interferometer for anyons does not allow direct observation of their exchange statistics, in contrast to the naive expectation illustrated in Fig. 1.8. Instead, the **HOM** ratio [Eq. (4.21)] probes the non-universal scaling dimension  $\delta$  of the quasi-particle-hole pairs created at the **QPC**.

## 4.4 Interpreting the braiding phase erasure

In this section, we provide a physical interpretation for the exchange phase erasure observed in the **HOM** interferometry for anyons based on the methods introduced in Refs. [44, 45]. Fractional statistics is rendered invisible for a time-resolved injection of anyons in the single-**QPC** Laughlin **FQH** setup depicted in Fig. 4.1. However, as discussed in the previous sections, the presence of the statistical exchange phase  $\vartheta$  in the current and noise expressions indicates braiding between injected anyons and the quasi-particle-hole excitations at the **QPC**. Because point-like tunneling prohibits spatial closed-loop trajectories of one quasiparticle around another, we may argue that the braiding processes occur in the time domain. To develop this point of view, we rearrange the expression for the noise in Eq. (4.14) into an interference pattern between different quantum states.

$$S_{HOM}^{(11)} \propto \int_{-\infty}^{\infty} \frac{dt}{T} \int_{-\infty}^{\infty} dt' \left[ {}_+ \langle t, \tau_d | t', \tau_d \rangle_+ + {}_+ \langle t', \tau_d | t, \tau_d \rangle_+ \right. \\ \left. + {}_- \langle t, \tau_d | t', \tau_d \rangle_- + {}_- \langle t', \tau_d | t, \tau_d \rangle_- \right], \quad (4.25)$$

where  $\tau_d = t_d - t_u$  corresponds to the tunable time delay between the arrival of the injected anyons at the **QPC**. The quantum states in Eq. (4.25) are defined with respect to the **HOM** auxiliary state  $|\varphi\rangle$  as the following:

$$|t, \tau_d\rangle_- = A(t) |\varphi\rangle \quad |t, \tau_d\rangle_+ = A^\dagger(t) |\varphi\rangle, \quad (4.26)$$

$${}_-\langle t, \tau_d| = \langle\varphi| A^\dagger(t) \quad {}_+\langle t, \tau_d| = \langle\varphi| A(t), \quad (4.27)$$

The auxiliary state in the above equations is solely dependent on  $\tau_d$  and is defined as  $|\varphi\rangle = \psi_u^\dagger(0)\psi_d^\dagger(\tau_d) |0\rangle$ . This auxiliary state, which varies based on the delay  $\tau_d$ , is obtained through a straightforward change of variables using  $\tau_d = t_d - t_u$ . By definition, the operator  $A(t)$  creates a quasiparticle in the upper edge ( $u$ ) and a quasi-hole in the lower edge ( $d$ ) with a charge  $q\nu$  at time  $t$ . Correspondingly its Hermitian conjugate  $A^\dagger(t)$  creates a quasi-hole and a quasiparticle in the upper ( $u$ ) and lower edge ( $d$ ), respectively. As elaborated in Sec. 4.2, products of the form  $\langle A^\dagger(t)A(t') \rangle_{qp}$  acquires the braiding phase  $\vartheta$  only when the arrival times coincide with the quasi-particle-hole pair creation times  $t$  and  $t'$  at the **QPC**. To proceed with our interpretation, we assume  $t' > t_u, t_d > t$  without loss of generality. From a more physical point of view, this implies:

$|t, \tau_d\rangle_\pm$ : Tunneling quasi-particle-hole pairs are excited *before* the arrival of the injected anyons at the **QPC** (the state  $|t, \tau_d\rangle_-$  is depicted in Fig. 4.4a).

$|t', \tau_d\rangle_\pm$ : Tunneling quasi-particle-hole pairs are excited *after* the arrival of the injected anyons at the **QPC** (the state  $|t', \tau_d\rangle_-$  is depicted in Fig. 4.4b).

To understand the braiding mechanisms occurring at the **QPC** within the time window  $(t', t)$ , we examine the inner product of the quantum states with the index  $k = -$  in Eq. (4.25). These components represent interference between the creation of quasiparticles in the upper edge and quasiholes in the lower edge [corresponding to the tunneling operator  $A(t)$ ] at the **QPC** at times  $t, t'$ . The complex conjugate of a quantum state in the inner product terms of Eq. (4.25) creates interference loops by reversing the paths traced by the injected and excited quasiparticles in the time domain.

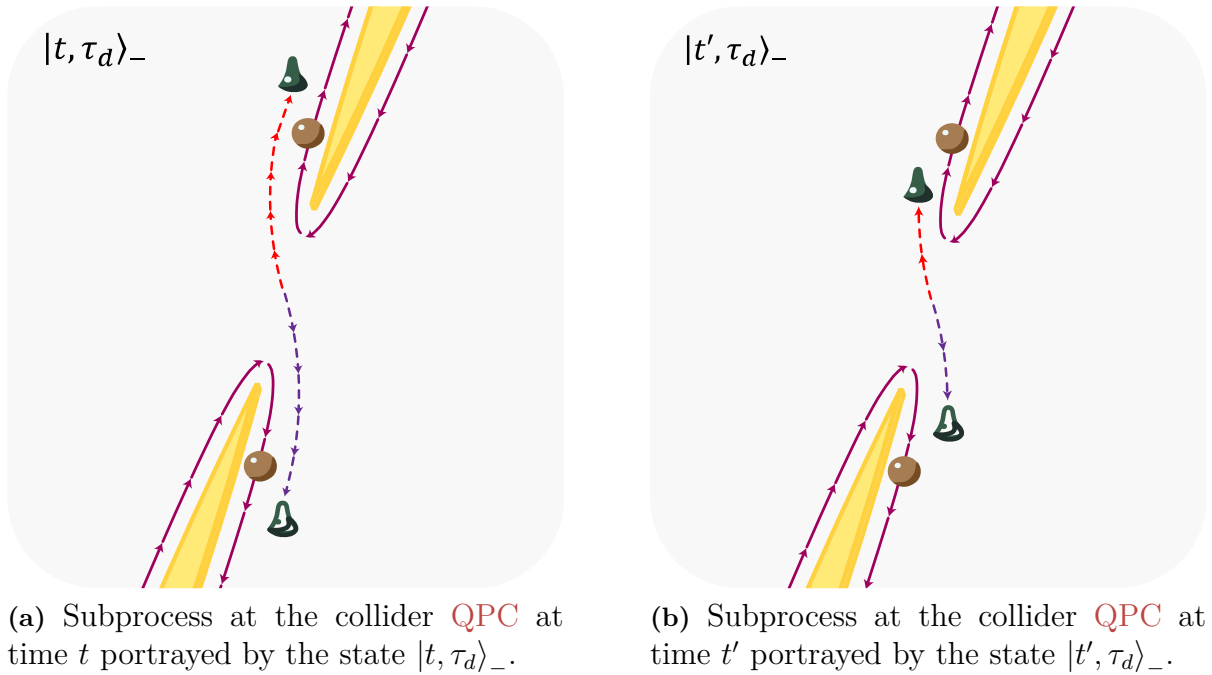
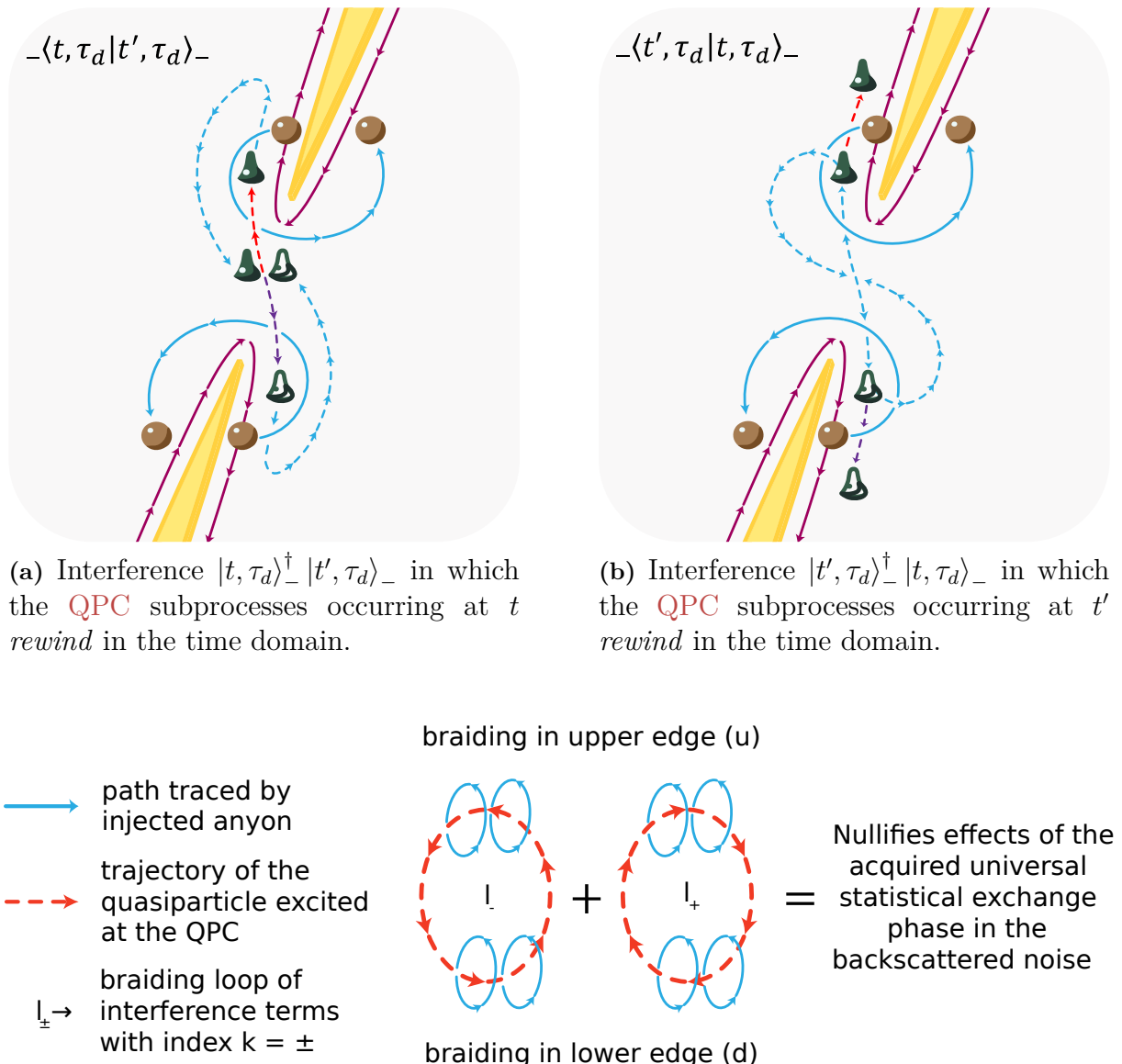


**Figure 4.4:** Pictorial representation of the subprocesses occurring at the tunneling QPC of the setup in the Laughlin sequence with  $\nu = 1/(2n + 1)$  depicted in Fig. 4.1. The subprocesses at times  $t$  and  $t'$  share the same spatial location of the injected anyons (brown spheres with solid purple trajectories).  $\tau_d$  is the tunable delay governing the arrival times of the upper ( $u$ ) and lower edge ( $d$ ) anyons at the QPC. Tunneling quasiparticle-hole pairs (green peaks with a dotted red trajectory for quasiparticle and white peaks with a dotted violet trajectory for its hole) are excited at the QPC at  $t$  and  $t'$  due to thermal or quantum (vacuum) fluctuations. Based on the assumption  $t' > t_u, t_d > t$ , the quasi-particle-hole pair creation at time  $t$  happens before the arrival of the injected anyons as depicted in (a). In comparison, the excitation at  $t'$  occurs after the injected anyons have passed the collider QPC as shown in (b).

These time domain braiding processes are illustrated in Fig. 4.5. Particle trajectories at a later time interval overlap with the paths traced by particles preceding in time, as shown in Figs. 4.5a and 4.5b. The closed-loop interference trajectories ( $l_-$ ), generated by rewinding the time axis, braid the quasiparticle excitations (portrayed by dotted red trajectories) with the injected anyons in an anti-clockwise direction. Likewise, the interference components with the index  $k = +$  from Eq. (4.25) correspond to braiding processes between the injected anyons and the tunneling quasiparticles in a clockwise direction ( $l_+$ ). Superposing the counteracting interference loops cancels any effects of the acquired braiding phase  $\vartheta$  from the backscattered noise<sup>2</sup>, as shown in Fig. 4.5c. Moreover, as demonstrated in

<sup>2</sup>The interpretation holds for unsymmetrized noise discussed in Chapter 3. In such a scenario, the HOM noise is given only by two interference terms  $S_{HOM}^{(11)} \propto \int_{-\infty}^{\infty} dt \int_{-\infty}^{\infty} dt' {}_+ \langle t, \tau_d | t', \tau_d \rangle_+ + {}_- \langle t, \tau_d | t', \tau_d \rangle_-$ . It results in a single braiding process (depicted by the blue loop in Fig. 4.5c) between the injected anyon and the tunneling quasiparticle excited at the QPC, occurring in both the upper and lower edges (i.e., the loops  $l_{\pm}$  would only consist of two blue loops instead of four). Likewise, the interference loops compensate each other, eliminating the braiding angle effects in the HOM noise. Notably, both forms of backscattered noise are equivalent and lead to the same physical interpretation.



(c) Pictograph depicting the different interference loops arising at the collider QPC that negate the braiding effects in the HOM noise.

**Figure 4.5:** Time domain braiding between the injected anyons and the quasi-particle-hole excitations at the QPC at times  $t$  and  $t'$ . The blue trajectories depicted in (a) and (b) denote the *rewound* path in the time axis corresponding to the interference between the quantum states with the index  $k = -$ . The trajectories occurring at later time intervals cut through (overlap) and superimpose on the traced paths preceding in time. In the subprocess (a), the quasi-particle-hole pairs excited at time  $t$  rewind to form the interference loop that braids the injected anyons. Considering the path traced only by the excited quasiparticle (in red trajectories), the braiding happens in an anticlockwise direction. Likewise, in the subprocess (b), the excitations at  $t'$  are reversed in time to braid the injected anyons also in a counterclockwise direction (with respect to quasiparticle). On the contrary, in the interference subprocesses with an index  $k = +$  from Eq. (4.25), the tunneling quasiparticles braid the injected anyons in a clockwise direction. Coalescing these two counterbalancing interference loops [as portrayed in (c)] demonstrates the erasure of the effects of the acquired braiding phase in the HOM noise.

Sec. 4.3, simultaneous arrival of injected anyons at the QPC with zero time delay  $\tau_d = 0$  assigns a trivial phase to the products of the form  $\langle A^\dagger(t)A(t') \rangle_{qp} = {}_+\langle t, 0 | t', 0 \rangle_+$  leading to a vanishing HOM noise as depicted in Fig. 4.3. The interference pattern in Eq. (4.25) can be reformulated into a summation of the squared magnitude of the superposition of two quantum states as follows:

$$S_{HOM}^{(11)} \propto \int_{-\infty}^{\infty} \frac{dt}{T} \int_{-\infty}^{\infty} dt' | |t, t_0\rangle_{\pm} + |t', t_0\rangle_{\pm} |^2 - | |t, t_0\rangle_{\mp} - |t', t_0\rangle_{\mp} |^2. \quad (4.28)$$

The superposition of the states with index  $k = -$  corresponding to the tunneling operator  $A(t)$  gives us the interference between the creation of a quasiparticle in the upper edge ( $u$ ) and quasihole in the lower edge ( $d$ ). Whereas the components with index  $k = +$  linked to  $A^\dagger(t)$  entail the reverse scenario of quasihole in ( $u$ ) and quasiparticle in ( $d$ ).

The outlined time domain interference processes are possible only when the injected anyon passes through the collider QPC without tunneling to the counter-propagating edge mode. This scenario of braiding with the QPC quasiparticle excitations dominates the conventional collision of two injected anyons in the low-temperature regime  $V_{applied} > k_b\theta$ . In the latter case, injected anyons collide with each other after direct tunneling at the QPC. The suppression of the conventional anyon collisions can be attributed to the slow decay of the quasiparticle correlations (as described by the Green's function) due to their Laughlin fractional filling factor  $\nu = 1/(2n + 1) < 1$ . The slow decay of the correlation function permits a larger time window ( $t', t$ ) of interaction between the quasiparticles that promote braiding processes at the QPC within the span  $t' > t_u, t_d > t$  or  $t' < t_u, t_d < t$ .

This signatory behavior of anyons is also reflected in our analysis of the quasiparticle tunneling current with voltage drives in Chapter 3. It is implied by the slowly decreasing tunneling current in the DC regime by  $\langle I_T(t) \rangle \propto V_{applied}^{2\nu-1}$  and by an exponential decay in the AC regime  $\langle I_T(t) \rangle \propto e^{\pm i q \nu \int_0^t d\tau V_{AC}(\tau)}$  for  $\nu < 1$  (from the photoassisted coefficients  $p_l$ , cf. Appendix C). This behavior is in sharp contrast to the case of electrons with  $\nu = 1$ , where the current is non-zero only when the injected electronic pulse arrives at the QPC. This feature suggests that the contribution to the tunneling current and noise is mainly due to the direct fermionic collisions (interference between injected electrons) occurring at the QPC within the short time span  $t \simeq 0$ , suppressing any non-trivial interference effects transpiring before or after the arrival times at the QPC [45, 63]. Moreover, braiding of electrons lacks conventional meaning, as the acquired phase becomes trivial  $e^{2i\vartheta} = 1$ , where  $\vartheta = \nu\pi$ . Notably, it also implies that the soliton excitation of the compact bosons developed in Sec. 4.2 [cf. Eqs. (4.4) and (4.5)] would be incompatible with electrons. One cannot extend it directly to fermions by taking  $\nu = 1$  (compared to our approach in Chapter 3) [83]. To summarize, the conventional interference of the injected electronic pulses is promoted by the short-time interactions ( $t \simeq 0$ ) for electrons with  $\nu = 1$ . It enables the investigation of their inherent Fermi-Dirac statistics through HOM interferometry. However, the long-time correlations ( $t' > t_u, t_d > t$  or  $t' < t_u, t_d < t$ ) of anyons with  $\nu < 1$ , allow non-trivial counterbalancing braiding processes that cancel the effects of the acquired statistical exchange phase in the HOM noise.



# 5

## Conclusion

In this thesis, we explored the idea of Hong-Ou-Mandel interferometry to anyons in the Laughlin sequence with filling factor  $\nu = 1/(2n+1)$ ,  $n \in \mathbb{Z}^+$ , to investigate their fractional statistics. As detailed in Chapter 1, the fluctuations observed in the **HOM** experiment are known to provide insights into the quantum statistics of indistinguishable particles when they are fermions or bosons. Our theoretical model of anyonic **HOM** was developed for the fractional quantum Hall effect, which offers a reliable and well-established platform for hosting anyons. Moreover, the feasibility of implementing interferometry components (anyon sources, waveguides, and quasiparticle beam splitter) in quantum Hall systems was instrumental in the recent experimental demonstration of anyon statistics.

Chapter 2 introduced theoretical tools for understanding anyon collisions in a Laughlin **FQH** setup. These included time evolution pictures, Landau levels in the **FQH** regime, one-dimensional chiral edge modes, bosonization, and quasiparticle creation operators. The subsequent chapters focused on deriving and interpreting the backscattered current and noise resulting from quasiparticle interactions at the collider **QPC** in the limit  $V_{\text{applied}} > k_B\theta$ . A summary of the main results and conclusions are:

- A single-**QPC FQH** collider in the Laughlin sequence, driven by conventional voltage sources, exhibits a vanishing **HOM** noise ratio for synchronized collisions ( $\tau_d = 0$ ) at fractional filling factors. This behavior of the noise ratio arises from the inability of conventional voltage sources to emit a single time-resolved fractionally charged quasiparticle through any of the Lorentzian, sinusoidal, or square voltage drives. Therefore, the Pauli dip observed at fractional filling factors exposes the inherent fermionic nature of the excitations induced by the voltage sources into the Laughlin **FQH** setup [Chapter 3].
- By modeling an ideal time-resolved anyon source with an auxiliary state, we obtained a vanishing tunneling current at zero time delay that also leads to a disappearing **HOM** noise. This behavior arises due to the single-**QPC** geometry of the Laughlin **FQH** setup, which results in the **HOM** configuration at null delay being equivalent to maintaining the system at equilibrium (zero net bias  $\Delta V = 0$ ), leading to vanishing observables. Furthermore, the suppression of **HOM** noise ratio for anyons does not indicate Fermi-Dirac statistics; instead, it points to a complex interaction of quasiparticles at the collider **QPC** [Chapter 4].
- Extending the auxiliary state approach to compute the **HOM** noise ratio  $\mathcal{R}(\tau_d)$  reveals the inverse relationship between the width of the anyonic **HOM** dip and temperature  $\theta$ . It contrasts with the case of electrons, where the width of the Pauli dip remains temperature-independent and only exhibits a linear relationship with the temporal extension of the interfering electronic wavepackets. Despite this sig-

natory feature, the anyonic **HOM** ratio fails to capture information about fractional statistics. Instead, it probes the non-universal scaling dimension of the tunneling quasi-particle-hole pairs excited at the collider **QPC** due to thermal or quantum (vacuum) fluctuations [Chapter 4].

- The point-like tunneling prohibits spatial closed-loop trajectories of one quasiparticle around another; however, reformulating the backscattered noise into an interference pattern reveals time domain braiding between the injected anyons and the quasi-particle-hole excitations at the **QPC**. The slow decay of the quasiparticle correlations (Green's function) with  $\nu < 1$  facilitates a long-time interaction window  $(t', t)$  between the injected anyons and **QPC** tunneling quasiparticles that dominates the direct collision of two injected anyons at the **QPC**. It promotes temporal braiding subprocesses between the injected anyons and the **QPC** quasiparticles within  $t' > t_u, t_d > t$  or  $t' < t_u, t_d < t$ . However, the counterbalancing time-dependent interference loops negate the effects of the acquired statistical exchange phase in the **HOM** noise. It is strikingly different for electrons with  $\nu = 1$ , where the main contribution to the tunneling current and noise is from direct collisions occurring at the **QPC** within the short period  $t \simeq 0$  [Chapter 4].

In a nutshell, fractional statistics is rendered invisible in the standard Hong-Ou-Mandel interference of anyons. The noise ratio does not display any explicit trace of anyon statistics because the universal braiding phase cancels out in the zero-frequency backscattered noise. Instead, the **HOM** ratio gives access to the anyon scaling dimension  $\delta$ , which is another important property of the FQH edge. In particular, the scaling dimension can be used to infer the influence of interactions [58, 85], edge reconstruction effects [86], or even to distinguish between various proposed edge theories in exotic FQH states [87].

# 6

## Outlook

Possible extensions of this work addressing the questions that were not tackled in this thesis project are outlined below:

- We only focused on computing the zero-frequency noise in **HBT** and **HOM** configurations to probe the statistical exchange phase of anyons. Investigating the finite frequency noise in the collider setup offers a potential avenue to access information about the universal braiding phase.
- We modeled ideal time-resolved anyon sources with the auxiliary state composed of quasiparticle creation operators. Although there are proposals of voltage sources capable of exciting single quasiparticles with fractional charge  $q\nu$ , they cannot be realized experimentally [63]. It would be interesting to explore practical setups that could serve as optimal time-resolved sources of single anyons.
- This work was devoted to studying Abelian anyons in the Laughlin sequence. Nevertheless, there is scope for generalization to non-Abelian anyons and more intricate **FQH** setups consisting of multiple counter and copropagating edge modes with intra- and inter-channel interactions [82, 88].

Several research paradigms are currently underway to investigate anyons and probe their fractional statistics. Below, we present a selection of a few alternative methodologies:

- Our study concentrated on utilizing the Hong-Ou-Mandel interferometry to probe the quantum statistics of anyons. However, there are other interference techniques capable of revealing fractional statistics. Direct observation of anyonic braiding statistics was reported utilizing a multipath Fabry–Pérot interferometer at fractional filling factor  $\nu = 1/3$  [13]. Braiding of anyons was also demonstrated in a two-path Mach-Zehnder interferometer with bulk filling tuned to  $\nu = 2/5$  comprising edge modes at  $\nu = 1/3$  [89].
- Our study centers around the exotic physics of the fractional quantum Hall effect to understand the properties of anyons. Researchers are also exploring complementary testbeds, such as ultracold atoms in an optical lattice, to realize and investigate anyons [90].



# Bibliography

- <sup>1</sup>R. Feynman, “The Feynman lectures on physics”, <https://www.feynmanlectures.caltech.edu/> (2017).
- <sup>2</sup>G. Bacciagaluppi and A. Valentini, *Quantum theory at the crossroads* (Cambridge University Press, Oct. 2009).
- <sup>3</sup>J. Fröhlich, “Statistics of fields, the Yang-Baxter equation, and the theory of knots and links”, in *Nonperturbative quantum field theory* (Springer US, 1988), pp. 71–100.
- <sup>4</sup>G. Moore and N. Read, “Nonabelions in the fractional quantum Hall effect”, *Nuclear Physics B* **360**, 362–396 (1991).
- <sup>5</sup>X. G. Wen, “Non-abelian statistics in the fractional quantum Hall states”, *Phys. Rev. Lett.* **66**, 802–805 (1991).
- <sup>6</sup>C. Nayak, S. H. Simon, A. Stern, M. Freedman, and S. Das Sarma, “Non-abelian anyons and topological quantum computation”, *Rev. Mod. Phys.* **80**, 1083–1159 (2008).
- <sup>7</sup>J. M. Leinaas and J. Myrheim, “On the theory of identical particles”, *Il Nuovo Cimento B Series* **11** **37**, 1–23 (1977).
- <sup>8</sup>G. A. Goldin, R. Menikoff, and D. H. Sharp, “Particle statistics from induced representations of a local current group”, *Journal of Mathematical Physics* **21**, 650–664 (1980).
- <sup>9</sup>G. A. Goldin, R. Menikoff, and D. H. Sharp, “Representations of a local current algebra in nonsimply connected space and the Aharonov–Bohm effect”, *Journal of Mathematical Physics* **22**, 1664–1668 (1981).
- <sup>10</sup>F. Wilczek, “Magnetic flux, angular momentum, and statistics”, *Phys. Rev. Lett.* **48**, 1144–1146 (1982).
- <sup>11</sup>F. Wilczek, “Quantum mechanics of fractional-spin particles”, *Phys. Rev. Lett.* **49**, 957–959 (1982).
- <sup>12</sup>A. Kitaev, “Fault-tolerant quantum computation by anyons”, *Annals of Physics* **303**, 2–30 (2003).
- <sup>13</sup>J. Nakamura, S. Liang, G. C. Gardner, and M. J. Manfra, “Direct observation of anyonic braiding statistics”, *Nature Physics* **16**, 931–936 (2020).
- <sup>14</sup>H. Bartolomei, M. Kumar, R. Bisognin, A. Marguerite, J.-M. Berroir, E. Bocquillon, B. Plaçais, A. Cavanna, Q. Dong, U. Gennser, Y. Jin, and G. Fève, “Fractional statistics in anyon collisions”, *Science* **368**, 173–177 (2020).
- <sup>15</sup>J.-Y. M. Lee, C. Hong, T. Alkalay, N. Schiller, V. Umansky, M. Heiblum, Y. Oreg, and H.-S. Sim, “Partitioning of diluted anyons reveals their braiding statistics”, *Nature* **617**, 277–281 (2023).
- <sup>16</sup>M. Ruelle, E. Frigerio, J.-M. Berroir, B. Plaçais, J. Rech, A. Cavanna, U. Gennser, Y. Jin, and G. Fève, “Comparing fractional quantum Hall Laughlin and Jain topological orders with the anyon collider”, *Phys. Rev. X* **13**, 011031 (2023).

- <sup>17</sup>P. Glidic, O. Maillet, A. Aassime, C. Piquard, A. Cavanna, U. Gennser, Y. Jin, A. Anthore, and F. Pierre, “Cross-correlation investigation of anyon statistics in the  $\nu = 1/3$  and  $2/5$  fractional quantum Hall states”, *Phys. Rev. X* **13**, 011030 (2023).
- <sup>18</sup>Y. Blanter and M. Büttiker, “Shot noise in mesoscopic conductors”, *Physics Reports* **336**, 1–166 (2000).
- <sup>19</sup>K. Kobayashi and M. Hashisaka, “Shot noise in mesoscopic systems: from single particles to quantum liquids”, *Journal of the Physical Society of Japan* **90**, 102001 (2021).
- <sup>20</sup>C. K. Hong, Z. Y. Ou, and L. Mandel, “Measurement of subpicosecond time intervals between two photons by interference”, *Physical Review Letters* **59**, 2044–2046 (1987).
- <sup>21</sup>S. Ol’khovskaya, J. Splettstoesser, M. Moskalets, and M. Büttiker, “Shot noise of a mesoscopic two-particle collider”, *Phys. Rev. Lett.* **101**, 166802 (2008).
- <sup>22</sup>A. Marguerite, E. Bocquillon, J.-M. Berroir, B. Plaçais, A. Cavanna, Y. Jin, P. Degiovanni, and G. Fève, “Two-particle interferometry in quantum Hall edge channels (Phys. Status Solidi B 3/2017)”, *Physica Status Solidi B* **254**, 1770215 (2017).
- <sup>23</sup>A. Marguerite, C. Cabart, C. Wahl, B. Roussel, V. Freulon, D. Ferraro, C. Grenier, J.-M. Berroir, B. Plaçais, T. Jonckheere, J. Rech, T. Martin, P. Degiovanni, A. Cavanna, Y. Jin, and G. Fève, “Decoherence and relaxation of a single electron in a one-dimensional conductor”, *Phys. Rev. B* **94**, 115311 (2016).
- <sup>24</sup>E. Bocquillon, V. Freulon, J.-M. Berroir, P. Degiovanni, B. Plaçais, A. Cavanna, Y. Jin, and G. Fève, “Coherence and indistinguishability of single electrons emitted by independent sources”, *Science* **339**, 1054–1057 (2013).
- <sup>25</sup>D. Arovas, J. R. Schrieffer, and F. Wilczek, “Fractional statistics and the quantum Hall effect”, *Phys. Rev. Lett.* **53**, 722–723 (1984).
- <sup>26</sup>V. Freulon, A. Marguerite, J.-M. Berroir, B. Plaçais, A. Cavanna, Y. Jin, and G. Fève, “Hong-Ou-Mandel experiment for temporal investigation of single-electron fractionalization”, *Nature Communications* **6**, 6854 (2015).
- <sup>27</sup>E. Bocquillon, F. D. Parmentier, C. Grenier, J.-M. Berroir, P. Degiovanni, D. C. Glattli, B. Plaçais, A. Cavanna, Y. Jin, and G. Fève, “Electron quantum optics: partitioning electrons one by one”, *Phys. Rev. Lett.* **108**, 196803 (2012).
- <sup>28</sup>I. Taktak, M. Kapfer, J. Nath, P. Roulleau, M. Acciai, J. Splettstoesser, I. Farrer, D. A. Ritchie, and D. C. Glattli, “Two-particle time-domain interferometry in the fractional quantum Hall effect regime”, *Nature Communications* **13**, 5863 (2022).
- <sup>29</sup>E. H. Hall, “On a new action of the magnet on electric currents”, *American Journal of Mathematics* **2**, 287 (1879).
- <sup>30</sup>K. v. Klitzing, G. Dorda, and M. Pepper, “New method for high-accuracy determination of the fine-structure constant based on quantized Hall resistance”, *Phys. Rev. Lett.* **45**, 494–497 (1980).
- <sup>31</sup>D. Tong, “Lectures on the quantum Hall effect”, <https://www.damtp.cam.ac.uk/user/tong/qhe.html> (2016).
- <sup>32</sup>R. B. Laughlin, “Anomalous quantum Hall effect: an incompressible quantum fluid with fractionally charged excitations”, *Phys. Rev. Lett.* **50**, 1395–1398 (1983).
- <sup>33</sup>X. G. Wen and A. Zee, “Classification of abelian quantum Hall states and matrix formulation of topological fluids”, *Phys. Rev. B* **46**, 2290–2301 (1992).
- <sup>34</sup>F. D. M. Haldane, “Fractional quantization of the Hall effect: a hierarchy of incompressible quantum fluid states”, *Phys. Rev. Lett.* **51**, 605–608 (1983).

- <sup>35</sup>D. C. Tsui, H. L. Stormer, and A. C. Gossard, “Two-dimensional magnetotransport in the extreme quantum limit”, *Phys. Rev. Lett.* **48**, 1559–1562 (1982).
- <sup>36</sup>J. P. Eisenstein and H. L. Stormer, “The fractional quantum Hall effect”, *Science* **248**, 1510–1516 (1990).
- <sup>37</sup>F. Wilczek, *Fractional statistics and anyon superconductivity* (World Scientific, Oct. 1990).
- <sup>38</sup>C. C. Dean and M. Pepper, “The transition from two- to one-dimensional electronic transport in narrow silicon accumulation layers”, *Journal of Physics C: Solid State Physics* **15**, L1287–L1297 (1982).
- <sup>39</sup>H. van Houten and C. Beenakker, “Quantum point contacts”, *Physics Today* **49**, 22–27 (1996).
- <sup>40</sup>C. L. Kane and M. P. A. Fisher, “Nonequilibrium noise and fractional charge in the quantum Hall effect”, *Phys. Rev. Lett.* **72**, 724–727 (1994).
- <sup>41</sup>L. Saminadayar, D. C. Glattli, Y. Jin, and B. Etienne, “Observation of the  $e/3$  fractionally charged Laughlin quasiparticle”, *Phys. Rev. Lett.* **79**, 2526–2529 (1997).
- <sup>42</sup>R. de-Picciotto, M. Reznikov, M. Heiblum, V. Umansky, G. Bunin, and D. Mahalu, “Direct observation of a fractional charge”, *Nature* **389**, 162–164 (1997).
- <sup>43</sup>B. Rosenow, I. P. Levkivskyi, and B. I. Halperin, “Current correlations from a mesoscopic anyon collider”, *Phys. Rev. Lett.* **116**, 156802 (2016).
- <sup>44</sup>B. Lee, C. Han, and H.-S. Sim, “Negative excess shot noise by anyon braiding”, *Phys. Rev. Lett.* **123**, 016803 (2019).
- <sup>45</sup>J.-Y. M. Lee and H.-S. Sim, “Non-abelian anyon collider”, *Nature Communications* **13**, 6660 (2022).
- <sup>46</sup>B. Bransden and C. Joachain, *Quantum mechanics* (Prentice Hall, 2000).
- <sup>47</sup>H. Bruus and K. Flensberg, *Many-body quantum theory in condensed matter physics - an introduction*, English (Oxford University Press, United States, 2004).
- <sup>48</sup>R. Kubo, “The fluctuation-dissipation theorem”, *Reports on Progress in Physics* **29**, 255–284 (1966).
- <sup>49</sup>C. L. Kane and M. P. A. Fisher, “Edge-state transport”, in *Perspectives in quantum Hall effects* (Wiley-VCH Verlag GmbH), pp. 109–159.
- <sup>50</sup>E. Miranda, “Introduction to bosonization”, *Brazilian Journal of Physics* **33**, 1 (2003).
- <sup>51</sup>P. M. Lavrov, O. V. Radchenko, and I. V. Tyutin, “Jacobi-type identities in algebras and superalgebras”, *Theoretical and Mathematical Physics* **179**, 550–558 (2014).
- <sup>52</sup>C. Gerry and P. Knight, *Introductory quantum optics* (Cambridge University Press, Oct. 2004).
- <sup>53</sup>D. C. Mattis, “New wave-operator identity applied to the study of persistent currents in 1d”, *Journal of Mathematical Physics* **15**, 609–612 (1974).
- <sup>54</sup>S. Mandelstam, “Soliton operators for the quantized sine-Gordon equation”, *Phys. Rev. D* **11**, 3026–3030 (1975).
- <sup>55</sup>P. D. Francesco, P. Mathieu, and D. Sénéchal, *Conformal field theory* (Springer New York, 1997).
- <sup>56</sup>X.-G. Wen, “Edge transport properties of the fractional quantum Hall states and weak-impurity scattering of a one-dimensional charge-density wave”, *Phys. Rev. B* **44**, 5708–5719 (1991).
- <sup>57</sup>C. L. Kane and M. P. A. Fisher, “Contacts and edge-state equilibration in the fractional quantum Hall effect”, *Phys. Rev. B* **52**, 17393–17405 (1995).

- <sup>58</sup>G. Zhang, I. V. Gornyi, and C. Spånslätt, “Delta- $T$  noise for weak tunneling in one-dimensional systems: interactions versus quantum statistics”, *Phys. Rev. B* **105**, 195423 (2022).
- <sup>59</sup>X.-G. Wen, “Topological orders and edge excitations in fractional quantum hall states”, in *Field theory, topology and condensed matter physics* (Springer Berlin Heidelberg), pp. 155–176.
- <sup>60</sup>F. Dolcini, R. C. Iotti, A. Montorsi, and F. Rossi, “Photoexcitation of electron wave packets in quantum spin Hall edge states: effects of chiral anomaly from a localized electric pulse”, *Phys. Rev. B* **94**, 165412 (2016).
- <sup>61</sup>A. Ambardar, *Digital signal processing: a modern introduction* (Thomson, 2007).
- <sup>62</sup>J. Rech, D. Ferraro, T. Jonckheere, L. Vannucci, M. Sasseti, and T. Martin, “Minimal excitations in the fractional quantum Hall regime”, *Phys. Rev. Lett.* **118**, 076801 (2017).
- <sup>63</sup>T. Jonckheere, J. Rech, B. Grémaud, and T. Martin, “Anyonic statistics revealed by the Hong-Ou-Mandel dip for fractional excitations”, *Phys. Rev. Lett.* **130**, 186203 (2023).
- <sup>64</sup>R. H. Brown and R. Q. Twiss, “A test of a new type of stellar interferometer on sirius”, *Nature* **178**, 1046–1048 (1956).
- <sup>65</sup>R. H. Brown and R. Q. Twiss, “Correlation between photons in two coherent beams of light”, *Nature* **177**, 27–29 (1956).
- <sup>66</sup>L. Vannucci, “Electron quantum optics at fractional filling factor: minimal excitation states and interferometry”, *PhD Thesis*, <https://iris.unige.it/handle/11567/929893> (2018).
- <sup>67</sup>M. Acciai, “Single - electron dynamics in topologically protected systems”, *PhD Thesis*, <https://iris.unige.it/handle/11567/987592> (2019).
- <sup>68</sup>M. H. Pedersen and M. Büttiker, “Scattering theory of photon-assisted electron transport”, *Phys. Rev. B* **58**, 12993–13006 (1998).
- <sup>69</sup>P. K. Tien and J. P. Gordon, “Multiphoton process observed in the interaction of microwave fields with the tunneling between superconductor films”, *Phys. Rev.* **129**, 647–651 (1963).
- <sup>70</sup>L. P. Kouwenhoven, S. Jauhar, K. McCormick, D. Dixon, P. L. McEuen, Y. V. Nazarov, N. C. van der Vaart, and C. T. Foxon, “Photon-assisted tunneling through a quantum dot”, *Phys. Rev. B* **50**, 2019–2022 (1994).
- <sup>71</sup>M. Moskalets and M. Büttiker, “Floquet scattering theory of quantum pumps”, *Phys. Rev. B* **66**, 205320 (2002).
- <sup>72</sup>V. S. Rychkov, M. L. Polianski, and M. Büttiker, “Photon-assisted electron-hole shot noise in multiterminal conductors”, *Phys. Rev. B* **72**, 155326 (2005).
- <sup>73</sup>C. L. Kane and M. P. A. Fisher, “Shot noise and the transmission of dilute Laughlin quasiparticles”, *Phys. Rev. B* **67**, 045307 (2003).
- <sup>74</sup>C. L. Kane and M. P. A. Fisher, “Transmission through barriers and resonant tunneling in an interacting one-dimensional electron gas”, *Phys. Rev. B* **46**, 15233–15262 (1992).
- <sup>75</sup>J. Keeling, I. Klich, and L. S. Levitov, “Minimal excitation states of electrons in one-dimensional wires”, *Phys. Rev. Lett.* **97**, 116403 (2006).
- <sup>76</sup>C. Mora, “Anyonic exchange in a beam splitter”, [10.48550/ARXIV.2212.05123](https://arxiv.org/abs/10.48550/ARXIV.2212.05123) (2022).
- <sup>77</sup>G. Arfken, H. Weber, and F. Harris, *Mathematical methods for physicists: a comprehensive guide* (Elsevier Science, 2013).
- <sup>78</sup>B. Rosenow and B. I. Halperin, “Nonuniversal behavior of scattering between fractional quantum Hall edges”, *Phys. Rev. Lett.* **88**, 096404 (2002).

- <sup>79</sup>E. Papa and A. H. MacDonald, “Interactions suppress quasiparticle tunneling at Hall bar constrictions”, *Phys. Rev. Lett.* **93**, 126801 (2004).
- <sup>80</sup>D. Ferraro, A. Braggio, M. Merlo, N. Magnoli, and M. Sassetti, “Relevance of multiple quasiparticle tunneling between edge states at  $\nu = p/(2np + 1)$ ”, *Phys. Rev. Lett.* **101**, 166805 (2008).
- <sup>81</sup>A. Braggio, D. Ferraro, M. Carrega, N. Magnoli, and M. Sassetti, “Environmental induced renormalization effects in quantum Hall edge states due to  $1/f$  noise and dissipation”, *New Journal of Physics* **14**, 093032 (2012).
- <sup>82</sup>R. Kumar, S. K. Srivastav, C. Spånslätt, K. Watanabe, T. Taniguchi, Y. Gefen, A. D. Mirlin, and A. Das, “Observation of ballistic upstream modes at fractional quantum Hall edges of graphene”, *Nature Communications* **13**, 213 (2022).
- <sup>83</sup>N. Schiller, Y. Shapira, A. Stern, and Y. Oreg, “Anyon statistics through conductance measurements of time-domain interferometry”, [10.48550/ARXIV.2301.00021](https://arxiv.org/abs/10.48550/ARXIV.2301.00021) (2023).
- <sup>84</sup>T. Jonckheere, J. Rech, C. Wahl, and T. Martin, “Electron and hole Hong-Ou-Mandel interferometry”, *Phys. Rev. B* **86**, 125425 (2012).
- <sup>85</sup>N. Schiller, Y. Oreg, and K. Snizhko, “Extracting the scaling dimension of quantum Hall quasiparticles from current correlations”, *Phys. Rev. B* **105**, 165150 (2022).
- <sup>86</sup>R. Sabo, I. Gurman, A. Rosenblatt, F. Lafont, D. Banitt, J. Park, M. Heiblum, Y. Gefen, V. Umansky, and D. Mahalu, “Edge reconstruction in fractional quantum Hall states”, *Nature Physics* **13**, 491–496 (2017).
- <sup>87</sup>I. P. Radu, J. B. Miller, C. M. Marcus, M. A. Kastner, L. N. Pfeiffer, and K. W. West, “Quasi-particle properties from tunneling in the  $\nu = 5/2$  fractional quantum Hall state”, *Science* **320**, 899–902 (2008).
- <sup>88</sup>C. Spånslätt, Y. Gefen, I. V. Gornyi, and D. G. Polyakov, “Contacts, equilibration, and interactions in fractional quantum Hall edge transport”, *Phys. Rev. B* **104**, 115416 (2021).
- <sup>89</sup>H. K. Kundu, S. Biswas, N. Ofek, V. Umansky, and M. Heiblum, “Anyonic interference and braiding phase in a mach-zehnder interferometer”, *Nature Physics* **19**, 515–521 (2023).
- <sup>90</sup>J. Kwan, P. Segura, Y. Li, S. Kim, A. V. Gorshkov, A. Eckardt, B. Bakkali-Hassani, and M. Greiner, “Realization of 1d anyons with arbitrary statistical phase”, [10.48550/ARXIV.2306.01737](https://arxiv.org/abs/10.48550/ARXIV.2306.01737) (2023).
- <sup>91</sup>I. Gradshteyn and I. Ryzhik, *Table of integrals, series, and products* (Elsevier Science, 2014).



# A

## Bosonic Green's Function

In this Appendix we evaluate the equilibrium bosonic Green's function [66, 67]

$$\mathcal{G}(x, t) = \langle \phi(x, t) \phi(0, 0) \rangle - \langle \phi^2(0, 0) \rangle. \quad (\text{A.1})$$

The calculations are presented for the right moving chiral bosonic field evolving as  $\phi_R(x, t) = \phi(x - vt, 0)$ , where  $v$  is the velocity of the edge mode, according to the Hamiltonian

$$H_0 = \frac{v}{4\pi\nu} \int dx (\partial_x \phi_R)^2 = \frac{v}{\nu} \sum_{k>0} k b_k^\dagger b_k, \quad (\text{A.2})$$

The bosonic field operators can be expressed in terms of the bona fide bosonic creation and annihilations operators as

$$\phi(x - vt, 0) = i\sqrt{\frac{2\pi\nu}{L}} \sum_{k>0} \frac{e^{-\alpha k/2}}{\sqrt{k}} [b_k e^{ik(x-vt)} - b_k^\dagger e^{-ik(x-vt)}]. \quad (\text{A.3})$$

Thermal excitations exist at finite temperature  $\theta$ , and the bona fide bosonic operators satisfy the following Bose-Einstein distribution equilibrium averages

$$\langle b_k^\dagger b_{k'} \rangle = \delta_{kk'} \frac{1}{e^{\frac{vk}{k_B\theta}} - 1} \quad \langle b_k b_{k'}^\dagger \rangle = \delta_{kk'} \frac{e^{\frac{vk}{k_B\theta}}}{e^{\frac{vk}{k_B\theta}} - 1}. \quad (\text{A.4})$$

Inserting (A.3) in (A.1) and using the relations in (A.4) gives

$$\begin{aligned} \phi(x - vt, 0) &= \frac{2\pi\nu}{L} \sum_{kk'>0} \frac{e^{-\alpha(k+k')/2}}{\sqrt{kk'}} \delta_{kk'} \left[ \frac{e^{\frac{vk}{k_B\theta}}}{e^{\frac{vk}{k_B\theta}} - 1} e^{ik(x-vt)} + \frac{1}{e^{\frac{vk}{k_B\theta}} - 1} e^{-ik(x-vt)} - \frac{e^{\frac{vk}{k_B\theta}} + 1}{e^{\frac{vk}{k_B\theta}} - 1} \right], \\ &= \frac{2\pi\nu}{L} \sum_{k>0} \frac{e^{-\alpha k}}{k} \left[ \cos(k(x - vt)) \frac{e^{\frac{vk}{k_B\theta}} + 1}{e^{\frac{vk}{k_B\theta}} - 1} + i \sin(k(x - vt)) \frac{e^{\frac{vk}{k_B\theta}} - 1}{e^{\frac{vk}{k_B\theta}} - 1} - \frac{e^{\frac{vk}{k_B\theta}} + 1}{e^{\frac{vk}{k_B\theta}} - 1} \right], \\ &= \frac{2\pi\nu}{L} \sum_{k>0} \frac{e^{-\alpha k}}{k} \left[ \cos(k(x - vt)) \coth\left(\frac{vk}{2k_B\theta}\right) + i \sin(k(x - vt)) - \coth\left(\frac{vk}{2k_B\theta}\right) \right], \\ &= \frac{2\pi\nu}{L} \sum_{k>0} \frac{e^{-\alpha k}}{k} \left[ \coth\left(\frac{vk}{2k_B\theta}\right) (\cos(k(x - vt)) - 1) + i \sin(k(x - vt)) \right]. \end{aligned} \quad (\text{A.5})$$

Applying the continuum limit

$$\sum_{k>0} \rightarrow \frac{L}{2\pi} \int_0^\infty dk,$$

results in

$$\mathcal{G}(x, t) = \nu \int_0^\infty dk \frac{e^{-\alpha k}}{k} \left[ \coth \left( \frac{vk}{2k_B\theta} \right) (\cos(k(x-vt)) - 1) + i \sin(k(x-vt)) \right]. \quad (\text{A.6})$$

We split Eq. (A.6) into zero-temperature and finite temperature contributions as  $\mathcal{G}(x, t) = \mathcal{G}^{(0)}(x, t) + \mathcal{G}^{(\theta)}(x, t)$ , where

$$\mathcal{G}^{(0)}(x, t) = \nu \int_0^\infty dk \frac{e^{-\alpha k}}{k} [e^{ik(x-vt)} - 1], \quad (\text{A.7})$$

$$\mathcal{G}^{(\theta)}(x, t) = \nu \int_0^\infty dk \frac{e^{-\alpha k}}{k} \left[ \left( \coth \left( \frac{vk}{2k_B\theta} \right) - 1 \right) (\cos(k(x-vt)) - 1) \right]. \quad (\text{A.8})$$

Note that Eq. (A.8) vanishes in the limit of  $\theta \rightarrow 0$ . We now evaluate the temperature independent Green's function. Introducing the variable  $y = \alpha k$  and expanding the exponential in Eq. (A.7) as a power series

$$\nu \int_0^\infty dy \left( \sum_{n=0}^\infty \frac{1}{n!} \left( \frac{iy(x-vt)}{\alpha} \right)^n - 1 \right) e^{-y} y^{-1} = \nu \sum_{n=1}^\infty \frac{1}{n!} \left( \frac{i(x-vt)}{\alpha} \right)^n \int_0^\infty dy e^{-y} y^{n-1}. \quad (\text{A.9})$$

The integral in (A.9) is equal to the Euler's Gamma function  $\Gamma(n-1) = (n-1)!$

$$\mathcal{G}^{(0)}(x, t) = \nu \sum_{n=1}^\infty \frac{1}{n} \left( \frac{i(x-vt)}{\alpha} \right)^n = \nu \ln \left( \frac{\alpha}{\alpha - i(x-vt)} \right). \quad (\text{A.10})$$

For the temperature dependent Green's function, we introduce the variables  $y = \alpha k$ , energy cut-off  $\omega_c = \frac{v}{\alpha}$ , and expand the trigonometric functions using Euler's formula.

$$\begin{aligned} \mathcal{G}^{(\theta)}(x, t) &= \nu \int_0^\infty dy e^{-y} y^{-1} \frac{1}{e^{\frac{\omega_c y}{k_B\theta}} - 1} \left( e^{i\frac{y}{\alpha}(x-vt)} + e^{-i\frac{y}{\alpha}(x-vt)} - 2 \right), \\ &= \nu \int_0^\infty dy \left[ \frac{e^{-y(1+i\frac{1}{\alpha}(x-vt))}}{ye^{\frac{\omega_c y}{k_B\theta}} \left( 1 - e^{-\frac{\omega_c y}{k_B\theta}} \right)} + \frac{e^{-y(1-i\frac{1}{\alpha}(x-vt))}}{ye^{\frac{\omega_c y}{k_B\theta}} \left( 1 - e^{-\frac{\omega_c y}{k_B\theta}} \right)} - \frac{2e^{-y}}{ye^{\frac{\omega_c y}{k_B\theta}} \left( 1 - e^{-\frac{\omega_c y}{k_B\theta}} \right)} \right]. \end{aligned} \quad (\text{A.11})$$

To rearrange (A.11) in the form of Hurwitz Zeta function [91]

$$\zeta(\gamma, z) = \frac{1}{\Gamma(\gamma)} \int_0^\infty dt \frac{e^{-zt}}{t^{1-\gamma}(1-e^{-t})}, \quad (\text{A.12})$$

setting  $y \rightarrow y \frac{k_B\theta}{\omega_c}$  and rewriting (A.11)

$$\mathcal{G}^{(\theta)}(x, t) = \nu \int_0^\infty dy \left[ \frac{e^{-y \left( 1 + \frac{k_B\theta}{\omega_c} + i \frac{k_B\theta}{\omega_c \alpha} (x-vt) \right)}}{y^{1-0} (1 - e^{-y})} + \frac{e^{-y \left( 1 + \frac{k_B\theta}{\omega_c} - i \frac{k_B\theta}{\omega_c \alpha} (x-vt) \right)}}{y^{1-0} (1 - e^{-y})} - \frac{2e^{-y \left( 1 + \frac{k_B\theta}{\omega_c} \right)}}{y^{1-0} (1 - e^{-y})} \right], \quad (\text{A.13})$$

$$\begin{aligned} \mathcal{G}^{(\theta)}(x, t) &= \lim_{\gamma \rightarrow 0} \Gamma(\gamma) \zeta \left( \gamma, \left( 1 + \frac{k_B \theta}{\omega_c} + i \frac{k_B \theta}{\omega_c \alpha} (x - vt) \right) \right) + \\ &\quad \Gamma(\gamma) \zeta \left( \gamma, \left( 1 + \frac{k_B \theta}{\omega_c} - i \frac{k_B \theta}{\omega_c \alpha} (x - vt) \right) \right) - 2\Gamma(\gamma) \zeta \left( \gamma, \left( 1 + \frac{k_B \theta}{\omega_c} \right) \right). \end{aligned} \quad (\text{A.14})$$

By using the expansions that are valid for  $\gamma \rightarrow 0$  [91]

$$\begin{aligned} \Gamma(\gamma) &= \frac{1}{\gamma} + \mathcal{O}\left(\frac{1}{\gamma^2}\right), \\ \zeta(\gamma, z) &= \frac{1}{2} - z + \gamma \left( \ln \Gamma(z) + \frac{1}{2} \ln 2\pi \right) + \mathcal{O}(\gamma^2), \end{aligned} \quad (\text{A.15})$$

and property of the Euler Gamma function  $\Gamma(x)\Gamma(x^*) = \Gamma(x)\Gamma^*(x) = |\Gamma(x)|^2$

$$\mathcal{G}^{(\theta)}(x, t) = \nu \ln \left( \frac{|\Gamma(1 + \frac{k_B \theta}{\omega_c} - i \frac{k_B \theta}{v} (x - vt))|^2}{\Gamma(1 + \frac{k_B \theta}{\omega_c})^2} \right). \quad (\text{A.16})$$

Now, we combine Eq. (A.10) and Eq. (A.16) to obtain

$$\mathcal{G}(x, t) = \nu \ln \left( \frac{\alpha}{\alpha - i(x - vt)} \frac{|\Gamma(1 + \frac{k_B \theta}{\omega_c} - i \frac{k_B \theta}{v} (x - vt))|^2}{\Gamma(1 + \frac{k_B \theta}{\omega_c})^2} \right). \quad (\text{A.17})$$

Since the energy cut-off  $\omega_c$  is the largest scale in the calculations, Eq. (A.17) can be simplified in the regime  $\omega_c \gg k_B \theta$ , using the identity

$$|\Gamma(1 + iy)|^2 = \frac{\pi y}{\sinh(\pi y)}, \quad (\text{A.18})$$

$$\mathcal{G}(x, t) = \nu \ln \left( \frac{\alpha}{\alpha - i(x - vt)} \frac{\pi k_B \theta \left( \frac{x}{v} - t \right)}{\sinh\left(\pi k_B \theta \left( \frac{x}{v} - t \right)\right)} \right). \quad (\text{A.19})$$

Equations (A.17) and (A.19) are the Green's functions calculated for a right moving chiral bosonic field. Repeating the above calculations for a left moving chiral bosonic field evolving as  $\phi_L(x, t) = \phi(x + vt, 0)$ , will result in similar equations with change in signs. The composite expression of the Green's function for both the right and left moving chiral bosonic fields is given as

$$\mathcal{G}_{L/R}(x, t) = \nu \ln \left( \frac{\alpha}{\alpha \pm i(x \pm vt)} \frac{|\Gamma(1 + \frac{k_B \theta}{\omega_c} - i \frac{k_B \theta}{v} (x \pm vt))|^2}{\Gamma(1 + \frac{k_B \theta}{\omega_c})^2} \right), \quad (\text{A.20})$$

$$\mathcal{G}_{L/R}(x, t) = \nu \ln \left( \frac{\alpha}{\alpha \pm i(x \pm vt)} \frac{\pi k_B \theta \left( \frac{x}{v} \pm t \right)}{\sinh\left(\pi k_B \theta \left( \frac{x}{v} \pm t \right)\right)} \right). \quad (\text{A.21})$$

# B

## Fourier Transform of the Green's Function

### B.1 Finite temperature Green's function

In this Appendix we calculate the Fourier Transform  $P_{2\nu}(E)$  of the Green's function  $G^2(t)$  [66], where  $G(t) = e^{\mathcal{G}(0,t)}$ . The Fourier Transform is defined as

$$P_{2\nu}(E) = \int_{-\infty}^{\infty} dt e^{-iEt} \left( \frac{\alpha}{\alpha \pm i(\pm vt)} \frac{|\Gamma(1 + \frac{k_B\theta}{\omega_c} - ik_B\theta(\pm t))|^2}{\Gamma(1 + \frac{k_B\theta}{\omega_c})^2} \right)^{2\nu}. \quad (\text{B.1})$$

The calculations can be simplified by rewriting the Green's function in B.1 and using the recurrence relation  $\Gamma(1 + \gamma) = \gamma\Gamma(\gamma)$ .

$$\begin{aligned} G(t) &= \frac{1}{1 + i(\omega_c t)} \frac{\Gamma(1 + \frac{k_B\theta}{\omega_c} + ik_B\theta t) \Gamma(1 + \frac{k_B\theta}{\omega_c} - ik_B\theta t)}{\Gamma(1 + \frac{k_B\theta}{\omega_c})^2}, \\ &= \frac{1}{1 + i(\omega_c t)} \frac{k_B\theta (1 + i(\omega_c t)) \Gamma(\frac{k_B\theta}{\omega_c} + ik_B\theta t) \Gamma(1 + \frac{k_B\theta}{\omega_c} - ik_B\theta t)}{\omega_c \Gamma(1 + \frac{k_B\theta}{\omega_c})^2}, \\ &= \frac{k_B\theta \Gamma(\frac{k_B\theta}{\omega_c} + ik_B\theta t) \Gamma(1 + \frac{k_B\theta}{\omega_c} - ik_B\theta t)}{\omega_c \Gamma(1 + \frac{k_B\theta}{\omega_c})^2}. \end{aligned} \quad (\text{B.2})$$

To rearrange B.2 in the form of Gamma function identity [91]

$$\Gamma\left(\frac{1}{2} + iy\right) \Gamma\left(\frac{1}{2} - iy\right) = \frac{\pi}{\cosh(\pi y)}, \quad (\text{B.3})$$

we make a change of variable  $t = t - i(2k_B\theta)^{-1}$  in B.2 and select a suitable contour in the complex plane [77] to keep the limits of the integral in B.1 unaltered along the real axis. In the regime  $\omega_c \gg k_B\theta$ , we obtain

$$\begin{aligned} P_{2\nu}(E) &= \int_{-\infty}^{\infty} dt e^{\frac{-E}{2k_B\theta}} e^{-iEt} \left( \frac{k_B\theta \Gamma(\frac{1}{2} + ik_B\theta t) \Gamma(\frac{1}{2} - ik_B\theta t)}{\omega_c \Gamma(1)^2} \right)^{2\nu}, \\ &= e^{\frac{-E}{2k_B\theta}} \int_{-\infty}^{\infty} dt (\cos(Et) - i \sin(Et)) \left( \frac{\pi k_B\theta}{\omega_c \cosh(\pi k_B\theta t)} \right)^{2\nu}. \end{aligned} \quad (\text{B.4})$$

The  $\sin(Et)$  function within the integral vanishes because its an odd function of the variable  $t$ . Therefore, we obtain

$$P_{2\nu}(E) = 2e^{\frac{-E}{2k_B\theta}} \int_0^\infty dt \cos(Et) \left( \frac{\pi k_B\theta}{\omega_c \cosh(\pi k_B\theta t)} \right)^{2\nu}. \quad (\text{B.5})$$

Now we expand the trigonometric functions using Euler's identities

$$P_{2\nu}(E) = 2e^{\frac{-E}{2k_B\theta}} \int_0^\infty dt \frac{e^{iEt} + e^{-iEt}}{2} \left( \frac{2\pi k_B\theta e^{-\pi k_B\theta t}}{\omega_c(1 + e^{-2\pi k_B\theta t})} \right)^{2\nu}. \quad (\text{B.6})$$

Introducing the variable  $z = e^{-\pi k_B\theta t}$  such that  $dz \rightarrow (-\pi k_B\theta z)dt$

$$P_{2\nu}(E) = 2e^{\frac{-E}{2k_B\theta}} \frac{(2\pi k_B\theta)^{2\nu-1}}{(\omega_c)^{2\nu}} \int_0^1 dz z^{2\nu-1} (z^{\frac{iE}{\pi k_B\theta}} + z^{-\frac{iE}{\pi k_B\theta}}) \left( \frac{1}{1+z^2} \right)^{2\nu}. \quad (\text{B.7})$$

To rearrange (B.7) in the form of Euler Beta function [91]

$$\mathcal{B}(\gamma, w) = \int_0^1 dt t^{\gamma-1} (1-t)^{w-1}, \quad (\text{B.8})$$

we introduce the variable  $y = \frac{z^2}{z^2+1}$  such that  $1-y = \frac{1}{z^2+1}$  and  $dy \rightarrow \frac{2z}{(z^2+1)^2} dz$

$$P_{2\nu}(E) = e^{\frac{-E}{2k_B\theta}} \frac{(2\pi k_B\theta)^{2\nu-1}}{(\omega_c)^{2\nu}} \int_0^{1/2} dy \left( \frac{z^2}{1+z^2} \right)^{\nu-1} \left( \frac{1}{1+z^2} \right)^{\nu-1} ((z^2)^{\frac{iE}{2\pi k_B\theta}} + (z^2)^{-\frac{iE}{\pi k_B\theta}}),$$

We treat the integral separately and simplify it as follows:

$$\begin{aligned} &= \int_0^{1/2} dy \left( \frac{z^2}{1+z^2} \right)^{\nu-1} \left( \frac{1}{1+z^2} \right)^{\nu-1} \left[ (z^2)^{\frac{iE}{2\pi k_B\theta}} \frac{(z^2+1)^{\frac{iE}{2\pi k_B\theta}}}{(z^2+1)^{\frac{iE}{2\pi k_B\theta}}} + (z^2)^{-\frac{iE}{2\pi k_B\theta}} \frac{(z^2+1)^{-\frac{iE}{2\pi k_B\theta}}}{(z^2+1)^{-\frac{iE}{2\pi k_B\theta}}} \right], \\ &= \int_0^{1/2} dy (y)^{\nu-1+\frac{iE}{2\pi k_B\theta}} (1-y)^{\nu-1-\frac{iE}{2\pi k_B\theta}} + \int_0^{1/2} dy (y)^{\nu-1-\frac{iE}{2\pi k_B\theta}} (1-y)^{\nu-1+\frac{iE}{2\pi k_B\theta}}. \end{aligned}$$

Making a change of variable of  $y = 1-y$  in the second integral will result in

$$P_{2\nu}(E) = e^{\frac{-E}{2k_B\theta}} \frac{(2\pi k_B\theta)^{2\nu-1}}{(\omega_c)^{2\nu}} \int_0^1 dy (y)^{\nu+\frac{iE}{2\pi k_B\theta}-1} (1-y)^{\nu-\frac{iE}{2\pi k_B\theta}-1}, \quad (\text{B.9})$$

$$P_{2\nu}(E) = e^{\frac{-E}{2k_B\theta}} \frac{(2\pi k_B\theta)^{2\nu-1}}{(\omega_c)^{2\nu}} \mathcal{B}\left(\nu + \frac{iE}{2\pi k_B\theta}, \nu - \frac{iE}{2\pi k_B\theta}\right). \quad (\text{B.10})$$

Using the representation of  $\mathcal{B}(\gamma, w)$  in terms of Gamma functions

$$\mathcal{B}(\gamma, w) = \frac{\Gamma(\gamma)\Gamma(w)}{\Gamma(\gamma+w)}, \quad (\text{B.11})$$

$P_{2\nu}(E)$  can be written in simpler form as

$$P_{2\nu}(E) = \frac{e^{\frac{-E}{2k_B\theta}}}{\Gamma(2\nu)\omega_c} \left( \frac{2\pi k_B\theta}{\omega_c} \right)^{2\nu-1} \left| \Gamma\left(\nu + \frac{iE}{2\pi k_B\theta}\right) \right|^2. \quad (\text{B.12})$$

## B.2 Temperature independent Green's function

The Fourier transform of the temperature independent Green's function can be calculated by taking the zero temperature limit of Eq. (B.12). However, this section presents a simple alternative method of its derivation using Eq. (A.10)

$$G(t) = e^{\mathcal{G}^{(0)}(0,t)} = \exp\left\{\nu \ln\left(\frac{\alpha}{\alpha \pm i(\pm vt)}\right)\right\} = \left(\frac{1}{1 + i\omega_c t}\right)^\nu. \quad (\text{B.13})$$

The Fourier Transform is defined as

$$P_{2\nu}(E) = \int_{-\infty}^{\infty} dt e^{-iEt} G^2(t) = \int_{-\infty}^{\infty} dt e^{-iEt} \left(\frac{1}{1 + i\omega_c t}\right)^{2\nu}. \quad (\text{B.14})$$

Equation (B.14) is in the form of the following integrals [91] (3.382 - Eqs. 6 and 7)

$$\begin{aligned} \int_{-\infty}^{\infty} dx (\beta + ix)^{-\nu} e^{-ipx} &= 0 && \text{for } p > 0, \\ &= \frac{2\pi e^{\beta p} (-p)^{\nu-1}}{\Gamma(\nu)} && \text{for } p < 0, \\ \int_{-\infty}^{\infty} dx (\beta - ix)^{-\nu} e^{-ipx} &= \frac{2\pi e^{-\beta p} (p)^{\nu-1}}{\Gamma(\nu)} && \text{for } p > 0, \\ &= 0 && \text{for } p < 0, \end{aligned} \quad (\text{B.15})$$

valid for  $\text{Re}\{\nu\} > 0$  and  $\text{Re}\{\beta\} > 0$ .

Using B.15, the temperature independent  $P_{2\nu}(E)$  can be expressed as

$$P_{2\nu}(E) = \frac{2\pi e^{\frac{E}{\omega_c}} (-E)^{2\nu-1}}{\Gamma(2\nu) \omega_c^{2\nu}} \Theta(-E). \quad (\text{B.16})$$

# C

## Photoassisted Coefficients

In this Appendix we detail the calculation of the photoassisted coefficients  $p_l$  [66] for a sinusoidal time-dependent voltage pulse  $V_{sin}(\tau)$  driving the anyon collider setup out of equilibrium. As seen in the current and noise calculations presented in the main text,  $V(\tau)$  appears as a phase factor with the form

$$\exp\left\{\pm iq\nu \int_{-\infty}^t d\tau V(\tau)\right\}. \quad (\text{C.1})$$

The time-dependent voltage pulse can be interpreted as a periodic AC signal riding over a DC bias, thus decomposing the signal into  $V(\tau) = V_{DC} + V_{AC}(\tau)$ . Considering a periodic signal with period  $T$  and frequency  $\Omega$ ,

$$q\nu \int_0^T d\tau [V_{DC} + V_{AC}(\tau)] = q\nu T V_{DC} + q\nu \int_0^T d\tau V_{AC}(\tau). \quad (\text{C.2})$$

Setting  $Q\Omega = q\nu V_{DC}$ , Eq. (C.1) can be written as

$$\exp\left\{\pm iq\nu \int_0^t d\tau V(\tau)\right\} = e^{\pm iQ\Omega t} e^{\pm iq\nu \int_0^t d\tau V_{AC}(\tau)}. \quad (\text{C.3})$$

The second phase factor on the right hand side of Eq. (C.3) can be written as a complex exponential Fourier series

$$e^{\pm iq\nu \int_0^t d\tau V_{AC}(\tau)} = \sum_{l=-\infty}^{\infty} p_l e^{\pm il\Omega t}. \quad (\text{C.4})$$

The complex exponential Fourier series coefficients are given by

$$p_l = \int_{-\frac{T}{2}}^{\frac{T}{2}} dt \frac{1}{T} e^{\mp il\Omega t} e^{\pm iq\nu \int_0^t d\tau V_{AC}(\tau)}. \quad (\text{C.5})$$

We now detail the evaluation of  $p_l$  for  $V_{AC}(\tau) = V_{AC} \sin(\Omega\tau)$

$$p_l = \int_{-\frac{T}{2}}^{\frac{T}{2}} dt \frac{1}{T} e^{\mp il\Omega t} e^{\pm iq\nu V_{AC} \int_0^t d\tau \sin(\Omega\tau)} = \int_{-\frac{T}{2}}^{\frac{T}{2}} dt \frac{1}{T} e^{\mp il\Omega t} e^{\mp iq\nu V_{AC} \Omega^{-1} \cos(\Omega\tau)} e^{\pm iq\nu V_{AC} \Omega^{-1}}.$$

Setting  $W\Omega = q\nu V_{AC}$ . As seen in the main text the photoassisted coefficients appear as  $|p_l|^2$  in the calculations. Therefore, we can ignore the global phase factor  $e^{\pm iW\Omega}$ .

$$p_l = \int_{-\frac{T}{2}}^{\frac{T}{2}} dt \frac{1}{T} e^{il\Omega t} e^{iW \cos(\Omega\tau)} = \frac{1}{2\pi} \int_{-\frac{\pi}{\Omega}}^{\frac{\pi}{\Omega}} dt \Omega e^{il\Omega t} e^{iW \cos(\Omega\tau)}.$$

Introducing the variable  $z = \Omega t$ , we obtain

$$\frac{1}{2\pi} \int_{-\pi}^{\pi} dz e^{i(lz+W \cos(z))} = \frac{1}{2\pi} \int_{-\pi}^{\pi} dz [\cos(lz + W \cos(z)) + i \sin(lz + W \cos(z))]. \quad (\text{C.6})$$

The  $\cos$  function in the above integral is odd over the period  $[-\pi, \pi]$  (it can be verified by plotting the function). Therefore, the integral of the  $\cos$  function evaluates to 0.

$$p_l = \frac{i}{\pi} \int_0^{\pi} dz \sin(lz + W \cos(z)) \quad (\text{C.7})$$

Using the identity  $\sin(A+B) = \sin(A)\cos(B) + \sin(B)\cos(A)$ , we obtain

$$\frac{i}{\pi} \int_0^{\pi} dz \sin(lz) \cos(W \cos(z)) + \frac{i}{\pi} \int_0^{\pi} dz \cos(lz) \sin(W \cos(z)). \quad (\text{C.8})$$

By Cauchy integral theorem [77], we can verify that

$$\int_0^{\pi} dx \cos(\cos(x)) e^{ix} = 0, \quad (\text{C.9})$$

$$\int_0^{\pi} dx \cos(\cos(x)) \cos(x) = -i \int_0^{\pi} dx \cos(\cos(x)) \sin(x). \quad (\text{C.10})$$

Using Eq. (C.10), we can rewrite Eq. (C.8) as

$$-\frac{1}{\pi} \int_0^{\pi} dz \cos(W \cos(z)) \cos(lz) + \frac{i}{\pi} \int_0^{\pi} dz \cos(lz) \sin(W \cos(z)). \quad (\text{C.11})$$

Equation (C.11) is in the form of the following integrals [91] (3.715 - Eqs. 13 and 18)

$$\begin{aligned} \int_0^{\pi} dz \sin(z \cos(x)) \cos(nx) &= \pi \sin\left(\frac{n\pi}{2}\right) J_n(z), \\ \int_0^{\pi} dz \cos(z \cos(x)) \cos(nx) &= \pi \cos\left(\frac{n\pi}{2}\right) J_n(z). \end{aligned} \quad (\text{C.12})$$

Using C.12, the photoassisted coefficient can be  $p_l$  can be expressed as

$$p_l = -\cos\left(\frac{l\pi}{2}\right) J_l(W) + i \sin\left(\frac{l\pi}{2}\right) J_l(W) = -e^{-i\frac{l\pi}{2}} J_l(W). \quad (\text{C.13})$$

Ignoring the global phase factor we have

$$p_l = -J_l(W), \quad (\text{C.14})$$

where  $J_l(W)$  is the Bessel function of the first kind.

# D

## Integral of the Equilibrium Green's Function

In this Appendix, we evaluate the integral of the equilibrium Green's function. As outlined in the main text, we encounter two analogous forms of definite integrals in current and noise calculations that need to be evaluated in two distinct regions. The general form of the first integral is

$$\int_{-\infty}^m dt' \mathcal{J}(t-t') = \int_{-\infty}^m dt' \left[ \frac{\pi k_B \theta \alpha}{\sinh(\pi k_B \theta (t-t'))} \right]^{4\delta}. \quad (\text{D.1})$$

We express the hyperbolic sinusoidal function in exponential form

$$(2\pi k_B \theta \alpha)^{4\delta} \int_{-\infty}^m dt' \left[ \frac{1}{e^{\pi k_B \theta (t-t')} - e^{-\pi k_B \theta (t-t')}} \right]^{4\delta}. \quad (\text{D.2})$$

Setting  $z = e^{-2\pi k_B \theta (t-t')}$  leads to  $dt' = (2\pi k_B \theta)^{-1} z^{-1} dz$ , altering the upper and lower integral limits as  $m \rightarrow e^{-2\pi k_B \theta (t-m)}$  and  $-\infty \rightarrow e^{-\infty} = 0$ .

$$(2\pi k_B \theta)^{4\delta-1} \alpha^{4\delta} \int_0^{e^{-2\pi k_B \theta (t-m)}} dz (1-z)^{(1-4\delta)-1} z^{2\delta-1} \quad (\text{D.3})$$

The integral in Eq. (D.3) is in the form of the incomplete Beta function [91]

$$\mathcal{B}(x; a, b) = \int_0^x t^{a-1} (1-t)^{b-1}, \quad (\text{D.4})$$

yielding the subsequent result

$$\int_{-\infty}^m dt' \mathcal{J}(t-t') = (2\pi k_B \theta)^{4\delta-1} \alpha^{4\delta} \mathcal{B}(e^{-2\pi k_B \theta (t-m)}, 2\delta, 1-4\delta). \quad (\text{D.5})$$

The general form of the second integral we encounter in the main text is

$$\int_m^\infty dt' \mathcal{J}(t'-t) = \int_m^\infty dt' \left[ \frac{\pi k_B \theta \alpha}{\sinh(\pi k_B \theta (t'-t))} \right]^{4\delta}. \quad (\text{D.6})$$

Setting  $z = e^{2\pi k_B \theta (t-t')}$  yields  $dt' = -(2\pi k_B \theta)^{-1} z^{-1} dz$ ,  $m \rightarrow e^{2\pi k_B \theta (t-m)}$ ,  $\infty \rightarrow 0$ , and

$$\int_m^\infty dt' \mathcal{J}(t'-t) = (2\pi k_B \theta)^{4\delta-1} \alpha^{4\delta} \mathcal{B}(e^{2\pi k_B \theta (t-m)}, 2\delta, 1-4\delta). \quad (\text{D.7})$$

DEPARTMENT OF MICROTECHNOLOGY AND NANOSCIENCE - MC2  
CHALMERS UNIVERSITY OF TECHNOLOGY

Gothenburg, Sweden

[www.chalmers.se](http://www.chalmers.se)



**KU LEUVEN**

**CHALMERS**  
UNIVERSITY OF TECHNOLOGY



Erasmus  
Mundus